IN VIVO IDENTIFICATION OF PERIODONTIUM MSCS AND THEIR RESPONSE TO PERIODONTITIS

A Dissertation

by

WENJING LUO

Submitted to the Office of Graduate and Professional Studies of
Texas A&M University
in partial fulfillment of the requirements for the degree of

DOCTOR OF PHILOSOPHY

Chair of Committee,	Hu Zhao
Committee Members,	Jian Q. Feng
	Lynne A. Opperman
	Yongbo Lu
Head of Department,	Larry L. Bellinger

August 2019

Major Subject: Oral Biology

ABSTRACT

Periodontium is the supporting tissue for teeth and is composed of alveolar bone, periodontal ligament (PDL), gingiva and cementum. Periodontal tissues are known to undergo constant turnover supported by the stem cell population. However, this process remain poorly understood because of the failure to identify and locate periodontium mesenchymal stem cells (MSCs) in vivo. Advanced periodontitis, which results in periodontium impairment (including alveolar bone loss and PDL space enlargement), is a major cause of tooth loss in adults. However, why MSCs fail to maintain periodontium integrity in infectious conditions is largely unknown.

The goal of my thesis was to test a dual hypothesis: the transcription factor glioma-associated (Gli1) + cells surrounding the neurovascular bundle (NVB) inside PDL are periodontium MSCs, which play a critical role in periodontal tissue turnover and injury repair under the control of Wnt-ß-catenin signaling. Secondly, during periodontitis pathogenesis, the bioactivity of Gli1+ periodontium MSCs is compromised. To test the hypothesis, we used newly developed tissue clearing and multiple imaging techniques in Gli1-CreERT2; Ai14 transgenic fluorescent reporter mice line, plus the conditional knockout strain in combination with the ligation-periodontitis model. Our key findings were: 1). The newly developed tissue clearing method revealed a three-dimensional view of Gli1+ MSCs distribution in adult mouse molar periodontium for the first time. 2). The Gli1+ cells surrounding NVB are periodontium MSCs, which actively maintain periodontium integrity during the animal`s adult stage. Likewise, to facilitate this integrity, 3). Wnt signaling is essential in the regulation of Gli1+ MSCs. However,

we also discovered that a loss of ß-catenin within the Gli1+ MSCs (Gli1-CreERT2; ß-catenin loxP; Ai14 line) leads to severe periodontal tissue defects. For example, 4). over-activated Wnt signaling within Gli1+ MSCs (Gli1-CreERT2; ß-catenin-(Exon3) loxP; Ai14 line) leads to periodontium overgrowth in vivo. 5). Periodontitis also inhibits Gli1+ MSC' activation and lineage commitment activity. 6). Accordingly, chronic periodontitis compromises Gli1+ MSC maintenance. In addition to the issues above, PDL vasculature is compromised in advanced periodontitis. 8). Lastly, we found out that Wnt signaling activity is downregulated during periodontitis while 9) over-activation of Wnt signaling within Gli1+ MSCs restores normal periodontal morphology.

Overall, our study found a reliable in vivo marker to label adult mouse molar periodontium MSCs and successfully localized them for the first time. Therefore, our work provides an effective animal model to further study the in vivo response of periodontal MSCs on pathological conditions, thereby providing insight for treatment planning in dental clinics. We further demonstrated the impact of infectious periodontitis on Gli1+ MSCs and revealed part of the mechanism behind the persistence of advanced periodontitis.

ACKNOWLEDGEMENTS

At this moment, all of my memories resurfaced in my mind. I still remember the first day I came here knowing nothing about my upcoming life. I was freaked out. However, Nancy toured me around the building and introduced me to a big warm family. Suddenly, I felt relieved. Everybody was so nice. The seniors helped me fit in with the environment and professors were supportive. All of the faculty was ready to assist you at any time. On the first day, I could really see myself enjoying the next four years of Ph.D. study life.

I would like to thank my Ph.D. advisor, Dr. Hu Zhao for supporting me during the past four years. Dr, Zhao is a talented, ambitious, and knowledgeable young scientist. Under his guidance, I realized how charming science could be. He took me to numerous lectures and I had the opportunity to meet and know many outstanding scientists in various fields. My horizons were broadened and I really learned a lot. Though I made a multitude of mistakes during the past three years, Dr. Zhao has always patiently taught me and helped me with troubleshooting. I'm very grateful for his scientific advice, insightful discussions, and suggestions. He has been so supportive and gave me the freedom to pursue my career dream. I really appreciate his support no matter if I go back to China for a job interview or travel for dental school interviews.

I would also like to thank my committee members for their guidance and support throughout the whole course of this research. Dr. Jian Q. Feng’s positive attitude on life, and research affects me considerably. He has offered many constructive suggestions not only about research but also regarding my future career plans. Dr. Lynne A. Opperman,

our department head, has been taking good care of not only myself but all graduate students. Her wisdom and elegant speech, behavior, and attitude are what I need to learn in my entire lifetime. She consistently gave great advice during the committee meetings. Furthermore, her insight always inspired me to think about this project in another perspective. She demonstrated great efforts in teaching me how to write a decent proposal and perform a clear oral presentation as well. In addition, Dr. Yongbo Lu's kind heart and rationality have inspired me to do better. He is always available for all of the students and he cares about them. I still remember once I asked a question in a seminar and the entire audience including even the invited speaker did not take it seriously. Yet, Dr. Lu found me after the seminar and told me his viewpoints- that was touching.

Likewise, our program director, Dr. Kathy Svoboda, has been helpful in providing advice many times during my graduate school career. She has helped to guarantee the graduation process for my fellow classmates and I. Her work included teaching us us how to write, present, and conduct experiments appropriately. Dr. Larry L. Bellinger, Associate Dean for Research & Graduate Studies, also helped to ensure scientific research goes on smoothly here. Moreover, Dr. M. Douglas Benson used to help perform spinal cord injury for us. His humor and meticulous attitude about research impress me greatly. Moreover, he helped me substantially with my preliminary exams. Besides, Dr. Xiaohua Liu and I often talked during lunchtime in the break room. He has been really nice and gave me some suggestions about my career development. Next, I can tell Dr. Chunlin Qin is a very responsible mentor. Each time we met in the elevator

or the hallway, "How's everything going on?" was always the first thing he asked. When I complained about stress, he provided useful ideas. Dr. Qian Wang and I also had a wonderful research trip in Puerto Rico. Further, I rotated in Dr. L-Bruno Ruest`s lab during my very first semester. He taught the very basic but important genotyping and cryo-sectioning techniques. In addition, Dr. Hua Zhang and Dr. Shuzhen Wang have also been so gentle and considerate. Meanwhile, Dr. Groppe`s lessons were inspiring and cultivated our critical thinking ability. Besides, Drs. Tao, Kramer, and Xiaofang Wang`s care and compliments really cheered me up. The department is so supportive and lovely-it wouldn`t be like that without the service of Nancy, Marge, Jeanne, Valeria, Darla, Kim, Richard, Jill, and Willie.

Thanks also go to my lab mates. Dr. Yi Men was a postdoc in our lab. We had discussions with each other and came up with good ideas. Dr. Shiwen Zhang not only helped me with lab work but was a good listener when I felt stressed and disappointed. Yating Yi and I collaborated in another project and supported each other when facing an overwhelming workload. Furthermore, I co-authored a paper with Dr. Dian Jing and we worked together in a big project. She let me know how to handle interpersonal relationships as well. Secondly, the short-term visiting students Sirong Shi and Xiaoru Shao helped everyone in the lab perform genotyping and change medium.

I also thank Dr. Wooping Ge, a collaborator from UT Southwestern Medical Center. Our lab had a joint meeting with his lab many times and he offered constructive suggestions about our projects. Accordingly, I appreciate all the efforts of his lab members: Dr. Xiaofei Gao, Dr. Fei Cheng, Dr. Yihui Wang, and Dr. Hong Wang. Dr. Bo

Shen, (also from UTSW) helped enormously with flow cytometry experiments and microCT scanning.

To be honest, I encountered lots of tough situations during my four years of study life. I suffered from a heavy workload and complicated interpersonal relationship issues. I could not pull through without my friends' support. Bei Chang and I have been classmates for over ten years. We turned pretty close when we both came to TAMU College of Dentistry and shared our pleasures and troubles. She has always been there to support and help me. Ke Wang, Yongxi Liang, and I had a happy time in the student office together. Next, I want to thank Runyi Mao for listening to my complaints patiently each time we went for dinner. Another important group was Jingya Wang, Chi Ma, Yan Jing, Ju Wang, Zhiai Hu, Xudong Xie, Yuanchao Li, Ruixin Wu, Lu Han, and Hui Li who all taught me research techniques. I would also like to thank the entire population of graduate students in the program for their company. Too many to list here but you know who you are!

Finally, I really want to thank family members: my mother, father, sister, brother-in-law, and nephew for their unconditional love and care. Without them, I wouldn’t have been able to pursue my dream in such a carefree environment. I love them so much and I would not have made it this far without them. They are the ones who always love me no matter how mean I was sometimes. They are my spiritual pillar. Also, I want to thank Adrian N. Morales for backing me up and encouraging me to stand up for myself. His advice and guidance led me to maturity.

CONTRIBUTORS AND FUNDING SOURCES

Contributors

This work was supervised by a thesis committee consisting of Dr. Hu Zhao [advisor, Department of Restorative Sciences], Dr. Jian Q. Feng [Department of Biomedical Sciences], Dr. Lynne A. Opperman [Department of Biomedical Sciences], and Dr. Yongbo Lu [Department of Biomedical Sciences].

The work conducted for section one and two was completed by a cooperation between Dr. Yi Men (postdoc in our lab) and I. Flow cytometry of Gli1+ MSCs relative number counting was performed by Dr. Bo Shen of UTSW. All other work was conducted independently by the student.

Funding Sources

This work was made possible in part by the Department of Biomedical Sciences as well as Department of Restorative Sciences under the NIH/NIDCR K08 (K08DE025090) and NINDS R21 (5R21NS099950) grant. Its contents are solely the responsibility of the authors and do not necessarily represent the official views of the National Institutes of Health.

NOMENCLATURE

MSCs	Mesenchymal Stem Cells
CD	Cluster of Differentiation
DPSCs	Dental Pulp Stem Cells
SHED	Stem Cells of Human Exfoliated Deciduous Teeth
PDLSCs	Periodontal Ligament Stem Cells
SCAP	Apical Papilla Stem Cell
DFSCs	Dental Follicle Stem Cells
GMSC	Gingival Mesenchymal Stem Cells
TGF-β1	Transforming Growth Factor-β1
FGF-2	Fibroblast Growth Factor-2
HA	Hydroxyapatite
TCP	Tricalcium Phosphate
DSPP	Sialophosphoprotein
Oct-4	Octamer-Binding Transcription Factor 4
PDL	Periodontal Ligament
PDLMSCs	Periodontal Ligament Mesenchymal Stem Cells
αSMA	Alpha Smooth Muscle Actin
Axin2	Axis Inhibition Protein 2
DSCs	Dental Stem Cells
NVB	Neurovascular Bundle
NG2	Neuron-Glial Antigen 2

SCA1	Spinocerebellar Ataxia Type 1
THY1	Thy-1 Cell Surface Antigen
IHH	Indian Hedgehog
SuMSCs	Suture Mesenchymal Stem Cells
BMP	Bone Morphogenetic Protein
CXCL12	C-X-C Motif Chemokine Ligand 12
SHH	Sonic Hedgehog
SCF	Stem Cell Factor
TGFß	Transforming Growth Factor β
PCP	Planar Cell Polarity
Lgr5	Leucine-Rich Repeat-Containing G-protein Coupled Receptor 5
Rac1	Ras-Related C3 Botulinum Toxin Substrate 1
RhoA	Ras Homolog Gene Family, Member A
PKC	Protein Kinase C
JNK	c-Jun N-Terminal Kinases
FzD	Frizzled
FYN	Proto-Oncogene Tyrosine-Protein Kinase
LRP	Lipoprotein Receptor-Related Proteins
APC	Adenomatous Polyposis Coli
CK1	Casein Kinase1
GSK3	Glycogen Synthase Kinase 3
Dvl	Disheveled Protein

TCF	T Cell Factor
LEF	Lymphoid-Enhancing Factor
ROR2	Tyrosine Kinase-Like Orphan Receptor 2
RYK	Receptor Tyrosine Kinase
DAMM1	Disheveled Activator of Morphogenesis 1
JNK	c-Jun Amino-Terminal Kinase
PLC	Phospholipase C
IP3	Inositol Triphosphate 3
DAG	Diacylglycerol
PIP2	Phosphatidylinositol-4,5-Bisphosphate
ER	Endoplasmic Reticulum
CaMKII	Calmodulin-Dependent Protein Kinase II
NFAT	Nuclear Factor of Activated T-Cells
MAPKs	Mitogen-Activated Protein Kinases
TAK1	TGF-β Activated Kinase 1
NLK	Nemo-Like Kinase
LEF1	Lymphoid Enhancer-Binding Factor 1
STAT3	Signal Transducer and Activator of Transcription 3
EMT	Epithelial–Mesenchymal Transition
HF-MSCs	Hair Follicle Mesenchymal Stem Cells
Dkk3	Dickkopf3
TCF-4	Transcription Factor 4

IFE	Interfollicular Epidermal
$p21^{Cip1/Waf1}$	Cyclin-Dependent Kinase Inhibitor 1
sFRP4	Secreted Frizzled-Related Protein 4
BIO	6-Bromo-Indirubin-3'-Oxime
MHC	Major Histocompatibility Complex
NF-κB	Nuclear Factor Kappa-Light-Chain-Enhancer of Activated B Cells
TLR	Toll Like Receptor
IL-1	Interleukin 1
MYD88	Innate Immune Signal Transduction Adaptor
Hsp70s	70 Kilodalton Heat Shock Proteins
PRRs	Pattern Recognition Receptor
PAMPs	Pathogen-Associated Molecular Patterns
NLRs	Nucleotide-Binding Oligomerization Domain-Like Receptors
RLRs	Retinoic Acid-Inducible Gene-I-Like Receptors
CLRs	C-Type Lectin Receptors
AIM2	Absence in Melanoma 2
DNA	Deoxyribonucleic Acid
LPS	Lipopolysaccharides
TNFα	Tumor Necrosis Factor α
TIR	Interlukin-1 Receptor
IRAK-4	IL-1 Receptor-Associated Kinase-4
TRAF6	TNF Receptor Associated Factor 6

TAK1	Transforming Growth Factor Beta-Activated Kinase 1
IKK	IκB Kinase
MKKs	Mitogen-Activated Protein Kinases Kinase
MAPKs	Mitogen-Activated Protein Kinase
ERK	Extracellular Signal-Regulated Kinases
TRIF	TIR-Domain-Containing Adapter-Inducing Interferon-β
IRF3	Interferon Regulatory Factor 3
BM-MSCs	Bone Marrow Mesenchymal Stem Cells
AD-MSCs	Adipose Mesenchymal Stem Cells
mRNA	Messenger Ribonucleic Acid
GSK-3β	Glycogen Synthase Kinase 3β
PGE2	Prostaglandin E2
AKT	Protein Kinase B
PI3Ks	Phosphoinositide 3-Kinases
LRRFIP2	Leucine-Rich Repeat Flightless-Interacting Protein 2
DAMPs	Damage Associated Molecular Patterns
LRR	Leucine-Rich Repeat
CARD	Caspase Recruitment Domain
PYD	Pyrin Domain
NLRA	Acidic Transactivating Domain
RIP2	Receptor-Interacting Protein Kinase 2
BIRs	Baculovirus Inhibitor Repeats

ASC	Speck-Like Protein
MCP-1	Monocyte Chemoattractant Protein 1
hUCBMSCs	Human Umbilical Cord Blood-Derived Mesenchymal Stem Cells
LYPD6	Ly6/PLAUR Domain–Containing Protein 6
FoxD3	Foxhead Box D3 Protein
IFN	Interferon
XIAP	X-Linked Inhibitor of Apoptosis Protein
FLIP	FLICE-Like Inhibitory Protein
RUNX2	Runt-Related Transcription Factor 2
COX2	Cyclooxygenase-2
ROS	Reactive Oxygen Species
NADPH	Reduced Form of Nicotinamide Adenine Dinucleotide Phosphate
NOX4	NADPH Oxidase 4
HIFs	Hypoxia-Inducible Factors
NRX	Nucleoredoxin
ECs	Endothelial Cells
NFP	Neurofilament Protein
DHH	Desert Hedgehog
PFA	PFA Paraformaldehyde
EDTA	Ethylenediaminetetraacetic Acid
PBS	Phosphate-Buffered Saline
RT	Room Temperature

PEGASOS	Polyethylene Glycol (PEG) Associated Solvent System
EDTP	N,N,N',N'-Tetrakis(2-hydroxypropyl) Ethylenediamine
TB	Tert-Buturnol
BB	Benzyl Benzoate
R.I	Refraction Index
NIR	Near-Infrared
TIFF	Tagged Image File Format
DAPI	4′, 6-Diamidino-2-Phenylindole
PES	Polyethersulfone
DMEM	Dulbecco's Modified Eagle's Medium
3D	Three Dimension
PBST	Phosphate-Buffered Saline With Triton
P1	Postnatal Day 1
SHG	Second Harmonic Generation
PDGFR	Platelet-Derived Growth factor Receptor
TGG	Trigeminal Ganglion
NIH	National Institutes of Health
NIDCR	National Institute of Dental and Craniofacial Research
Micro-CT	Micro Computed Tomography
ABL	Alveolar Bone Loss
CEJ	Cementoenamel Junction
AC	Alveolar Crest

H&E	Hemotoxylin and Eosin
EdU	5-Ethynyl-2'-Deoxyuridine
MI	Myocardial Infarction
FITC	Fluorescein Isothiocyanate
TRITC	Tetramethylrhodamine
HBSS	Hanks' Balanced Salt Solution
PCR	Polymerase Chain Reaction
Cdh5	Vascular Endothelial-Cadherin
NK	Natural Killer
Tregs	Regulatory T Cells
RANKL	Receptor Activator of Nuclear Factor Kappa-B Ligand
Pg	Porphyromonas Gingivalis
CMC	Carboxymethylcellulose
CGRP	Calcitonin Gene-Related Peptide
OCN	Osteocalcin
COL-1	Collagenase 1
PMNs	Polymorphonuclear Neutrophils

TABLE OF CONTENTS

LIST OF FIGURES

Page

LIST OF TABLES

Page

1. INTRODUCTION

1.1. Identified Dental and Craniofacial MSCs

Craniofacial tissue and tooth loss are a big issue in dental clinical practice, impacting patients' physiological and psychological health. Nowadays, regenerative therapy has become a hotspot in dental medicine research. Mesenchymal stem cells (MSCs) are promising therapy candidates. Namely, orofacial MSCs are ready to harvest. Their high proliferation rate and multipotency deem them a unique cell source for tissue engineering and cell-based therapies not only in dentistry but also in general [1] [2] [3] [4] [5]. Recently, many dental and craniofacial MSCs were identified, such as dental pulp stem cells (DPSCs) [6] [2], stem cells from human exfoliated deciduous teeth (SHED) [7] [3], periodontal ligament stem cells (PDLSCs) [4], apical papilla stem cells (SCAP) [5], dental follicle stem cells (DFSCs) [8] and gingival MSCs (GMSCs) [9] . Furthermore, to date there have been several dental stem cell banks for human use around the world. They are in the USA (Bioeden, Stem Save, Store a Tooth), Europe (Bergen, Future Health), India (Stemade Biotech), Japan (Teeth Bank, Advanced Center of Tissue Engineering, Hiroshima University, Nogoya University) and China (National Dental Stem Cells Bank, Taipai Medical University). However, only a few stem cell-based therapies were registered as clinical trials and none of them have been established as the standard protocol for oral and craniofacial tissue regeneration so far. This lack of knowledge is also experienced in other study settings which would benefit from the use of these cells.

For instance, there are three minimal criteria based on previous studies to define MSCs in vitro, including trilineage differentiation ability, specific surface marker expression (such as CD73, CD90, or CD105), and adherence to a plastic plate [10] [11]. Yet, in vitro culture does not faithfully replicate an actual in vivo situation due to a different microenvironment [12]. On the

other hand, a variety of MSCs derived from embryonic mesoderm were identified in situ such as bone marrow [13] , skeletal muscle [14], adipose tissue [15], endometrium [16], synovial membrane [17], menstrual fluid [18], umbilical cord blood [19] [20] and bone [1] since around 2010. However, although lineage tracing and label-retaining techniques have become the gold standard for the in vivo identification of many other MSCs as of late [21], application in identifying dental and craniofacial MSCs remains deficient [22]. In spite of the current problematic nature of craniofacial MSCs study, there is some background knowledge on dental pulp MSCs, which will be briefly explained in the next section.

1.1.1. Dental MSCs (DSCs)

1.1.1.1. DPSC

The first identified dental MSCs were dental pulp stem cells (DPSCs) in the early 2000s from human adult third molar pulp [2]. These cells were characterized by osteogenic, chondrogenic, and adipogenic differentiation ability together with highly active proliferation and self-renewal. Their in vitro expression profile indicates they are positive for typical MSC surface markers such as CD44/73/90/146/105 and Strol but negative for CD34, CD45, and CD14. In addition, under special conditions with transforming growth factor-β1 (TGF-β1) and/or fibroblast growth factor-2 (FGF-2), DPSCs can differentiate into odontoblast-like cells [23]. In fact, transplantation studies demonstrated that DPSCs generated functional dentin/pulp-like complexes in immunocompromised mice [2] [24] [25] when mixed with hydroxyapatite-tricalcium phosphate (HA/TCP) scaffolds. The newly formed pulp tissue is vascularized and the outer dentin-like structure contains dentinal tubules and expresses sialophosphoprotein (DSPP) [2] [26]. Besides, DPSCs are found to form myoblast-like cells and induce endogenous axon guidance [27] [28] [29]. For instance, engrafted DPSCs can be involved in the treatment of stroke and heart infarction by

promoting neurogenesis, gliogenesis, vasculogenesis and muscle regeneration [30] [31] [32] [33]. Additionally, DPSCs have already been used to replace dead pulp tissue in patients after traumatic dental injuries. In fact, hDPSC implantation led to dental pulp regeneration with normally functioning blood vessels and sensory nerves during a twenty-four month follow up observation [34]. In addition to the MSCs found in human molar pulp, there are SHEDs, which differ from DSPCs in several ways.

1.1.1.2. SHEDs

SHEDs are stem cells isolated from human exfoliated deciduous incisor pulp [3]. Their proliferation rate is much higher than bone marrow MSCs or DPSCs [2] [35] [36]. Further, they highly express embryonic stem cell pluripotency markers including Oct4, Nanog, SSEA 3,4, TRA-1-60 and TRA-1-81 as well as MSC markers CD105, CD146, Stro-1, and CD29, but are negative for CD31 and CD34 [37]. Moreover, SHED could undergo osteogenic, chondrogenic, adipogenic, neurogenic, myogenic, endothelial and odontoblastic differentiation [37] [35]. However, transplanted SHED can only give rise to odontoblast-like cells and dentin-like structure instead of complete dentin-pulp complex [2] [3]. Though also derived from dental pulp, SHED displayed higher osteoinductive potential than DPSCs. Therefore, they are regarded as a possible cell source for calvaria and mandible bone defect repair [3] [38] [39] [40]. In addition, SHED have been discovered to express a nerve tissue-specific marker called nestin with an optimized induction medium and help treat neurodegenerative diseases [41] [42]. Another type of cell beyond SHEDs is SCAPs, which we will uncover with a focus on proliferation levels in comparison to DPSCs.

1.1.1.3. SCAPs

SCAPs are extracted from the apical papilla tissue which is loosely attached to human immature permanent teeth root apex. They are supposed to participate in root development. The

SCAP variety was discovered because of its strong STRO-1 expression activity [5]. SCAP in vitro expression profile showed the expression of CD73, CD44, CD105, CD146, and CD166. They are able to give rise to odontoblast, osteoblast, neural cells and adipocytes [5 43]. Compared with DPSCs, SCAPs are more robust in terms of proliferation level, migration ability and telomerase activity which may be related to developing tissue origin [5 44]. SCAP is also majorly used in bio-teeth root formation [5]. Besides SCAPs, DFSCs play a large role in dental development.

1.1.1.4. DFSCs

The dental follicle is a loose mesenchymal connective tissue which surrounds the developing tooth at its early stage. This tissue houses cementoblasts, osteoblasts, PDL progenitor cells, and plays a critical role in whole tooth development. The first group of DFSCs was harvested from an impacted human third molar's dental follicle [8]. They express MSC markers Notch1, STRO-1, nestin, CD105, CD44, and CD29 while being negative for hematopoietic markers CD34 and CD117 in vitro [45 8]. DFSCs, like SCAP, are derived from developing tissue and are featured with high plasticity, stemness, and multipotency. They can give rise to osteoblasts, chondrocytes, adipocytes, cementoblasts, and neurons in vitro [8 46]. Also, under proper culture conditions, DFPCs can differentiate into cementum [8]. Moreover, both in vivo and in vitro models verified their potential in PDL regeneration [47]. For instance, transplanted DFSCs could regenerate root-like tissue with pulp-dentin complex and PDL-cementum complex in the host alveolar socket in combination with dentin matrix and an HA scaffold [46 48].

1.1.1.5. GMSCs

On the other hand, gingival MSCs have their own positives apart from DFSCs, such as an easy isolation from the gingiva lamina propria layer (with minimum discomfort to patients) via gingivectomy and de-epithelialization during standard periodontal surgeries [49]. They highly

express pluripotency-related markers such as Oct-4, SSEA-4, and STRO-1 but with decreased expression of MSCs surface markers such as CD29, CD90 and CD105 [50 9 51]. Likewise, GMSCs have self-renewal capability. Their population doubling time is about thirty to fifty hours in vitro. Further, they are committed to osteoblastic, adipocytic, chondrocytic, endothelial, and neural directions [51 52 9]. Various in vivo transplantation experiments in connection to these discoveries have been performed for skin wound healing, tendon and periodontal regeneration including alveolar bone, cementum and PDL [49].

1.1.1.6. Mouse Incisor MSCs

The above DSCs are isolated from human dental tissues and are mostly defined based on in vitro cellular properties. However, the response of MSCs in vivo to physiological and pathological conditions is more meaningful in terms of clinical application. The mouse incisor provides an excellent model for dental MSC study. It grows continuously throughout life, implying DSCs are highly active and respond quickly to inner and external stimulus [53].

Generally, MSCs in any tissue or organ are heterogeneous, consisting of various sub-populations with different molecular characteristics [54 55 56 57]. Through lineage tracing analysis on transgenic mice, Gli1 was identified as one of the in vivo markers for mouse incisor MSCs. Gli1+ MSCs are located in the apical region surrounding the neurovascular bundle (NVB) [58 59]. They actively proliferate following injury, while also giving rise to undifferentiated dental mesenchyme and odontoblasts. Correspondingly, Gli1+ mouse incisor MSCs are typically negative for CD44, CD146, CD105, CD73, NG2, or Sca1 in vivo; while under ex vivo culture, Gli1+ MSCs meet minimal criteria for expressing classic MSCs surface markers. Any subsequent population is under the regulation of sonic hedgehog (SHH), secreted by the sensory

nerves within the incisor mesenchyme. The blockage of the Hedgehog signaling pathway via denervation leads to dentin differentiation defects [59].

Furthermore, NG2+ cells have been found surrounding all of the arteries inside the incisor [54]. Lineage tracing results demonstrate that NG2+ pericytes represent a small portion of incisor MSCs or secondary progenitor cells because they can differentiate into odontoblasts during incisor growth and contribute to reparative dentin formation upon injury [54].

In addition, flow cytometry indicates that CD90/Thy1+ cells accounted for 30% of incisor MSCs. Under tissue homeostasis, CD90/Thy1+ MSCs tend to be quiescent. Upon mechanical injury, they activate rapidly to re-establish incisor length[60].

1.1.1.7. PDLMSCs

While the other aforementioned types of MSCs are important, PDLMSCs are especially promising due to their regenerative potential in animals and around titanium implants. The first group of PDLMSCs was isolated from extracted human 3rd molar PDL in 2004 [4] [5]. PDLMSCs show high levels of STRO-1, CD44, CD90, CD105, and CD146 expression during in vitro culture. They can form colonies on culture dishes and undergo multi-potential differentiation into osteoblasts, chondrocytes, adipocytes, neurons, and even hepatocytes [61]. Actually, when transplanted into immunocompromised mice, these cells can re-establish PDL tissue [47]. Also, in clinical trials, researchers have employed these cells to avoid dento-alveolar ankylosis or replacement resorption in delayed avulsed teeth transplantation [62]. Accordingly, extensive research is ongoing to explore PDLMSC potential in periodontal disease treatments. Even to the present, transplanted PDLMSCs exhibit excellent periodontium regenerating capacity in mice, rats, dogs and mini-pigs [63] [64] [65]. In addition, some researchers have now started to apply autologous PDLMSCs in clinical trials to establish PDL attachment around titanium implants

plus treat intrabony and peri-implant defects [66] [67]. Improved clinical outcomes and defect reconstruction hold great potential for PDLSCs as an exciting source for periodontal tissue repair.

The first related study for PDLMSC in vivo identification was done by Roguljic et al in 2013 [68]. In this paper, they concluded that αSMA+ cells could serve as periodontal progenitor cells giving rise to cementocytes and osteoblasts [68]. Wnt-responsive Axin2+ cells have been found to be a quiescent population within PDL proper, but turn proliferative upon tooth extraction. This population migrates from the PDL remnant to the tooth extraction socket center and differentiate into osteoblasts and osteocytes [69]. Recently, PTHrP+ cells have gained notice by being involved in mice molar root development by giving rise to PDL and alveolar bone [70]. But αSMA+ cells' labeling efficiency was fairly low even seven weeks after lineage tracing-only a small portion of periodontium was derived from them. Axin2+ cells' expression is not specific. They were multipotential and widely expressed in adult mouse molars including osteoblasts, odontoblasts, PDL cells and so on. In fact, PTHrP+ cells contribution to adult periodontal tissue turnover is minor. Hence, all three of these in vivo markers for periodontal MSCs are not ideal. In this project, we aim to identify a reliable in vivo marker for adult molar periodontium MSCs which can precisely give rise to the whole periodontium in adult mouse molars effectively and efficiently.

1.1.2. Craniofacial SuMSCs

Most of the craniofacial bones share the same developmental origin with dental mesenchymal tissues—the cranial neural crest. Namely, craniofacial sutures are the major osteogenic sites during postnatal development. Gli1+ cells are found to be the suture MSCs (SuMSCs) supporting craniofacial bone physiological turnover and injury repair [71]. Gli1+ cells do not express CD44, CD73, or CD146 in vivo but do express all of the typical MSC markers in

vitro and undergo tri-lineage differentiation. The specific ablation of Gli1+ cells caused craniosynostosis and severe osteoporosis. Further, Indian Hedgehog (IHH) from the osteogenic front regulates Gli1+ SuMSC. Blockage of the IHH signaling pathway leads to severe osteoporosis but no craniosynostosis, suggesting its regulation is limited to MSCs lineage commitment activity instead of maintenance [71]. Further research indicates that bone morphogenetic protein (BMP)-IHH signaling synergistically balances Gli1+ SuMSCs mediated osteogenesis and osteoclastogenesis activity [72].

Axin2 is another marker for the SuMSC population. In particular, Axin2 knockout causes premature suture closure in mice [73]. Axin2+ cells have long-term self-renewal, clonal expanding, and differentiation abilities during calvarial development and homeostatic maintenance. These cells specifically reside in the suture midline, co-localized with slow-cycling cells. They are also highly responsive to calvaria injury. Lineage tracing analysis shows that Axin2+ cells constitute 46% of cells residing in the skeletogenic mesenchyme and that number increases to 98% during damage-induced repair [74]. All of the aforementioned activity can be impacted by the MSCs niche.

1.2. Wnt Signaling Regulation in the MSCs Niche

The stem cell niche is the microenvironment where stem cells reside, containing various critical regulating factors. Crosstalk between various niche signals keeps stem cells in a dynamic balance [75] [76]. Niche components include the perivascular nerve, endothelial cells, special megakaryocytes (which secrete various bioactive proteins such as SHH [59], SCF [77], CXCL12, 4 [78]), and TGFß [79] to participate in MSC maintenance, quiescence, activation, lineage commitment activity, and so on. In fact, when niche components are ablated, stem cells fail to respond to tissue regeneration cues [80], underscoring the significance of the niche in dictating stem cell behavior [81]. Additionally, tissue regeneration-based studies report that the majority of engrafted

MSCs die within days and the remaining small percentage is not enough to replace lost tissue [82]. Therefore, the low survival percentage of transplanted MSCs could be ascribed to the niche loss during transplantation.

Further, several lines of evidence suggest that a critical player in regulating the MSCs niche is a group of proteins encoded by the Wnt gene family which was previously known for influencing various stages of embryonic development and cell fate determination [83] [84]. In adults, Wnt has been proven to be important for MSC bioactivity in various types of mesenchyme tissues such as the maintenance of hair follicle MSCs [85], preservation of Lgr5+ intestinal stem cell proliferation and pluripotency, liver homeostasis [86], respiratory epithelial MSC renewal, and differentiation [87, 88] (which includes osteogenic differentiation of bone marrow MSCs [89]). Besides these processes, there are many other factors which are influenced by Wnt.

1.2.1. Wnt Signaling Pathway

The Wnt protein family was first found in 1976 due to the fact that one gene mutation resulted in *Drosophila melanogaster* wing loss [90]. Moreover, throughout the past decades, researchers consistently found that the Wnt signaling cascade was important for embryonic development and tissue homeostasis in adulthood through regulating various cellular activities covering proliferation, survival, apoptosis, angiogenesis, and cell polarity [91] [92]. Thanks to extensive studies on Wnt signaling, two classical pathways have been well-established, including canonical and non-canonical pathways based on the difference of downstream responsive elements to Wnt ligands. Specifically, the canonical pathway is mediated by ß-catenin, playing indispensable roles in governing MSC activity. Until now, three non-canonical signaling pathways have been characterized: the planar cell polarity pathway (Wnt-PCP pathway) through Rac1 and RhoA, a Wnt/calcium pathway involving protein kinase C (PKC) and c-Jun N-terminal

kinases (JNK), and the Wnt5a/frizzled (FZD) pathway regulating tumor metastasis via proto-oncogene tyrosine-protein kinase (FYN). Nevertheless, the Wnt signaling system is complicated by the presence of different subtypes including LRPs, WNTs, FZDs, regulatory inhibitors, interaction between canonical and non-canonical pathways, and crosstalk with other signaling pathways. Throughout the abundant varieties of Wnt, there are many signaling steps involved, which will be further explained in the following sections.

1.2.1.1. Canonical Wnt Signaling

The ß-catenin dependent canonical Wnt pathway appears to be evolutionarily conserved in both vertebrates and invertebrates and plays a dual role in adherent junctions and transcriptional regulation [93 94 95]. The receptors in Wnt signaling pathways include a single-pass transmembrane co-receptor LRP 5/6 and seven-transmembrane signaling receptor FZD. The key element is a destruction complex consisting of scaffold protein Axin, adenomatous polyposis coli (APC), and casein kinase1 (CK1). Without Wnt ligands, the destruction complex in the cytoplasm is activated to phosphorylate downstream ß-catenin. APC binds ß-catenin and CK1 primes the protein for subsequent phosphorylation mediated by recruited glycogen synthase kinase 3 (GSK3) at threonine and serine residues. The phosphorylated ß-catenin is then degenerated by E3 ubiquitin ligase and transferred to proteasomes (Fig. 1B). With Wnt ligands bonded, disheveled (Dvl) protein is recruited by Fzd. Consequently, phosphorylated Dvl inhibits GSK3 through phosphorylation. Thus, ß-catenin is protected from GSK3-dependent phosphorylation. Unphosphorylated ß-catenin is then translocated into the nucleus where it displaces the co-repressor Groucho from the transcriptional factor Groucho/ T cell factor/lymphoid-enhancing factor (TCF/LEF) complex, thereby triggering the transcription of Wnt target genes which mediates MSCs' bioactivity [96 97 98] (Fig. 1A).

1.2.1.2. Non-Canonical Wnt Signaling

Non-Canonical Wnt pathway research is ongoing. So far, two distinct pathways have been well-identified with different impacts on cell activities. One is the Wnt-PCP, pathway, which begins from Wnt binding to Fzd, either through a tyrosine kinase-like orphan receptor 2 (ROR2) or a receptor tyrosine kinase (RYK). Similarly, Dvl is recruited and activated. The following cascade is mediated by the associated disheveled activator of morphogenesis 1 (DAMM1) or Dvl associated small signaling G-protein Rac1. DAMM1 activates the small G-protein Rho through a guanine exchange factor [49]. Consequently, the downstream Rho-associated protein kinase is activated by a regulating cytoskeleton [99]. Alternatively, Rac1 can activate transcription factors via c-Jun amino-terminal kinase (JNK) activation, which is involved in cytoskeleton modification as well as targeting gene expression regulating cell survival, movement, and polarity [100] [101] (Fig. 1C).

Secondly, the Wnt-calcium pathway is involved in cell movement and cell adhesion regulation. For instance, phosphorylated Dvl triggers phospholipase C (PLC) activation and the formation of inositol triphosphate (IP3) and diacylglycerol [102] from the cell membrane component phosphatidylinositol-4,5-bisphosphate (PIP2). First, IP3 binds to its receptor on the endoplasmic reticulum (ER) membrane, resulting in the release of intracellular calcium [98] [100] [101]. Calcium movement in cytoplasm then activates calcium-/calmodulin-dependent protein kinase II (CaMKII), which causes nuclear import attributed to an activated T cell family of transcription factors (NFAT) via mitogen-activated protein kinases (MAPKs) phsphyorylation [103]. Meanwhile, DAG activates PKC and MAPKs which are all targeted at NFAT inside the nucleus to govern cell movement and adhesion. In addition, the non-canonical Wnt-calcium pathway has been reported to inhibit the canonical Wnt/b-catenin pathway, because CaMKII could trigger TGF-b

activated kinase 1 (TAK1) phosphorylation. This action in turn enhances the activity of the nemo-like kinase (NLK), leading to lymphoid enhancer-binding factor 1 (LEF1) ß-catenin/DNA dissociation [104] (Fig. 1D). Recently, another special non-canonical pathway was been discovered to facilitate epithelial-mesenchymal transition in cancer [105]. Upon Wnt5a ligand binding, Fzd2 exclusively recruits and phosphorylates Dvl. The following activation and nuclear transportation pertaining to signal transducer and activator of transcription 3 (STAT3) by FYN triggers cell migration-related target gene expression. Consequently, abnormal cell migration occurs, which underlies EMT and tumor cell invasion responsible for tumor metastasis (Fig. 1E).

1.2.2. The Function of Wnt Signaling in Regulating MSCs Activity

While non-canonical signaling is connected to cancerous activity, canonical Wnt signaling is known to be one of the most critical stem cell niche regulating pathways for tissues such as the hair follicle, intestinal epithelium, respiratory epithelia and epidermis [106] [107] [108] [109]. For example, Wnt signaling is significant in the maintenance of hair follicle MSC (HF-MSC) undifferentiated status. Furthermore, Axin2 is the reporter protein of the canonical Wnt pathway found constantly expressed in the outer bulge of HF-MSC niche. Without Wnt, HF-MSCs lose their stemness and exit the quiescent phase to contribute to hair growth in the inner bulge, where most of the differentiated cells are located and Wnt inhibitor-Dickkopf3 (Dkk3) is localized [85]. Short-range canonical Wnt signaling has been proven to be important for the preservation of Lgr5+ intestine stem cells via Wnts secreted by Paneth cells or Gli1+ cells [110, 111] [86]. Moreover, genetic disruption of the pathway's ultimate effectors TCF4 [112] [113] or β-catenin (Ctnnb1) [114] are associated with the demise of intestinal crypts. Similarly, Dkk1 collapses intestinal architecture deriving from the counteraction to the Wnt cascade [115] [116]. Likewise, overactivation of the Wnt pathway increases intestinal stem cell numbers after the administration of Wnt agonist R-

spondin-1(RSPO1) [105]. Furthermore, recent investigation indicates that the Wnt targeted gene c-Myc directly represses cell cycle inhibitor cyclin-dependent kinase inhibitor 1 (p21Cip1/Waf1), and thus facilitates mesenchymal stem cell proliferation [117]. Expectedly, c-Myc ablation results in the exhaustion of intestinal progenitor cells as the result of G1 arrest and concomitant differentiation [118]. Moreover, Wnt/ß-catenin signaling is necessary for activation and proliferation of Axin2+ interfollicular epidermal (IFE) progenitor cells [119]. These Axin2-expressing cells produce Wnt signals as well as long-range secreted Wnt inhibitors, suggesting an autocrine regulatory mechanism for stem cell self-renewal [119]. Correspondingly, SuMSCs express Axin2 and are characteristic of long-term self-renewal and clonal expansion during calvarial development and homeostatic maintenance [74]. Not long ago,, an exogenous Wnt 3a protein delivered in the form of liposomes was found to accelerate craniofacial tissue healing [120] [98], which suggests a potential therapeutic strategy to promote MSC-based tissue regeneration via high levels of the Wnt signaling pathway [121]. In the liver, Wnt proteins secreted by central vein endothelium are found to regulate adjacent Axin2+ cells for self-renewal g and liver homeostasis [57]. Similarly, Axin2+ -Wnt responsive cells are proven to contribute to lung epithelial self-renewal and differentiation [87]. Numerous studies underscore the importance of Wnt signaling as a powerful stem cell factor that controls stemness, self-renewal, and proliferation of multiple adult stem cell populations [122]. What's more, the Wnt signaling pathway exerts non-identical impacts on MSCs tri-lineage differentiation [81].

1.2.2.1. Wnt and MSCs Adipogenic Differentiation

The Wnt signaling pathway inhibits MSCs adipogenic differentiation. It has been demonstrated that Wnt antagonists secreted frizzled-related protein 4 (sFRP4), and their associated Dkk1 expression level is higher in adipogenic differentiated MSCs than

undifferentiated MSCs [123]. One example of this concept is that a short 48 hour treatment with sFRP1 and sFRP4 on human MSCs was seen to upregulate adiponectin secretion [124] [98]. In clinics, a few researchers attempted to test out the relationship between Wnt activity, obesity, and diabetes. The sFRP4 level was concluded to be positively related to impaired glucose and triglyceride metabolism. Some researchers even use sFRP4 as a predictor of type II diabetes mellitus [125]. Conversely, a previous study showed that GSK-3ß inhibitor-6-bromo-indirubin-3'-oxime (BIO) could inhibit MSC adipogenesis as a result of enhanced Wnt signaling [126]. In brief, all of this evidence depicts inhibitory regulation of Wnt on MSCs differentiation into adipocytes, implying the possibility to treat obesity with Wnt activators. However, this claim remains under extensive investigation.

1.2.2.2. Wnt and MSC Chondrogenic Differentiation

Generally speaking, there are many controversies on the functions of Wnt pathways in MSC chondrogenesis, which may come from complicated interactions within the Wnt signaling network. On one hand, enhanced chondrogenesis activity on sFRP1-deficient mice highlights the positive effect of Wnt signaling on MSCs' chondrogenic differentiation [127]. Activation of non-canonical Wnt after Wnt5a ligand binding was also seen to induce the chondrogenesis of MSCs derived from the chicken wing bud [128]. An in vitro study showed that overexpression of Wnt3a was associated with the chondrogenic differentiation of C3H10T1/2 murine mesenchymal cells [129]. Increase of pre-cartilage condensation in ex vivo MSCs cultured in the presence of Wnt5a protein further confirmed Wnt signaling's supporting effect on MSCs chondrogenesis [128]. Indeed, the related underlying mechanism of the procedure indicates Wnt5a activates non-canonical Wnt pathways but blunts the canonical one. On the other hand, one study reported reduced expression of chondrogenic-specific markers such as collagen II, Sox9, and aggrecan after continuous

treatment with Wnt1 protein for twenty-one days, while treatment with the Wnt antagonist Dkk1 increased their expression in human adipose-derived MSCs [130]. To make the matter even more complicated, many in vitro studies consistently emphasize the importance of suppressed Wnt signaling during chondrogenesis. For example, sFRP1 and Dkk1 could help with human MSC chondrogenesis at the initial stage indicated by enhanced glycosaminoglycan synthesis, Sox9, and type II collagen expression [131]. These Wnt antagonists also exhibit a chondrogenesis-promoting effect in long-term pellet cultures [132]. Most of these conclusions are based on an in vitro study where the concentration of Wnt pathway regulators and the absence of other interacting pathways may be the reason behind the controversy.

1.2.2.3. Wnt and MSC Osteogenic Differentiation

Beyond the other functions above, it has been well-established that the Wnt signaling pathway is indispensable for MSC osteogenesis. The canonical Wnt signaling pathway activates differentiation of MSCs into osteoblasts [133]. In addition, the disruption of Wnt signaling by targeted destruction of LRP5 in mice has been shown to promote osteoporosis and low bone mass phenotype [134], while its overexpression leads to a high bone mass syndrome [135]. The Wnt/ ß-catenin signaling works as a "switch" favoring MSC osteogenesis at the expense of adipogenesis by modulating the availability of cell-type-specific transcription factors [136]. Recently, Src homology region 2 domain-containing phosphatase-1(SHP1) was found to bind to GSK3, suppressing its kinase activity. Hence, SHP1 deficient mice (mev/mev) developed osteoporosis as a result of increased ß-catenin degradation by phosphorylated GSK3. Cultured bone marrow MSCs extracted from the mutant mice also displayed less osteogenesis and more adipogenesis [89]. Further, Wnt antagonism has been reported to inhibit osteogenesis as expected. For instance, sFRP4 is reported to inhibit periodontal MSCs commitment to osteogenic

progenitor cells [137]. Additionally, sFRP1 overexpression is found to inhibit in vivo bone formation [138] and deteriorate osteoblast and osteocyte apoptosis [139]. Conversely, a lack of sFRP1 reduces apoptosis, accelerates MSC osteogenic differentiation, enhances trabecular bone formation, and improves fracture healing [140], confirming the inhibitory effect of Wnt antagonists on osteogenesis. Besides, sFRP3 represses the non-canonical Wnt pathway through binding to Wnt5a, which in turn blocks Wnt5a's inhibitory effect on the canonical pathway, promoting osteogenesis [137]. This fact further proves the positive regulation of the canonical Wnt pathway in MSCs osteogenic differentiation. Thus, the extensive crosstalk contributed by the Wnt signaling network during osteogenic differentiation can be considered when devising possible new therapeutic approaches for bone-related diseases.

1.3. Wnt Pathway Regulation on MSCs During Tissue Infection

MSCs have a niche homeostasis, which is influenced by inner and external microenvironments including pathogens, DNA damage, and metabolic stress. During homeostasis, the concerted action of local positive and negative regulatory niche signals helps keep adult MSCs in dynamic balance. However, if one stimulus goes beyond control, stem cells cannot maintain their normal function. For instance, microbiota are the external regulators which play a critical role in MSCs health. Furthermore, the absence of MHCII and a low expression level of class I endow MSCs with a low immunogenic properties, (which is also the basis of MSC tissue regeneration medicine [7]**)**, whereas tissue injury and the following healing process are accompanied by mild inflammation or even infection. Unexpected or prolonged infection always leads to tissue repair failure, suggesting implanted MSCs may be susceptible to the recipient`s immune system [137]. Thus, irreversible tissue loss under serious tissue infection conditions defines the inhibitory effect of infection-related signals on MSCs. In addition, MSCs seeded tissue

engineering shows low success rates in various tissues when injury sites are under severe infection despite the immunomodulatory properties.

To clarify, coordinated and precise cross-talk between microorganic endotoxins, inflammatory cells, cytokines, regulatory signaling cascades, and MSCs is critical for the success of tissue regeneration during the damage repair process [141]. Loss of harmony is associated with arrested MSC activity, which subsequently leads to wound healing defects, inflammatory disorders, and even malignant transformation [142]. In particular, the regenerative capacities of endogenous or transplanted stem cells are significantly modified by the immune microenvironment at the injury sites [143] [144] [145]. For example, it has been shown that recipient T cells negatively regulate autologous MSC mediated bone formation in mice and the NF-kB major transcription factor in both innate and adaptive immune response represses bone formation in rats [146]. Likewise, lung tumor cell-derived exosomes could educate naïve MSCs into pro-inflammatory MSCs (P-MSCs) by activating TLR2/IL1/MyD88 signaling through HSP70 [147]. Besides, radiation-induced injury produced damaged RNA strands, causing the death of crypt stem cells through TLR3 signaling [145]. Hence, an in-depth understanding of patterns and how the infectious niche governs MSCs behavior could provide insight into therapeutic avenues for restoring damaged tissues efficiently and effectively [143] [144].

Despite the fact that more information is necessary on some parts of MSCs, the mechanisms of tissue infection have been well studied, thanks to the continuous efforts of immunology researchers. Their work includes the recognition of typical pathogens, molecules, immune cell recruitment, inflammatory cytokines secretion, and molecular pathway interaction with local tissue cells such as MSCs. First, there are five classes of germline-encoded host-pathogen sensors which are collectively termed pattern recognition receptor (PRRs). These

elements can recognize the specific molecules on microorganisms, which are named pathogen-associated molecular patterns (PAMPs). However, PRRs include: (1) toll-like receptors (TLRs), which are transmembrane proteins located mainly at the cell surface (or in some cases, in endosomes), nucleotide-binding oligomerization domain-like receptors (NLRs) defined as intracellular sensors inside the cytoplasm, and (3) retinoic acid-inducible gene-I-like Receptors (RLRs) that are intracellularly located and are primarily involved in antiviral responses. PRRs also encompass: (4) C-type lectin receptors (CLRs), known as a carbohydrate-binding transmembrane receptor functioning in immune response to pathogens and apoptosis and (5) absence in melanoma 2 (AIM2)-like receptors specifically characterized by a pyrin domain and a DNA-binding HIN domain detecting intracellular microbial DNA. Each PRR triggers inflammatory pathways to fight against microorganisms in various forms, among which TLRs and NLRs are two key components in the innate immune response.

Some researchers hold the opinion that MSCs age rapidly under long term infection. Consequently, those aged stem cells are reported with a down-regulated Wnt pathway, which implies the inhibitory regulation of infection on stem cells through the Wnt pathway [148]. In fact, the TLR inflammatory pathway [149], inflammatory macrophages [150] and ROS [151] are reported to age or deplete the MSC population via Wnt signaling down-regulation. Moreover, some previous studies have indicated that the relationship between inflammatory signaling pathways and Wnt pathways may participate in the regulation of the immune system on MSCs. For example, tissue repair macrophages activate stem cells via Wnt pathway upregulation through secreting Wnt7b, Wnt10a, and progenitor cells through Wnt3a [150].

1.3.1. The Regulation of MSCs Through Crosstalk Between TLR and Wnt Signaling

1.3.1.1. TLR pathways

TLRs are dominantly expressed on the membranes of leukocytes including dendritic cells, macrophages, natural killer cells, along with T and B lymphocytes. Until now, thirteen members of the TLR family have been identified, of which TLR1, TLR2, TLR4, TLR5, TLR6, and TLR11 are expressed on the cell surface and TLR3, TLR7, TLR8, and TLR9 localize to the endosomal/lysosomal compartment. Notably,TLR12 and TLR13 are not found in humans [152]. In spite of this variation, each TLR binds and becomes activated by different ligands. For example, LPS exclusively binds to TLR4 but TLR4 can be activated by many other pathogens. Further, TLR3 can be activated by PolyI:C- a mismatched double-stranded RNA in viral infection [153]. Additionally, lipoteichoic acid [154], the immune-stimulant of Gram-positive bacteria, is recognized by TLR2. The downstream responsive adaptors are also different. Overall, TLR inflammatory pathways act via two major signaling cascades: a myeloid-differentiation primary-response protein 88 (MyD88)-dependent pathway and a MyD88 independent pathway which acts via type I interferons [155]. The dominant MyD88-dependent pathway originates from the cytoplasmic Toll/Interleukin-1 receptor (TIR) domain. Upon stimulation with extracellular PAMPs, MyD88 attaches to TLRs via the TIR domain and recruits IL-1 receptor-associated kinase-4 (IRAK-4) to TLRs. Then, the IRAK1/2/4 complex is connected to TNF receptor-associated factor 6 (TRAF6) after phosphorylation, and goes on to activate transforming growth factor beta-activated kinase 1 (TAK1). This procedure leads to IκB kinase complex activation [156]. Next, the downstream IκB kinase phosphorylates the inhibitory IκBα protein [157]. This phosphorylation dissociates IκBα from NF-κB. The free NF- κB is able to migrate into the nucleus to activate target genes responsible for pro-inflammatory cytokines transcription, such as

pro-IL-1 ß or pro-IL-18. Enhancement of the same target genes' transcription can also be mediated by activated mitogen-activated protein kinases kinase (MKKs) to phosphorylate mitogen-activated protein kinase (MAPKs), including c-Jun N-terminal kinase (JNK), extracellular signal-regulated kinases (ERK), and p38 [158]. Lastly, another related issue is that activation of MyD88-independent pathways occurs via TIR-domain-containing adapter-inducing interferon-β (TRIF) and TRAF3 when MyD88 is deficient. This action induces recruitment of IKKε/TBK1, phosphorylation of interferon regulatory factor 3 (IRF3), and expression of interferon-β (Fig. 2B). So far, the majority of TLR related inflammation is mediated by the MyD88-dependent pathway, whereas PolyI:C-TLR3 antiviral innate immunity is found independent on MyD88 [159] as described in Fig. 2A.

1.3.1.2. The Impact of TLR Signaling on MSCs and Interaction With the Wnt Pathway

Foremost, TLR and IL-1R ligands are highly expressed in tissue injury and wound repair sites [160]. TLR signaling substantially impacts the repair process [161]. Many in vitro studies have proven that MSCs express a number of TLRs. So far, consistent results have demonstrated expression of TLR 1, 2, 3, 4, 5, and 6 in adipose-MSCs and bone marrow-MSCs from both humans and mice at mRNA and protein levels, while inconsistent results have been reported on the expression of TLR 7 to 10 [162]. Besides, TLR/Myd88/ILR1 signaling inhibits BM-MSCs colony formation, proliferation, migration, and osteoblastic differentiation after activation by IL-1b. Interestingly, BM-MSCs are more vulnerable to inhibitory effects of TLR/Myd88/ILR1 signaling than osteoblasts [163]. For instance, Pevsner-Fischer et al. found that TLR2 activation reduced mouse BM-MSC differentiation into the three mesodermal lineages [164]. Likewise, the activation of the TLR4 or 2 pathway in a pro-inflammatory environment negatively regulates human AD-MSCs differentiation to adipocytes [165] [166]. However, the effect of TLR pathways on

MSCs lineage commitment potential varies depending on different culture conditions, tissue origins, and species [164]. Unfortunately, the most available evidence about the relationship between TLR pathways and MSCs is based on in vitro studies. MSC behavior in vivo in an inflammatory environment may be different. A good example of this scenario is the fact that in BMMSCs based calvaria regeneration, delivering Myd88-/- MSCs induced better regeneration compared to wild-type MSCs, while in vitro culture of Myd88-/- and wild-type MSCs showed equal ability to differentiate and proliferate [163].

To complicate this matter further, it is well-known that the oral cavity is subjected to daily assault from external microbiota, which may result in periodontitis. In periodontitis, LPS could cause periodontal tissue degeneration in a dosage-time-dependent fashion [167], which indicates the failure of periodontal MSCs to support physiological turnover and pathological wound repair. Although, modulation of Wnt/b-catenin signaling helps attenuate periapical bone lesions [168]. An in vitro study by Wang et al. demonstrated that LPS activated p38-MAPK and inhibited the canonical Wnt/b-catenin signaling pathway with an increased level of p38, c-Myc, cyclin D1 mRNA, and phosphorylated GSK-3b [169]. In the wound repair process, PGE2 is released from neighboring apoptotic cells that activate the Wnt/b-catenin pathway in MSCs via Wnt3. Researchers also discovered LPS enhanced Wnt5a expression through the TLR4/MyD88/phosphatidylinositol 3-OH Kinase/AKT/NF-kB/MAPK pathway, based on an in vitro study of human dental pulp stem cells [170] [171] and osteoblasts [172]. However, there is a paradox about the Pg-LPS influence on dental MSCs' function and the mediating pathways. It has been shown that Pg-LPS modified periodontal ligament stem cells' lineage commitment in inhibiting osteogenesis and stimulating fibrosis via the ERK1 2 signaling pathway [173]. Also, Pg-LPS inhibited osteogenic differentiation of BMMSCs [173]. However, LPS upregulated gingival

MSCs to proliferate without attenuation of their regenerative capacity and this positive effect is mediated through NF-kB but not the Wnt/b-catenin pathway. These results indicate that the effect of TLR pathways on MSCs lineage commitment potential varies depending on different culture conditions, tissue origins, and species [164].

The digestive system is another non-sterile environment exposed to microorganisms where infectious bowel diseases are quite common. Under infectious circumstances, intestinal MSCs can differentiate into inflammatory cells and secrete inflammatory cytokines such as IL-1b, IL-8, and TNF-a [174]. When treating intestinal MSCs with LPS, flow cytometry analysis showed that conditioned MSCs were arrested at the G1 phase, and cell pyroptosis was severe. Moreover, researchers have determined that LPS inhibits Wnt signaling by activating GSK3β, which then leads to a dramatic inhibition in enterocyte proliferation both in vitro and in vivo [175]. This particular phenomenon links the LPS/TLR4 pathway with Wnt signaling in terms of intestinal MSCs bioactivity regulation. What's more, Liu et al. found that AvrA, a bacterial effector protein present in certain intestinal microorganisms of Salmonella and E. coli, specifically upregulated the expression of Wnt genes and phosphorylation of β-catenin, leading to a marked increase in crypt proliferation [176].

All the above findings imply the influence of TLR inflammatory pathways on the regulatory Wnt pathway to MSCs. Undoubtedly, the molecular mechanism is partially uncovered and TLRs can modulate Wnt activity at different points with various terminal effects. First, TLRs can modulate b-catenin degradation through binding to LRP5/6 FzD receptor complex, promoting the function of the β-catenin destruction complex and subsequently blocking Wnt target gene expression. This behavior helps explain the fact that transient Wnt3a could counteract the inhibitory effect of Pg-LPS. Secondly, phosphorylation of TAK1 in TLRs signaling attributes

to NLK activation, which negatively relates to the canonical Wnt pathway downstream TCF/LEF transcription [177]. In contrast, TLRs can lead to the activation of AKT via interaction with P13K and IKK, thus inhibiting GSK3b, enhancing b-catenin expression and upregulating TCF/LEF transcription. TLR4/Myd88/LRRFIP2 has also been revealed as an activator of Wnt because it interacts with Dvl to activate catenin/LEF/TCF-dependent transcriptional activity [149].

1.3.2. The Regulation of MSCs Through Crosstalk Between NLRs and Wnt Signaling

1.3.2.1. NLRs Pathways

In addition to TLRs, vertebrates have evolved strategies to sense pathogens in cytosol [178]. Their bodies have NLRs- intracellular receptors which play key roles in innate immune system regulation by sensing PAMPs together with cell stress related damage associated molecular patterns (DAMPs) [152], entering the cell via phagocytosis or pores. NLRs are composed of three major domains- central NACHT (NOD- nucleotide-binding domain), C-terminal leucine-rich repeat (LRR) and the variable N-terminal interaction domain [160]. LRR recognizes ligands, while the central NACHT domain mediates ATP-dependent self-oligomerization. Furthermore, the N-terminal domain triggers homotypic protein interaction, which consists of a caspase recruitment domain (CARD) (on NLRC subfamily), pyrin domain (PYD) (NLRP), acidic transactivating domain (NLRA) or baculovirus inhibitor repeats (BIRs) (NLRB) [179].

NLRs mediate programmed cell death in an infectious condition by pyroptosis via inflammasome. This manifestation includes pyknosis, chromatin condensation, a DNA break, plasma membrane permeabilization, and cellular swelling [180]. After TLRs associated "priming" and "activating", NLR ligand uptake triggers inflammasome assembly and IL-1, IL-18 maturation. NLRs then directly bind to apoptosis associated speck-like protein (ASC), via its PYD domain, and the ASC binds to procaspase-1 via its CARD domain [181]. NLR signaling

driven pyroptosis can be achieved through the canonical or noncanonical inflammasome pathway. In the canonical inflammasome pathway, the combination of NLRs/ASC with pro inflammasome 1 transforms it into a functional caspase-1 and then composes into a multiprotein oligomer complex. Afterwards, the activated caspase-1 induces IL-1ß and IL-18 secretion from pro-IL-1ß and pro-IL-18. As a consequence, inflammatory immune cells are attracted, such as pro-inflammatory cytokines TNF-α and IL-6, including chemokines like IL-8, CXCL8, monocyte chemoattractant protein 1 (MCP-1) and an adhesion molecule are released. What's more, a K+ selective hemichannel on the inflammatory cell surface is open upon ATP binding. Subsequent K+ efflux causes pore formation on the cell membrane via pannexin-1 and extracellular pathogen. Influx then further deteriorates pyroptosis. Accordingly, the non-canonical pathway works synergistically with the canonical pathway. Released IL-1ß and IL-18 and proteolytic cleavage of Gasdermin-D into Gasdermin-N domain by caspase-4,5,11 then either directly activate caspase-1 or indirectly activate the canonical inflammasome/NLR pathway to induce pyroptosis [182] [183].

1.3.2.2. The Impact of NLR Signaling on MSCs and Interaction with the Wnt Pathway

In vitro studies displayed that hUCB-MSCs expressed bioactive NOD1 and 2 genes. Correspondingly, the administration of NLR agonists led to IL-8 production. Activated NLR pathways also enhance hUCB-MSC osteogenesis, chondrogenesis, and inhibit adipogenic differentiation, but have no remarkable effects on MSC proliferation [184]. Controversially, another in vitro BM-MSC culture study demonstrate increased adipogenesis and decreased osteogenesis of MSCs in the presence of NLRP3 inflammasome, which may due to the difference in tissue origins. Likewise, the inhibition of caspase-1 offered a novel therapeutic target for aging-related chronic inflammatory diseases like osteoporosis [185]. Though many disputations exist, the above

facts suggest pivotal roles of NLR pathways in MSC regulation. However, literature discussing the impact of NLR pathways on Wnt signaling is limited. The available evidence depicts that NLR pathways could negatively regulate Wnt pathways through a TAK/NLK cascade, while other researchers found NOD2 could upregulate Wnt in a non-canonical RIP2–TGFß–TAK1-independent manner [186]. As an alternative approach, NOD2 can stimulate and mediate the Wnt pathway through the Ly6/PLAUR domain-containing protein 6 (LYPD6), which synergizes the ligand-receptor combinations in the Wnt pathway [186].

1.3.3. Proinflammatory Cytokines and Their Impact on MSCs via the Wnt Pathway

While some varieties of MSCs have an established sensor system, it has been implied within various in vivo and in vitro studies that inflammatory cytokines secreted during tissue infection affect stem cells' bioactivity. In most cases, pro-inflammatory cytokines repress MSC behavior in various aspects. For instance, endogenous pro-inflammatory cytokine IL-1ß activates IL-1R/MyD88 signaling and thus impairs MSC proliferation, migration, and differentiation by inhibiting the Akt/GSK-3ß/ß-catenin pathway [163]. Similarly, a loss of function study proved that IL-1 ß initiated IL-1R/Myd88 signaling and depleted stem cells under in vitro culture conditions [187] [188]. In addition, IL-1ß was found to inhibit BMSCs osteogenesis by activating foxhead box D3 protein (FoxD3) mediated microRNA-496 expression [189]. Moreover, IFN-α works as a central mediator of adaptive immunity and its net effect under inflammation is to stimulate bone loss [190]. Likewise, a combination of IFN-γ and TNF-α can accelerate MSC apoptosis via internalization of FAS, with a reduction of the anti-apoptotic factors NF-κB, X-linked inhibitor of apoptosis protein (XIAP), and FLICE-like inhibitory protein (FLIP). TNF-α alone, however, induces MSC apoptosis in a dose-dependent manner. Meanwhile, administration of recombinant TNF-α inhibits MSC adipogenesis and osteoblastogenesis, therefore promoting bone resorption

[191] [192]. Accordingly, IFN-γ and TNF-α secreted from lymphocytes synergistically block MSC-based bone regeneration [146]. On the other hand, When treating bone marrow MSCs with IFN-γ alone or a combination of IFN-γ and TNF-α in vitro, we found that IFN-γ blocks osteogenic differentiation concomitant with SMAD Family Member 6 (SMAD6) up-regulation and inhibition of runt-related transcription factor 2 (RUNX2) [193]. Both IFNγ and TNFα promote the phosphorylation of the p38 MAPK, and this phosphorylation is associated with the downregulation of cyclooxygenase-2(COX2)/PGE2, which results in a gradual decrease in MSCs immunomodulatory ability [194].

1.3.4. ROS and Their impact on MSCs via the Wnt Pathway

Even if MSCs can detect infections, activation of the TLRs and the NLRs pathways triggers the production of a common byproduct: an antimicrobial reactive oxygen species called ROS [195]. ROS are short-lived oxygen-containing molecules in the form of free radicals including the superoxide anion (O2-), hydroxyl radical (OH), hydroxyl ion (OH-), or nitric oxide (NO). There are also nonradical varieties such as hydrogen peroxide (H_2O_2) [196]. Their production happens under different physiological and pathological circumstances aided by active enzymes [197]. Further, ROS is ubiquitously found in the extracellular space [198], plasma membrane [199] and intracellular compartments, including mitochondria [200], peroxisomes, ER [201] and cytosol [202], among which mitochondrial complexes I,III, and the corresponding NADPH oxidase isoform NOX4 are major sources of ROS production roles in MSCs regulatory niches [203]. However, many researchers now regard local hypoxia as the culprit for the failure of MSC based tissue regeneration and MSC aging [204] [205].

In addition, ROS is known to influence MSC survival in a concentration-dependent way. Generally speaking, the appropriate concentration of ROS is necessary and advantageous to

maintain cellular proliferation and survival but beyond that, too high ROS levels cause cellular damage and dysfunction after chemical reactions with RNA, DNA, proteins, and lipids [196] [206] [207]. Indeed, Eto et al. declared that AD-MSCs are extremely sensitive to oxygen concentrations so that only cells implanted less than 300mm from an oxygen source would survive and any others undergo apoptosis [208]. Meanwhile, extra ROS are attested to activate MAPK pathways and apoptotic proteins as well as suppress antiapoptotic pathways [208] [209].Then, antioxidants concordantly stimulate MSC proliferation [210].

In the larger context, ROS involvement in the regulation of MSCs differentiation is depicted by the dissimilarity in ROS level within differentiated and undifferentiated MSCs. During homeostasis, undifferentiated MSCs are supported more by glycolysis energy with higher levels of glycolytic enzymes and more lactate production. In contrast, MSC-differentiated osteoblasts rely more on oxidative mitochondrial metabolism [211]. In comparison to mature differentiated cells, MSCs exhibit relatively low levels of ROS but also low antioxidant activity, suggesting they are more sensitive to oxidative stress [212] [213] [214]. Actually, the impact of ROS on MSCs lineage differentiation varies depending on the dosage. In vivo and in vitro studies collectively suggest that excessive ROS could suppress osteogenesis but induce adipogenic differentiation [215]. Furthermore, highly defined levels of ROS activate MSC differentiation into chondrocytes [184], adipocytes [216], osteocytes [97] and neuronal cells [217] through enhanced activity of regulatory signaling pathways, including Wnt. Besides., an in vitro study has verified that the exogenous addition of H_2O_2 suppresses TCF-mediated transcription. Nonetheless, overexpression of ß-catenin and the application of antioxidants could rescue the inhibition. In addition, ROS increases with age, and aged MSCs are reported with a reduction of Wnt target genes such as Axin2 and Opg in thirty-one month old mice compared with four month old mice,

and thus diminishes osteogenesis [151]. Moreover, in vivo investigation revealed that irradiation injury could cause intestine tissue regeneration via activation of Wnt signaling achieved through the ROS-HIF-Wnt2b signaling axis [218]. One explanation of the mechanism behind this tissue change is that superoxide-generating NADPH oxidase (Nox) induces ROS production, which leads to the inactivation of nucleoredoxin (NRX) in the b-catenin destruction complex. This sequence activates the Wnt/b-catenin pathway [219]. Conversely, in the MSCs niche, binding of Wnt ligands to its receptor complexes triggers sequential activation of Src kinase, followed by Rac1 activation through Src-dependent tyrosine phosphorylation. Activated Rac1 then induces Nox1-derived ROS which, in turn, results in the oxidation of NRX. Afterwards, oxidative NRX detaches Dvl. Liberated Dvl subsequently suppresses the β-catenin destruction complex, resulting in stabilization of β-catenin and activation of Wnt signaling [219 220].

Therefore, as our literature review here indicates, the in vivo identification of periodontal MSCs and their niche is not precise, even to the present day. Also, their response to periodontal infectious diseases and the underlying mechanisms remain largely unclarified. Hence, these obstacles inspire this research project. Based on preliminary results, we hypothesize that Gli1+ MSCs are the dominant stem cell population within the periodontium and are regulated by canonical Wnt signaling pathway. Subject to periodontitis, Gli1+ MSCs are negatively regulated upon down-regulated Wnt cascades. In this project, we aim 1). to investigate if Gli1+ cells are the dominant and primitive MSCs for periodontium *in vivo*. 1a. To investigate if Gli1+ cells contribute to tissue turnover of the periodontium; 1b. To investigate if Gli1+ cells contribute to tissue homeostasis during periodontal tissue injury repair; 1c. To investigate if Gli1+ cells give rise to previously known MSCs marker positive cells; 2). To define the roles of canonical Wnt signaling within periodontium MSC niche. 2a. To determine canonical Wnt pathway blockage's

impact on the activation and apoptosis of Gli1+ MSCs. 2b. To determine the impact of canonical Wnt pathway over-activation on Gli1+ MSCs' activation; 3). To investigate the inhibitory regulation of Gli1+ MSCs under periodontitis. 3a. To investigate if periodontitis inhibits Gli1+ MSCs activation; 3b. To investigate if periodontitis inhibits Gli1+ MSCs maintenance; 3c. To investigate if periodontitis negatively regulates Gli1+ MSCs bio-activity through Wnt pathway.

Our findings will help solve some puzzles regarding the persistence of periodontitis, provide insights for effective and efficient periodontal tissue regeneration strategy.

2. GLI1+ CELLS ARE PERIODONTIUM MSCS IN ADULT MICE MOLARS

2.1. Introduction

Though MSCs have been thoroughly investigated in many other tissues, study of periodontal MSCs and their regulating niche is fairly limited [98]. During tooth development, PDL, alveolar bone and cementum all originate from cranial neural crest cells and undergo constant turnover which is supported by periodontal MSCs [221]. Specifically, the first group of verified periodontal stem cells was isolated from human molar PDL and cultivated in vitro [4]. Despite that discovery, the in vivo identification, localization, and regulatory niche are poorly understood. Hence, even when αSMA+ cells, Axin2+ cells, and PTHrP+ cells have been proven to be subpopulations of periodontal stem cells [68 69], they were determined with low labeling efficiency. The first goal of this project is to find a precise in vivo marker which could label dominant and primitive MSCs for periodontium and efficiently contribute to the majority of periodontium. Also, this marker may enable localization of a PDL niche for these cells and provide an efficient animal model for periodontal MSC in vivo study in the same way.

Furthermore, considering the similarities between MSCs and perivascular cells, MSCs were proposed to be located nearby pericytes in the perivascular niche within various tissues [222 223 224 225]. This knowledge helps to explain why MSCs are widely spread in the whole body [224]. In addition, MSCs within the perivascular niche either have close contact to endothelial cells (ECs), or reside in the adventitia matrix and do not contact ECs directly [226].

The periodontal ligament is a group of specialized connective tissue which links teeth and the highly vascularized alveolar bone. There are three principal sources of supportive blood vessels in this area, including apical vessels (in the apical region derived from vessels supporting dental pulp), perforating vessels (on the lateral side of teeth originating from lamina dura,

perforating the socket wall) and gingival vessels. Cervically, arterioles, venules, and the profuse capillary network within gingiva anastomose together, forming a complex blood vessel network. At the same time, the middle part of the PDL contains occluso-apically coursing arterioles and venules close to the alveolar wall, while the capillaries form vasculature loops at the regions close to the root surface. At the apical region, arterioles originate from vascular canals in the alveolar bone marrow and then course upwards, branching into an interconnected network of capillaries. These capillaries transform into hairpin loops pointing coronally. At the loop tip, capillaries enlarge in diameter and are irregular in shape. The capillaries then turn apically, running together into a vein. Moreover, venules coursing next to each other in the uniformly coronal-apical path show a palisade-like appearance. These blood vessels either leave the PDL through vascular canals or are confluent in the apex, forming a venous cap exiting through the apical foramen. Generally, the apical blood vessels are extremely dense compared to other parts of the tooth vascular complex with numerous confluent vessels. Accordingly, in the coronal 1/3 of the PDL, the complex vasculature system may be responsible for antimicrobial defense and rapid tissue turnover. Furthermore, in the middle 1/3 of the segment, vasculature supports the suspensory structures and the venous cap in the 1/3 of the apical region is presumed to cushion masticatory forces [227]. Accordingly, it has long been suggested that PDL stem cells/progenitors are located around blood vessels. For example, cultured PDLSCs were positive for pericyte markers, including CD146, NG2, and CD140b. When cultured with human umbilical cord endothelial cells, PDLSCs localized adjacent to endothelial cells just like pericytes [227]. However, the spatial relationship between PDLMSCs and blood vessels in vivo has not yet been identified.

Recently, Zhao et al. identified Gli1 as the marker of perivascular MSCs in mice incisors [59]. Later, more perivascular Gli1+ MSCs were localized in bone marrow, muscle, heart, lung,

liver, and kidney in vivo [228]. These Gli1+ cells form an extensive perivascular network and meet the minimal criteria of mesenchymal stem cells. Actually, to support stem cell homeostasis, SCF is primarily expressed by perivascular cells as a key niche component. For example, hematopoietic stem cell bioactivity was not repressed when SCF was conditional knocked out from hematopoietic cells, osteoblasts, and nestin+ cells, whereas if SCF was deleted from endothelial cells or perivascular stromal cells, HSC was completely gone. This absence implies importance of the perivascular niche for stem cell maintenance [229].

PDL is also heavily innervated for the functions of mechanoreception, nociception and reflexes. The nerve fibers are always closely related to blood vessels. Within the molar periodontal ligament, thick neurofilament protein (NFP) + nerve fiber bundles enter through slits at the alveolar socket bottom and thinner ones penetrate the PDL from the lateral wall of alveolar socket. Comparatively, nerve fibers are densely distributed around the molar root tip, similar to blood vessel patterns. These NFP-immunoreactive nerve fibers terminated in free endings. Besides these structures, a small group of coiled nerve endings exist in molar PDL [230].

Likewise, nerves always run along vasculature in adult tissues. In Dr. Zhao's paper, the Gli1+ mouse incisor MSCs were found surrounding only arterioles accompanied by nerves, aka the neurovascular bundle (NVB), which indicates the indispensable role of nerve in the MSC niche [59]. Correspondingly, Gli1+ MSCs are subjected to the precise regulation of Shh secreted from the inferior alveolar nerve. The ablation of Shh via inferior alveolar nerve denervation led to a decrease in label-retaining cells (LRCs) and the proliferating cell number, suggesting the regulation of Shh for MSCs' maintenance and activation. In fact, the whole incisor is susceptible to fracture with low odontogenic activity. Within the bone marrow space, norepinephrine-the neurotransmitter from the sympathetic nervous system yields osteoblast suppression and thus

reduces CXCL12 synthesis. Decreased CXCL12 then enforces nestin+ hematopoietic stem cells to migrate out of the bone marrow niche under the regulation of the nerve system [231] [232]. On a different note, parasympathetic innervation is essential for the undifferentiated status of keratin5+ epithelial progenitor cells during salivary gland organogenesis. Parasympathetic nerve apoptosis could compromise salivary gland stem cells or progenitor cells' regeneration capability after irradiation [233] [234].

Taking together with the above information in mind, we presume that periodontal MSCs are also surrounding the NVB, with the majority at the apical region where blood vessels and nerve fibers are confluent. PDL, alveolar bone, cementum, dentin, and the majority of cranial bones are all derived from cranial neural crest cells. Hence, the Hedgehog signaling pathway is essential for neural crest cells based embryonic development including tooth development. There are three Hh proteins highly conserved in mammals: sonic hedgehog (SHH), indian hedgehog (IHH), and desert hedgehog (DHH) [235]. DHH and IHH are mainly involved in embryonic development [236] [237] [238], while SHH is most widely expressed in adult tissues [239]. Shh signaling triggers downstream Gli to translocate into the nucleus, which promotes specific gene expression, including NANOG and SOX associated with stem cell self-renewal [240]. Similarly, recent studies revealed the Gli1+ cells as MSCs in various tissue [59] [228]. Gli1+ cells have already been proven to be the MSCs for various maxillofacial tissues such as craniofacial sutures and mice incisors [59] [71]. Considering the same developmental tissue origin, we presume that Gli1+ cells may also be MSCs inside mouse molar periodontal tissue in vivo.

2.2. Method and Materials

2.2.1. Animals and Tamoxifen Administration

All animal models used in this section, their source of origin, and original reference papers are listed in Table 3. In addition, all mice experiments were conducted in accordance with protocols approved by the Department of Animal Resources and the Institutional Animal Care and Use Committee of Texas A&M University College of Dentistry. Tamoxifen (Sigma, T5648) was dissolved in corn oil (Sigma, 47112U) (20 mg/ml) and injected intraperitoneally (i.p. 200 ml daily for two days).

2.2.2. Cryosection

Mandibles were carefully dissected and fixed in 4% PFA overnight at room temperature. Samples were then decalcified in 0.5M EDTA (Sigma-Aldrich, E9884) and shaken for seven days at 37 ℃. Afterwards, decalcified samples were dehydrated with a 30% sucrose solution for one hour and another 60% sucrose solution overnight at room temperature. Samples were then embedded in an OCT compound (Tissue-Tek, Sakura) under a stereomicroscope (Olympus) and immediately transferred into dry ice to solidify. The OCT block was set on a base and cut at 10μm thickness using a cryostat machine (Leica CM1850). Slides were incubated in 37 ℃ oven for at least one hour.

2.2.3. X-gal/ LacZ Staining Assay

Mice mandibles were fixed in a 0.5% glutaraldehyde solution (Sigma, G5882) containing 2mM $MgCl_2$ (Sigma, M8266) at 4℃ overnight and decalcified in 0.25M EDTA (Sigma, E9884) with 2mM $MgCl_2$ at 4℃ for one week. Next, samples were dehydrated with a gradient of 30% sucrose and 60% sucrose and 2mM $MgCl_2$ at 4℃ until the sample sank down. Frozen sections were then obtained. After PBS with 2mM $MgCl_2$ wash for 10min on ice, slices were postfixed in

cold 0.5% glutaraldehyde solution along with 2mM $MgCl_2$ for ten minutes (also on ice). Slides were rinsed with cold PBS plus 2mM $MgCl_2$ solution for 2*10min. ß-gal staining solution (Sigma, B4252) was used to stain LacZ positive cells at 37℃ for two days. Slides were then washed with PBS at RT twice for five minutes. Next, 4% PFA was used to postfix the slices at RT for thirty minutes. Then, Nuclear Fast Red was used to counterstain the slices for two minutes. After two-minute dehydration in 70% ethanol, Eosin was used to stain the cytoplasm. The slices were later dehydrated with gradient ethanol solutions at 80% and 95% for two minutes and then 100% 2*2min. At last, slides were mounted with mounting medium (Vol ratio xylene: permount =1:1).

2.2.4. PEGASOS Tissue Clearing Method

Mice were sacrificed by transcardial perfusion with 50ml 0.02% heparin-PBS (w/vol) (Sigma-Aldrich, 84020) and 20ml 4% PFA as described in a previous study 241 under the administration of xylazine and ketamine anesthetics (Xylazine 10-12.5 mg/kg; Ketamine, 80-100 mg/kg body weight). Mandibles were then collected and fixed in 4% PFA overnight at RT. Afterwards, samples were immersed in 0.5 M EDTA (pH=7.0) solution at 37°C to decalcify for four days. This step was followed by decolorization with a 25% (vol % in dH2O) EDTP solution (Sigma-Aldrich, 122262) for one day to remove remaining blood heme under constant shaking at 37°C. Then, the mandibles underwent stepwise delipidation at 37°C, shaking for six hours in each of the following sequentially: 30% (vol% in dH2O) Tert-Buturnol (TB, Sigma-Aldrich, 360538), 50%TB, 70%TB and overnight dehydration with TB-poly (ethylene glycol) methyl ether methacrylate average Mn500 (PEGMMA500) (Sigma-Aldrich, 447943) (vol ratio7:3). All the above mediums' pH was adjusted to 9.5 or above with 3% vol pure EDTP. Finally, samples

were immersed in the clearing medium benzyl benzoate (BB) (Sigma-Aldrich, B6630) -PEG-MMA500 (R.I=1.543) with 5% EDTP before imaging.

2.2.5. Two-Photon Imaging and Image Analysis

After PEGASOS clearing, transparent mandibles were placed in BBPEG-MMA RI matching medium and fixed in a cassette with a glass cover. Three-dimensional images were taken under a Zeiss LSM 780 two-photon microscope with 950nm pulsed NIR excitation and a Zeiss BiG two-channel nondescanned detector. Bone was then outlined by second harmonic generation (SHG). The endogenous tdTomato signal was captured with a 561nm visible laser. Afterwards, the FITC signal was imaged with a 488nm visible laser. Tiling or individual images were taken at 1024x1024 frame resolution with recommended Z stack interval and speed, and the pinhole for the internal detector was set as 1A.U. All raw image data was collected afterwards in a 16-bit TIFF format. Image 3D reconstructions were generated using Imaris X64 software.

2.2.6. The Periodontal MSCs' Culture and in Vitro Differentiation

Periodontal MSCs were obtained from the lower molars of mice as previously described [241]. Molars were extracted, placed on a culture peri-dish, and incubated with low glucose DMEM (Gibco, 11885084) + 10% fetal bovine serum (GIBCO, 16140071) containing ascorbic acid, glutamate (Gibco, 25030081), 50U/mL penicillin and 50U/mL streptomycin at 37°C in 5% CO2 atmospheric conditions. After two weeks, MSCs colonies were selected for a further osteogenic, adipogenic, or chondrogenic differentiation assay as previously described [71]. Cells were then seeded at 1x105 cells per well in a fibronectin-coated six well tissue culture plate using MSC Growth Medium Two (promocell, C-28009). Next, MSCs were induced with an osteogenic (Gibco, A1007201), chondrogenic (Gibco, A1007101) and adipogenic (Gibco, A1007001) differentiation medium for a respective fourteen to twenty-one days. The medium was changed

every third day. Then, cells were gently washed with Dulbecco's PBS w/o Ca2+/Mg2+ (promocell, C-40232) and Saccomanno fixation solution (Morphisto, #13881.00250) was added to fix the cellular monolayer. One hour later, cells were washed with distilled water. 2% Alizarin Red S (pH=4.1-4.3) (Sigma, A5533) was added for osteogenic differentiation detection. Cells were then incubated at RT in the dark for ten to fifteen minutes and washed with distilled water. 1% (in 3% acetic acid) Subsequently, Alcian Blue staining solution (Sigma, B8438) was used to detect cartilage extracellular matrix. After incubating in dark at RT for forty-five minutes, cells were washed with PBS. For the adipogenic differentiation assay, cells were preconditioned by incubating in 60% isopropanol solution (Sigma, W292907) for five minutes at RT. Cells were then incubated in Perilipin Solution (Morphisto #10396.00500) at RT for ten to fifteen minutes.

2.2.7. Immunofluorescent Staining

The following antibodies were used in our study: Anti-αSMA (Sigma, F3777, 1:200), Anti-β3-tubulin (R&D system, MAB1195, 1:20), Anti-Nestin (Millipore Sigma, MAB353, 1:100), Anti-CD 31 (BD Bioscience, 550274, 1:25), Anti-CD146 (BD Biosciences, 562230, 1:500), Anti-CD44 (BD Biosciences, 553134, 1:100), Anti-CD73 (BD Biosciences, 561545, 1:500), Anti-Periostin (Santa Cruz, sc-49480, 1:100), Anti-Col1(Abcam ab21286, 1:40), Anti-SP7 (Abcam ab22552, 1:100),CD34 (BD Biosciences, 560238, 1:500), Gs-iB4 (Invitrogen, I21411, 20µg/mL) and LepR (R&D systems, MAB497, 1:20). The secondary antibodies used in this study included goat anti-rabbit IgG (H+L) 488 (Invitrogen, A11034, 1:100), goat anti-rabbit IgG (H+L) 488 (Invitrogen, A11036, 1:100), goat anti-mouse IgG (H+L) 488 (Invitrogen, A11029, 1:100), donkey anti-rat IgG (H+L) 488 (Invitrogen A21208, 1:100), goat anti-rat IgG (H+L) 568 (Invitrogen, A11077, 1:100), and rat anti-mouse IgG (H+L) 568 (Invitrogen, A11004, 1:100). To conduct immunofluorescent staining, slides were first washed with PBST (1000ml

PBS+1ml TritonX100) for five minutes. 10% v/v 10x Casein blocking solution (Vector, SP5020) was used for blocking for 1 hour. Then, slices were incubated with 1st antibody overnight in a 4°C refrigerator. After PBST wash for 3*5min, a 1:100 diluted secondary antibody was added and incubated at RT for one hour. Slices were mounted with DAPI mounting medium (Vector laboratories, H-1200).

2.2.8. Injury Assay

For the molar injury assay, adult mice (6-8 weeks old) were anesthetized with an i.p injection of xylazine and ketamine (Xylazine 10-12.5 mg/kg; Ketamine, 80-100 mg/kg body weight). Next, mice were posted on a small animal plate in semisupination. A 25G needle was used to puncture holes at the furcation area into the alveolar bone of the right lower first molar. The left lower first molar was set as control.

2.3. Results

2.3.1. Gli1+ Cells Were Gradually Restricted to the Apical Region of Adult Molars During Postnatal Development

To investigate if Gli1+ cells were the dominant and primitive MSCs for periodontium in vivo, it was necessary to first determine the Gli1 gene expression pattern within the periodontium. We used Gli1-Lacz reporter mice and conducted LacZ staining on postnatal day 1 (P1), was well as P7, P21, P28, and P60 mice. At P1, strong LacZ staining was detected throughout the whole tooth germ, including the enamel organ, dental papilla, and the dental follicle (Fig. 3a, i). Similarly, at P7, a powerful LacZ signal was observed within 80% of tooth germ tissues (Fig. 3b, i). Also, Gli1+ cells number decreased with time. After P14, Gli1+ cells were gradually restricted to the root tip area (Fig. 3c, arrow in Fig. 3d), until at P28 and P60 when they were mainly located in apical PDL space (periodontal ligament) space (Fig. 3e, f,

arrow in Fig. 3e1, f1), with a few sparsely distributed in the pulp (asterisk in Fig. 3e2, f2) and other parts of PDL such as furcation areas (arrow in Fig. 3e2, f2). Furthermore, quantification indicates that the percentage of Gli1+ cells within the entire periodontium reduces from 100% at P1 to ~20% at P21 and maintains at ~5% from P30 to P90 (Fig. 3i).

Afterwards, Gli1-CreERT2; Ai14 mice of 6-8 weeks old were induced with tamoxifen for two days and cleared with the PEGASOS method to visualize Gli1+ cells distribution within their adult molars. Deep imaging of the lower first molar mapped the Gli1+ cells spatial distribution within the periodontium at a 3D scale. Moreover, Second Harmonic Generation (SHG in green) signal displayed type I collagen enriched hard tissue. Similarly, in adults, Gli1+ cells were found concentrated in root tip area (Fig. 3g, h, g1-g3, h1). Quantification results then indicated that two days after induction, ~60% of Gli1+ cells were located within the apical PDL space, ~15% in the middle 1/3 PDL space, and <10% in the cervical 1/3 PDL space. The rest of Gli1+ cells were sparsely distributed within the alveolar bones, cementum and pulp (Fig. 3j).

2.3.2. Gli1+ Cells Tightly Surrounded the Neurovasculature Bundle (NVB) and Multiplied Within PDL Along Vasculature

The distribution pattern of Gli1+ cells within periodontium was similar to that of the adult mice molar vasculature and nerve system. Specifically, Cdh5-Cre; Ai14 mice were used to label the vascular endothelium [242]. In addition, mandibles were harvested from six week old Cdh5-Cre; Ai14 mice and cleared with the PEGASOS method to visualize the molar vasculature. Deep imaging revealed an enriched vascular network within the pulp chamber and PDL space in 3D without sectioning (Fig. 4a). We found that the molar root tip is the region where numerous blood vessels are confluent (arrow in Fig. 4b). Then, the mandibles of adult Synapsin-CreERT2; Ai14 mice were collected and cleared to display nerve distribution pattern of adult mice molar

roots. Deep imaging showed nerve fibers within root pulp (arrowhead in Fig. 4c) and the inferior alveolar nerve (arrow in Fig. 4c). Correspondingly, intensive nerve fibers gathered at the root tip area. Thus, the 3D reconstruction of tooth vasculature and nerve helps explain why most Gli1+ cells gather around root apical regions. To further investigate the spatial relationship between Gli1+ cells and NVB, 6-8 week old Gli1-CreERT2;Ai14 mice were induced for four days and β3-Tubulin or GS-IB4 immunofluorescence staining were performed on horizontal cross-sections of molars to label respective nerves and vasculatures. Besides, all Gli1+ cells were found exclusively surrounding vasculatures (Fig. 4d). Moreover, local magnification indicated that Gli1+ cells had pare-vasculature located surrounding the pericytes (Fig. 4e). Additionally, Gli1+ cells were closely around nerve bundles (Fig. 4f). Molars were also collected at 3 days, 7 days or 14 days after tamoxifen induction. GS-IB4 staining was performed on horizontal sections and Gli1+ cells were found multiplying centered in blood vessels inside PDL within a short range (Fig. 4g,h, i).

2.3.3. Gli1+ Cells Were Negative for Periodontium Lineage Differentiation Markers and Express Typical MSCs Markers in Vitro

Stem cells were defined as undifferentiated cells [243]. In order to clarify if Gli1+ cells were MSCs, we further studied their expression profiles with immunofluorescence staining. To start, primitive Gli1+ cells were labeled two days after tamoxifen administration. CD44 did not show an obvious overlap with Gli1+ cells (Fig. 5a) and CD73 expression was not detected in the periodontium (Fig. 5b). However, CD146 was detected to surround vasculatures but rarely colocalized with Gli1+ cells (Fig. 5c). The absence of in vitro MSCs surface markers on Gli1+ cells suggested that in vitro could not faithfully replicate in vivo situations. Whereas immunofluorescence assays indicated that periostin (a widely accepted PDL specific marker [244])

was detected in almost the entire PDL except for the apical region where Gli1+ cells were located (Fig. 5d). To continue, Sp7 and type1 collagen were known to be expressed by respective osteoblasts and osteocytes. No obvious overlap between Gli1+ cells and Sp7 or type I collagen was noticed at the root tip (Fig. 5e,f). These results implied that Gli1+ cells were in a primitive undifferentiated state.

2.3.4. Gli1+ Cells Expressed Typical MSC Markers and Underwent Multi-Lineage Differentiation in Vitro

In larger context, the classical definition of the mesenchymal stem cell is set based on in vitro study. There are three criteria to determine MSCs: 1) the ability to attach to plastic culture dishes and undergo clonal culture, 2) high expression of typical surface markers (including CD44, CD146, CD73, etc; 3), and to be capable of experiencing osteogenic, chondrogenic, and adipogenic differentiation under defined culture conditions [245]. Therefore, to see if Gli1+ cells are stem cells, we performed an in vitro study. Gli1+ cells were labeled two days after tamoxifen injection. PDL cells were then collected from adult (6-8 weeks of age) Gli1-CreERT2; Ai14 mice molar root and cultured in vitro. Afterward, immunohistochemistry staining for cultured Gli1+ cells demonstrated that hematopoietic or endothelium markers including CD31 and CD34 were not present in the culture (Fig. 6a, b). Although, typical stem cell markers such as CD44, CD146 and CD73 were highly expressed in Gli1+ cells (Fig. 6c-e). Next, Gli1+ cells were positive for Sp7 but negative for periostin, αSMA, or nestin (Fig. 6f, h, i). Quantified results confirmed that Gli1+ cells were typical MSCs in vitro (Fig. 6j). Under in vitro culture condition, Gli1+ cells were found colonized and adhered to a culture dish (Fig. 6k). When induced, these Gli1+ cells displayed osteogenic differentiation with positive Alizarin red staining (Fig. 6l) and

chondrogenic differentiation with positive Alcian blue staining (Fig. 6m). No adipogenic differentiation was observed when performing perilipin staining (Fig. 6n).

2.3.5. Gli1+ MSCs Contributed to Periodontium Physiological Turnover in Adulthood

Adding to the parameters above, stem cells are supposed to support physiological tissue turnover [243]. To track the fate of Gli1+ cells within periodontium in vivo, lineage tracing was performed on 6-8 week old Gli1-CreERT2; Ai14 mice. Three days after tamoxifen induction, Gli1+ cells were found mainly located within the apical PDL area (Fig. 7a, a1) with some in the dental pulp (Fig. 7a2) and other segments of PDL, such as the furcation area (Fig. 7 a3). In time, more Gli1+ cells were detected within PDL 30 days after induction (Fig. 7b). During 60 days of tracing, we found Gli1+ cells could give rise to the entire PDL space (Fig. 7c), cementum (asterisk in Fig. 7c1), and alveolar bone (arrow in Fig. 7c3). A slight increase of Gli1+ cells was also observed in dental pulp (Fig. 7c2). This result was confirmed by 3D deep imaging results, which demonstrated that quite a few Gli1+ cells were in sparse distribution along the molar root (Fig. 7d, d') 3 days after induction while Gli1+ cells multiplied along the molar root 60 days after tamoxifen injection (Fig. 7e). Moreover, Gli1+ cells compromised the majority of cementum and alveolar bone areas (Fig. 7e'). Accordingly, our quantification result indicated that Gli1+ cells could give rise to 60% PDL cells thirty days after induction whereas the labeling efficiency could reach to 90~100% within PDL space 30 days after induction. Meanwhile, in terms of Gli1+ cells' lineage tracing in cementum, ~20% cementum cells were labeled by Gli1 30 days after tamoxifen administration. Furthermore, lineage tracing was performed for 60 days and ~50% cementum cells were labeled as Gli1 positive. Likewise, Gli1+ cells contributed to a small proportion of pulp and alveolar bone (Fig. 7f).

2.3.6. Gli1+ Cells Supported Periodontium Tissue Injury Repair

Stem cells are known to support not only tissue turnover in normal physiological conditions but are also involved in injury repair processes [243] [246]. To test if Gli1+ cells contribute to periodontal tissue injury repair, an injury model was conducted on adult Gli1-CreERT2; Ai14 mice. Two shots of tamoxifen were given after the injury. Then, molars were collected seven and thirty days later for Gli1+ cells tracing. Additionally, mice littermates were set as a control group without the punching injury. Lineage tracing results indicated that Gli1+ cells were highly active 7 days after injury (Fig. 8a). To illustrate, intensive Gli1+ cells were noticed gathering in the molar root tip and injury region-furcation area (arrow in Fig. 8a1). Compared with the control group (Fig. 8c, c1), we found that Gli1 activity was significantly increased thirty days post injury (Fig. 8b). In fact, more active Gli1+ cells were detected within the root tip and furcation PDL space. Further, a dramatic increase of osteocytes was found derived from Gli1+ cells in the injury area, indicating the contribution of Gli1+ cells to reparative alveolar bone formation (arrow in Fig. 8b1).

2.3.7. Multipotent Gli1+ Cells Gave Rise to the Entire Molar Periodontium at the Young Age

To analyze Gli1+ cells' contribution to molar periodontium at a young age. A lineage tracing assay was performed on P3, P7, and P14 Gli1-CreERT2; Ai14 mice. One month after injection, mandible bones were collected for confocal imaging as shown in Fig. 8d. Gli1+ cells from P3 mice could give rise to most dental pulp, except for portions of the crown and dentin (Fig. 9a, asterisks in Fig. 9a1). Specifically, the whole periodontium was labeled as Gli1 positive, including the entire PDL, alveolar bone (Fig. 9a2) and cementum (Fig. 9a3). Then, when induction started from P7, Gli1+ cells derived from dental pulp cells were slightly decreased,

especially in the crown pulp area (Fig. 9b, b1). Despite this finding, Gli1+ cells still supported complete PDL and cementum turnover (Fig. 9b2, b3). Next, we discovered that Gli1+ cells in P14 mice gave rise to PDL, cementum, alveolar bone, and root tip pulp (Fig. 9c, c1, c2, c3). Quantification results indicated that P3 Gli1+ cells were highly multipotent, contributing to 100% PDL, 100% cementum, 100% alveolar bone, 100% apical, 1/3 of root tip pulp, and ~60% dental pulp in other regions. Similarly, Gli1+ cells from P7 mice gave rise to 100% PDL, 100% cementum, 100% apical, 1/3 in root tip pulp, ~60% alveolar bone, and ~30% pulp in other areas. In contrast, Gli1+ MSCs multipotency slightly decreased in P14 mice. Gli1+ cells gave rise to 100% PDL and 100% cementum, as well as ~50% alveolar bone, ~90% apical, 1/3 of root tip pulp, and ~10% in other pulp areas (Fig. 9e).

2.3.8. Gli1+ Cells Were the Primitive Stem Cell Population of the Adult Molar Periodontium

To demonstrate that Gli1+ cells are the primitive stem cell population for adult molar periodontium, it is essential to analyze the expression profiles of other MSCs markers. Recently, MSCs or mesenchymal progenitor cells have been identified with specific gene markers in other mesenchymal tissues. For example, LeptinR and Gremlin 1 are regarded as the bone marrow MSCs markers [247] [55, 224, 248]. Likewise, NG2+ pericytes have been found to contribute to osteoblasts, chondroblasts, fibroblasts, adipocytes [249], myogenic cells [224], and odontoblasts [250], while αSMA+ cells are proposed to be periodontium progenitor cells [68]. Correspondingly, PDGFRα or PDGFRβ is thought to label adipose MSCs [54, 58]. For this reason, we repeated a lineage tracing assay on NG2-CE; Ai14, PDGFRβ-CE; Ai14, αSma-CE; Ai14 and LeptinR-Cre; Ai14 adult mice to define the fate of each particular cell group. Mandible sections were then analyzed to compare these markers' labeling efficiency with Gli1. Three days after injection,

NG2+ cells were mainly detected in alveolar bone (Fig. 10a, a2), with quite a few in PDL, cementum (Fig. 10a1), and dental pulp (Fig. 10a3). One month later, NG2 expressing cells were noticed in dental pulp (Fig. 10b1), but most NG2 + cells were mature cementocytes and osteocytes (Fig. 10b, asterisks in Fig. 10b2, arrow in Fig. 10b3). At the same time, the majority of PDL space was free of NG2+ cells. Further, the expression profile of PDGFRβ cells indicated that they were not the major periodontium MSCs in adult mouse molar. PDGFRβ+ cells were mainly located in the dental pulp (Fig. 10c, c3), part of cementum (asterisk in Fig. 10c1) and the bone marrow space (Fig. 10c2) three days after tamoxifen administration. Additionally, after tracing for one month, PDGFRβ+ cells expressed in pulp tissue (Fig. 10d, d3). On the other hand, PDGFR labeled cementum (asterisk in Fig. 10d1) and mature osteocytes in alveolar bone (arrow in Fig. 10d2) but PDL was sparsely labeled. Meanwhile, in αSMA-CreERT2; Ai14 mice, aSMA+ cells gave rise to very limited cells which were mainly around the artery (Fig. 11a, a1) two months after induction. Co-localization between aSMA+ cells and aSMA antibody immunofluorescent staining validated the lineage tracing results (arrow in Fig. 11b). In LeptinR-Cre; Ai14 mice, small groups of LepR+ cells were observed in PDL (Fig. 11c, c1,c2), alveolar bone (Fig. 11c2) and dental pulp (Fig. 11c3) at one month of age. The distribution pattern was similar to that of six month old mice but with more cells within PDL and alveolar bone (Fig. 11d, d1, d2). LeptinR + cells were identified as pericytes surrounding Gs-ib4 labeled blood vessels, which are in line with the previous study (Fig. 11e). Moreover, Gli1+ cells closely surrounded aSMA+ and LepR+ cells two days after induction in Gli1-CreERT2; Ai14 mice (Fig. 11f, g). In contrast, Gli1+ cells co-localized with aSMA+ cells 60 days after induction (Fig. 11h) and LepR+ cells were found derived from Gli1+ cells 30 days after induction (Fig. 11i). Therefore,

Gli1+ cells were demonstrated as the primitive stem cells giving rise to the subpopulation of aSMA+ and LepR+ cells.

2.4. Discussion

The classic definition of MSCs is based on a loose set of criteria according to a series of in vitro observation. However, through our investigation, the in vitro culture properties and expression profiles may not precisely represent in vivo MSCs characteristics, as shown in Fig. 5 and 6. These images show that the majority of Gli1+ cells do not express classical surface markers in vivo. Hence, two fundamental questions of periodontal MSCs study are centered on the in vivo identification and localization of these MSCs. Considering the same tissue origin with incisor pulp, we speculated Gli1 as one of the specific markers for molar periodontal MSCs. In adult molar periodontium, Gli1+ cells have been proven to be multipotent, contributing to physical tissue turnover and pathological injury repair and simultaneously remain in undifferentiated status under normal conditions. In this way, we successfully identified an in vivo marker for periodontal MSCs for the first time and as a result, related transgenic fluorescent reporter mouse models can be applied for periodontium studies. Besides, in comparison with other stem cell markers such as LeptinR, NG2, αSMA, PDGFRβ, and Gli1+, MSCs are endowed with higher labeling efficiency, indicating their multipotency and primitiveness. Although this information is true, we are not ruling out the possibility that there are other subpopulations of periodontal MSCs which could also support periodontium homeostasis.

We found Gli1+ MSCs localized perivasculature. However, the underlying mechanism for the perivasculature niche, which regulates MSCs such as the particular blood vessel type, secreted molecules, and regulatory signaling remains largely unknown. The co-

immunohistochemical staining results indicated that αSMA+ arteries comprise the MSC niche. Therefore, studies regarding the role of veins and capillaries are still needed.

Conversely, the previous study proved that nerves are indispensable in the MSC niche, since mouse incisor Gli1+ MSCs surround the only arterioles accompanied by nerves [59]. Though we displayed close spatial relationship between respective vasculature and Gli1+ cells, nerve, and Gli1+ cells, co-immunostaining of αSMA, β3-tubulin, and Gli1 are necessary to investigate if NVB is the only niche for periodontium Gli1+ MSCs. On another note, Shh is produced by trigeminal ganglion (TGG) sensory neurons, which can activate Gli1+ incisor MSCs [59]. In adult molars, it is possible to have a similar regulatory function. In background literature, Shh as a member of the mammalian Hedgehog (Hh) family and plays a key role during tooth development [252]. Actually, the Gli1 gene is one of the downstream target genes in Shh canonical signaling. Nevertheless, the role played by Shh/Gli signaling in PDL growth is largely unknown [253]. However, Shh from the dental epithelium has been proposed to regulate the differentiation of dental mesenchymal cells —their HH signaling is critical for stem cells' osteogenic commitment [254]. Unfortunately, we did not focus on this point during this project. In the future, more efforts should be spent on exploring the detailed regulation of nerve on periodontium MSCs through a denervation experiment and a Shh agonist and antagonist administration approach.

In addition, there are still a multitude of unveiled issues pertaining to the NVB niche. This piece contains not only nerves and arteries but also other cells, such as glial and endothelium varieties. These components secrete more than one type of molecule and participate in a complicated signaling network to regulate MSCs. It will be a big project to elucidate each contribution to the MSC niche. Furthermore, based on our current data, we presume that Gli1+

MSCs initially localize around NVB, go through self-renewal, give rise to daughter cells, and differentiate into terminal tissues within the short spatial range centered on each NVB niche.

Collectively, our discoveries help establish Gli1 as a reliable in vivo marker for adult molar periodontium and we will be able to have a good animal model to investigate periodontal MSCs related questions in vivo.

Lastly, an extremely noticeable feature of our study was application of the PEGASOS tissue clearing method to acquire 3D images of MSCs comprehensive distribution map within adult molars. PEGASOS tissue clearing workflow consists of fixation, decalcification, decolorization, delipidation, dehydration, and refraction index (R.I) matching as described previously [255]. After PEGASOS tissue clearing, the whole tooth turns transparent, thereby enabling the endogenous fluorescence to be directly visualized with a regular two-photon or confocal microscope. Images can then be acquired at differing depths of the tissue and re-constructed after to form a three-dimensional image stack [256] [257] [248] [255]. In contrast to the traditional 2D imaging process, PEGASOS tissue clearing needs no cut, which is more convenient and efficient. The 3D images could also provide more precise information and straightforward views. From this aspect, the PEGASOS aided 3D imaging technique will become a useful new tool for MSC studies.

3. CANONICAL WNT SIGNALING IS ESSENTIAL FOR PERIODONTAL MSCS REGULATION

3.1. Introduction

Insight into cross-talk between regulatory factors within MSCs and their niches is fairly important for both normal tissue homeostasis and disease conditions, as exemplified in tissue infection and injury. For instance, various craniofacial tissues were found responsive to Wnt signaling. Using an Axin2-lacz strain, researchers mapped the distribution of Wnt–responsive cells in the mouse incisor cervical loop and discovered that both stem cell populations and differentiated odontoblasts are $lacz^{hi}$ [258]. In subsequent lineage-tracing experiments on Axin2-Cre ERT2; R26mTmG/+, Wnt-responsive cells and their daughter cells were found in the pulp, cervical loop, odontoblastic, and ameloblastic layers [106]. With the same methods, Wnt responding cells were discovered to populate PDL space and the thin layer on the surface of alveolar bone. The cementoblasts close to the dentin surface are also responsive to the Wnt signal [259]. Likewise, knockout of Wnt signaling within osteoblasts led to the decrease of alveolar bone volume and density, cementum volume, as well as craniofacial bone thickness. In contrast, the Sharpey's fibers of Wnt conditional knockout mutant mice, within PDL turned unattached and disorganized along the entire root surface with time [260]. As a matter of fact, aberrantly elevated Wnt signaling has been shown potentially leading to cementum overgrowth, tooth impaction, and dental ankylosis [261]. Comparatively, the liposomal formulation of Wnt3a protein has been demonstrated to enhance autografts' osteogenic ability and rescue failure of oral implants [262] [263]. In fact, adenovirus Dkk1-treated mice showed decreased osteogenic markers expression and increased PDL width [264]. Though these studies have concluded that periodontal tissues are all Wnt-responsive or Wnt-dependent [260] while Wnt protein could work as a stem cell

activator in vitro, direct in vivo evidence of Wnt signaling`s significance to periodontal MSCs is lacking . In this project, we hope to define the roles of canonical Wnt signaling within the periodontium MSC niche. Through this investigation, we may obtain valuable information to start instigating periodontal tissue regeneration.

Hence, to an appropriate way to investigate the regulation of Wnt signaling to periodontium stem cells is using Wnt reporter or lineage tracing strains to demonstrate endogenous Wnt responsiveness within periodontal tissue. To date, various transgenic mice lines have been generated by directly placing the lacz or GFP gene behind the Wnt related genes' promotor. Other strains for lineage tracing of Wnt responsive cells involve using the Cre/ERT2 or rtTA/tTA (tet on/off system) inserted into Wnt target genes. Furthermore, in our studies, when crossing with Rosa26-tdTomato or GFP, the Wnt signaling activity or Wnt responding cells were conditionally visualized under the control of Wnt-responsive elements. Additionally, the available mice Wnt reporter strains are listed in Table 2. Among those reporter mice models, we choose Axin2-lacz as the real-time reporter for Wnt signaling activity because Axin2 is widely expressed throughout the whole body with consistent expression.

Overall, the stem cell niche integrates various molecular signals and mediates the balanced response of stem cells to the needs of organisms. For the first time, we are able to locate and study the regulating niche of the periodontal stem cells with the identification of Gli1+ MSCs in vivo. Therefore, to take our research further and determine the canonical Wnt pathway's regulation on Gli1+ periodontium MSCs, we performed a loss and gain of function study by using Gli1-CE; β-Cateninflox/flox; Ai14 and Gli1-CE; Ctnnbfl/-(exon3); Ai14. We hypothesize that blockage of canonical Wnt activity from Gli1+ MSCs will inhibit their activation and vice versa.

3.2. Materials and Methods

3.2.1. Animals and Tamoxifen Administration

The entirety of animal experiments were approved by the Texas A&M University Institutional Animal Care and Use Committee in accordance with guidelines from the NIH/NIDCR. Gli1-CreERT2 (JAX 007913) mice were crossed with Ai14 mice (JAX 007908) to generate Gli1-CreERT2;Ai14 mice. β-Catenin flox (JAX 004152) mice were bred to Gli1-CreERT2;Ai14 mice in order to generate Gli1-CreERT2;β-Catenin$^{flox/flox}$;Ai14 mice for the loss of function study. To further clarify, a group of, Ctnnbfl/-(exon3) mice participating in the study were kindly given by Dr. Jerry Feng of Texas A&M University College of Dentistry. When these specimens were crossed with Gli1-CreERT2;Ai14 mice, Gli1-CE; Ctnnbfl/-(exon3);Ai14 mice were generated for the gain of function study. Meanwhile, all mice were housed in a twelve hours light/dark cycle. Tamoxifen was dissolved in corn oil (20 mg/ml) and injected intraperitoneally (i.p.; 200 ml daily for two days) into G.T and Gli1-CreERT2;β-Catenin^{flox};Ai14 mice. As for Gli1-CE; Ctnnb$^{fl/-(exon3)}$;Ai14 mice, the dosage was deducted to 50 ml daily for two days.

3.2.2. X-Gal/ LacZ Staining Assay

Mice mandibles were fixed in 0.5% glutaraldehyde solution containing 2mM $MgCl_2$ at 4℃ overnight and decalcified in 0.25M EDTA with 2mM $MgCl_2$ at 4℃ for one week. Next, samples were dehydrated with a gradient of 30% and 60% sucrose with 2mM $MgCl_2$ at 4℃ until the sample sank down. Then, frozen sections were obtained. After PBS with a 2mM $MgCl_2$ wash for ten minutes on ice, slices were postfixed in a cold 0.5% glutaraldehyde solution with 2mM $MgCl_2$ for ten minutes on ice. Subsequently, slides were rinsed with cold PBS plus 2mM $MgCl_2$ solution for 2*10min. ß-gal staining solution was then used to stain LacZ positive cells at 37℃

for two days. Following this time period, slides were washed with PBS at RT twice for five minutes and 4% PFA was used to postfix the slices at RT for thirty minutes. Next, Nuclear Fast Red was used to counterstain the slices for two minutes. Then, after 2 minutes dehydration in 70% ethanol, Eosin was used to stain the cytoplasm. The slices were dehydrated with gradient ethanol solutions at 80% and 95% for two minutes and 100% 2*2min. At last, slides were mounted with mounting medium (Vol ratio xylene: permount =1:1).

3.2.3. Micro-CT Scanning and Assessment of Alveolar Bone Loss

The mice mandibles were analyzed with a high-resolution micro-CT scanner (Scanco Medical, Basserdorf, Switzerland). The scanning protocol was set at high resolution, and the X-ray energy settings were 70 kV and 114 μA (as previously described in 267). When scanning was complete, the slice stack was reconstructed into a three-dimensional model and evaluated in Imaris software. Namely, Alveolar Bone Loss (ABL) is represented by the linear distance of the Cementoenamel Junction (CEJ) to the Alveolar Crest (AC). The CEJ-AC distance becomes higher in accordance with severity of bone loss. Similarly, CEJ and AC were localized by two pinpoints in the "measurement" tab of Imaris.

3.2.4. H&E Staining

Slides were stained in Hematoxylin solution for three minutes and then rinsed with distilled water till the water was clear. After being dipped in 1%HCl-Alcohol for two seconds and rinsed with distilled water, slides were immersed in 1% ammonia (Vol% in distilled water) for ten seconds to undergo nuclear blue staining. Samples were then moved into Eosin solution and stained for thirty seconds to stain the cytoplasm. Moreover, tap water was used to remove extra Eosin stain. Then, slides were dehydrated with 80% EtOH and later mounted with xylene

based Permount solution (Vol ratio 1:1). Pictures were taken afterwards under a 40x objective using Olympus BX51 microscope.

3.2.5. EdU Incorporation Assay

5-ethynyl-2'-deoxyuridine (EdU) can incorporate into the proliferative DNA chain and be detected through its reaction with fluorescence azides. In particular, EdU staining is a highly sensitive and efficient method to assay cell proliferation activity. Also, reagents are almost 1/500th the size of an antibody molecule, so they easily penetrate intact hard tissue [265]. To perform EdU staining, adult mice were given an intraperitoneal injection of EdU (Invitrogen, #A10044) in a dosage of 60ug/g their body weight two hours before sacrifice. Next, cryo-section slices were incubated in an EdU labeling cocktail for 30 minutes following a PBST wash 3 * 5min. The labeling dye used contained Tris-buffered saline (100 mM final, pH 7.6), CuSO4 (4 mM final, Acros #197730010), Sulfo-Cyanine 3 Azide (2-5 uM final, Lumiprobe #D1330) and Sodium Ascorbate (100 mM final, made fresh each use, Acros #352685000).

3.2.6. Confocal Imaging Assay

Confocal images were captured under a Leica SP 5000 fluorescence microscope with filter settings for DAPI/FITC/TRITC and acquired using Leica LAS AF software. Laser energy was set at an equal rate of 40% for all sample imaging. Further, corresponding band-pass filters were set as for DAPI (Ex. 405 nm, BP410-490) and tdTomato (Ex. 543 nm, BP550-595). Tiling or individual images were taken at a 1024x1024 frame resolution, 200 Hz frequency with recommended Z stack interval while the pinhole for the internal detector was set as 1A.U. Then, the Gli1+ cells number was counted manually in six randomly chosen areas of interest within PDL space separately at root tip area, furcation, and interdental septum area. In the end, the

relative percentage of Gli1+ cells was calculated as Gli1+ cells number/total cells (DAPI+) number on both the ligation and non-ligation side.

3.2.7. Statistical Analysis

SPSS software version 21.0 was used for statistical analysis. A paired t-test was conducted for mean comparison. P value of less than 0.05 was considered statistically significant. *p<0.05, ** p<0.01, ***p<0.001. Furthermore, Prism 7 was used to display the quantification results. Data were shown as Mean ± SEM.

3.3. Results

3.3.1. Wnt Signaling Was Gradually Restricted to the Adult Molar Apical Region and Corresponded to Gli1+ MSCs Activity

Wnt signaling proteins have been proven essential for stem cell bioactivity in various other mesenchyme tissues. However, the direct evidence of Wnt regulation on periodontal MSCs in vivo is limited. To analyze the Wnt responsiveness within periodontium, we generated Axin2-LacZ reporter mice and performed lacZ staining on molars of different developmental stages. At P1, nearly the entire dental follicle and dental epithelium expressed Axin2 (Fig. 12a). Then, from P7 to P21, Wnt responsive cells were gradually restricted to the root tip area (Fig. 12b, c, d). At 1 month old, LacZ staining was particularly strong in the apical region (Fig. 12e). Also, Axin2+ Wnt-responsive cells were detected within the odontoblasts and cementoblasts (arrow in Fig. 12e1, asterisks in Fig. 12e2). In addition, to visualize the spatial relationship between Axin2+ cells and Gli1+ MSCs, Lacz/ß-Gal immunohistochemical staining was conducted on adult Gli1-CreERT2; Ai14; Axin2-Lacz mice two days after induction. Co-localization of Gli1+ cells and Axin2+ cells suggested the responsiveness of Gli1+ MSCs to Wnt signaling (arrow in Fig. 12f).

3.3.2. Blockage of the Canonical Wnt Pathway within Gli1+ MSCs led to Deactivation and Severe Periodontium Tissue Loss

The canonical Wnt pathway is mediated by β-Catenin. To investigate the potential regulatory effects of the Wnt pathway on Gli1+ periodontal MSCs, a Gli1-CreERT2; β-Cateninfl/fl mouse model was generated for Wnt signaling conditional loss of function study within Gli1+ cells after tamoxifen administration. Blockage of the canonical Wnt pathway prevented Gli1+ MSCs from populating the periodontium. As comparison, in the littermate control Gli1-CreERT2; Ai14 mice, Gli1+ MSCs were found mostly located in molar root apical regions (Fig. 13a). They could normally populate the entire PDL two months after tamoxifen administration (Fig. 13b). Further, in adult Gli1-CreERT2; β-Cateninfl/fl; Ai14 mice, the distribution pattern of Gli1+ cells was similar to Gli1-CreERT2; Ai14 mice three days after induction (Fig. 13a,g). There was no significant difference in Gli1+ cells percentage between control mice and mutant mice at the time, (Fig. 13m) which indicated that the canonical signaling pathway has no significant roles in the maintenance of Gli1+ periodontium MSCs. In contrast, later at two months after induction, Gli1+ MSCs in the mutant mice arrested at their original locations (mostly at the apical area) and failed to give rise to the major periodontium (Fig. 13h). Consequently, quantification results showed that in a normal condition, ~90% of PDL space was occupied by Gli1+ cells, while when β-catenin mediated canonical Wnt signaling was knocked out within Gli1+ cells for two months, the relative Gli1+ cells percentage in PDL decreased to ~15% (Fig. 13m). The decrease suggested that β-catenin conditional knocking out disrupted the activation of Gli1+ cells. 6 months after Wnt blockage, severe periodontal tissue loss was found on Gli1-CE;β-Cateninfl/fl mice. The alveolar bone height and density in the knockout mice reduced significantly (Fig. 13i,j) compared with control mice (Fig. 13c,d). In

addition, the distance between the CEJ and alveolar bone crest increased by two folds in mutant mice than in control mice (Fig. 13n). Correspondingly, histological sections displayed a significant reduction of alveolar bone amount and cementum volume (asterisk in Fig. 13k), disorganized PDL fiber, and widened PDL space (Fig. 13k,l) compared to the normal periodontium morphology in control mice (Fig. 13e,f). Based on both lineage tracing and micro-CT analysis data, we concluded that canonical Wnt signaling in mouse molar mesenchyme was critical for Gli1+ MSCs activation.

3.3.3. Constitutive Activation of Wnt Signaling Led to Periodontium Overgrowth and Enhanced Gli1+ MSCs Activation

To further demonstrate the role of Wnt pathways in Gli1+ periodontal MSCs regulation, gain of function study was performed on 6~8 week old Gli1-CreERT2; Ctnnbfl/-(exon3); Ai14 mice to over-activate Wnt signaling after two injections of tamoxifen. EdU incorporation was used to assay the proliferation status of Gli1+ cells. 3 days after induction, an increase in EdU+/Gli1+cells of mutant mice demonstrated a positive impact of the canonical Wnt signaling pathway on Gli1+ MSCs activation (arrow in Fig. 14a, d) compared with littermate control Gli1-CreERT2; Ai14 mice.. Correspondingly, abnormal cementum overgrowth was detected through micro-CT and H&E staining assays on mutant mice compared with control mice (arrow in Fig. 14b, e and Fig. 14c, f). On a different note, the mice`s striking phenotype changes implied the importance of Wnt signaling in periodontal tissue homeostasis. Gli1+ MSCs experienced enhanced activation especially the cementum area two weeks after Wnt over-activation, (Fig. 14g, h, asterisk in Fig. 14h1). Correspondingly, only ~60% PDL space and less than 10% cementum were occupied by Gli1+ cells in control mice (Fig. 14i, j). Meanwhile, Gli1+ MSCs in mutant mice could prompt ~90% PDL and ~90% cementum (Fig. 14i, j). Also, Gli1+ MSCs

gave rise to osteocytes in alveolar bone (arrow in Fig. 14h2), which did not occur in control mice. Thus, the reuslts above suggest that canonical Wnt signaling is critical for the homeostasis of Gli1+ MSCs participating in periodontal MSCs activation as well as lineage commitment.

3.4. Discussion

An abundance of data demonstrates that Wnt signaling is essential for periodontium development. For instance, the absence of Wnt signaling caused arrested periodontium formation during embryogenesis [266] and disrupted homeostasis in adulthood [267]. By employing reporter mice, we demonstrated that Wnt responsive cells gradually restrict to the root apex, which is similar to the dynamics of Gli1+ cells within molar periodontium. Afterwards, the co-localization of Gli1 and Axin2 suggested the presence of Wnt signaling within Gli1+ MSCs. In addition, we performed a loss of function study achieved through constructing a β-catenin conditional knockout mice model, which implied the importance of canonical Wnt signaling in the activation of MSCs. We also found that transient β-catenin knockout rarely affects Gli1+ MSCs maintenance. However, this phenomenon could be explained as the result of incomplete Wnt signaling blockage via an induction period of only three days. The decreased Gli1+ cell population within periodontium two months after tamoxifen injection may ascribe to initial Gli1+ MSCs apoptosis instead of or more than MSCs activation interruption. To solve this puzzle, cell proliferation and apoptosis should be further examined at different induction time points. Another issue to take into consideration is that the effects of the experiment may be time and dosage-dependent. Similarly, a gain of function study on Exon3 conditional knockout mice (with inhibited β-catenin expression) verified the upregulation of canonical Wnt signaling on Gli1+ periodontal MSCs. Wnt responsive cells then spread out the whole body. Thus, due to this activity we noticed a striking phenotype in Gli1-CreERT2; Ctnnbfl/-(exon3); Ai14 mice even

after a short time (two weeks) along with a small dosage (50ul/adult mouse) of tamoxifen induction. The resulting features included skin thickening, tachypnea, excessive secretion of sebum, osteopetrosis, and craniosynostosis (pictures not shown). The death rate was fairly high one month after induction. Likewise, in each area of periodontal tissue, consequent over-active Gli1+ cells were detected in both PDL and cementum but not in the alveolar bone. This finding may be related to the slow turnover rate of mature alveolar bone or a relatively short induction duration. Accordingly, previous studies implied that both osteoblasts and cementoblasts produce and respond to Wnt signaling [261]. However, the Wnt overaction is limited in our study to within Gli1+ MSCs and the daughter cells. Hence, we provided evidence in this manner that periodontal tissue overgrowth is initialized by the direct response of Gli1+ periodontal MSCs upon elevated canonical Wnt signaling.

As for future research directions, recent studies reported the antagonism between the canonical Wnt pathway and the noncanonical Wnt/Ca2+ pathway. For example, decreased β-catenin levels could activate the Wnt/Ca2+ pathway, restoring the lost osteogenic differentiation potential of PDLSCs [268]. Conversely, non-canonical Wnt/Ca2+ pathway mediated an elevated Ca2+ concentration in cytoplasm, which then activates TAK1 and NLK kinase, thus inhibiting TCF/β-catenin signaling [269]. Given the common crosstalk between canonical and noncanonical Wnt signaling, it is necessary to investigate the noncanonical Wnt signaling's role in periodontal MSCs regulation from this point forward.

Altogether, this section provided direct evidence that showed canonical Wnt signaling is important for Gli1+ periodontal MSCs' activation and the subsequent periodontal tissue homeostasis, which offers insight for stem cell strategies and in dental tissue defect treatment or engineering.

4. THE INHIBITORY REGULATION OF GLI1+ MSCS DURING PERIODONTITIS

4.1. Introduction

Adult periodontitis is a chronic periodontal tissue infection manifested by soft and hard tissue loss. Clinical signs of inflammation such as changes in color, contour, consistency, or bleeding on probing are noticed first. Furthermore, radiographic changes include loss of lamina dura, horizontal or vertical bone resorption, and thickening of the periodontal ligament space. Periodontal disease progression goes through four stages of lesions: initial, early, established, and advanced. The initial lesion is a protective response of resident leukocytes and endothelial cells to the bacterial biofilm. Besides, metabolic products produced by pathogenic microbes cause local vasculature vasodilatation while neutrophils chemotaxis toward the inflammation site fights against pathogen infiltration. Next, the early lesion stage is characteristic with additional neutrophils and the appearance of macrophages, lymphocytes, plasma cells, and mast cells. Then, in the established lesion stage, host body immunity switches from its innate immune response to an acquired immune response. Moreover, lymphocytes are the predominant immune cells and collagenolytic activity is increased during this time period. During advanced lesion stage, Irreversible attachment loss and bone loss are observed histologically and clinically.

37% of the adults in the United States suffer from severe periodontitis. This affliction is closely associated with systemic diseases including those of the liver, diabetes, atherosclerosis, MI, and stroke [270]. Worse yet, tissue wound repair is difficult to achieve during periodontitis [271]. Although simple tooth scaling and root planning can remove pathogenic insult and stop pathogenesis, it fails to restore periodontitis induced soft and hard tissue loss. Collectively, these observations suggest that chronic infections may significantly affect the function of periodontal MSCs— the progenitor cells of all periodontal tissues, even the alveolar bone, which has been

proven to be mainly derived from PDL [272]. Therefore, understanding the long-term effect of periodontitis on periodontal MSCs is a matter of key clinical importance.

LPS is well known as the major PAMP for periodontitis. LPS exclusively bonds to TLR4, leading to the production of cytokines, chemokines, and antimicrobial peptides. Previously, flow cytometry confirmed the heightened expression of the LPS-sensing TLRs2 and 4 on PDLSCs [273] [274]. Then, after P. gingivalis-LPS was added into culture medium, PDLSCs showed enhanced proliferation [275], while E. coli-LPS stimulation had no such effect [276]. Similarly, IL-1β/TNF-α, (known as the major inflammatory cytokines in periodontitis models) could decrease PDLSCs' population doubling time twenty-four hours after in vitro culture [277] with β-catenin pathway activation and noncanonical Wnt/Ca2+ pathway suppression [268]. Nevertheless, when the inflammatory stimulus exceeds a certain level, the effect is reversed. P. gingivalis-LPS42 as well as E. coli-LPS90 stimulation represses the osteogenic potential of PDLSCs, especially when combined with a hypoxic state or TNFα or IFN [278] [279] [280] [281] [282] , and promotes adipogenic and the chondrogenic differentiation abilities [276]. The impaired osteogenic differentiation of PDLSCs could be partly attributed to downregulated Wnt signaling after TNF-α /TNFR binding via NF-kB pathway [279] [280].

However, most of the above conclusions were drawn upon in vitro studies. The commonly implemented approach is to compare PAMP ligands' precondition of PDLSCs with unconditioned MSCs to determine if the pro-inflammatory environment could change MSCs bioactivity in vitro. In fact, the most available in vivo study was achieved through periodontitis model construction on various mammalians [283] [284] [285] [286]. To date, there have been several experimental models used to induce periodontitis in animals, among which the mechanical ligation model is well established and widely used due to high efficiency, repeatability and

convenient operation. Most importantly, the mechanical ligation model could ideally represent periodontitis pathogenesis in humans and simulate the infection outcome akin to what is observed in clinic [287].

Regardless of advances made so far, researchers were still unable to demonstrate MSC changes upon periodontal tissue infection due to the lack of an effective animal model. Thanks to previous efforts, we successfully identified an in vivo marker for periodontal MSCs - Gli1, therefore making it possible to further investigate the in vivo response of periodontal MSCs to tissue infection. In this thesis, we aim to investigate the periodontal MSC response to periodontitis in vivo and to unravel its underlying mechanism. Our findings will help solve some puzzles regarding the persistence of periodontitis for a better periodontal tissue regeneration strategy, especially during periodontitis.

4.2. Methods and Materials

4.2.1. Animals and Tamoxifen Administration

In this section, the same Axin2-lacZ, Gli1-CE;Ai14 and Gli1-CE;Ctnnb$^{fl/-(exon3)}$;Ai14 mice lines were used as in the previous section. All animal experiments were approved by Texas A&M University Institutional Animal Care and Use Committee in accordance with guidelines from the NIH/NIDCR. The same tamoxifen administration was also performed as previously described in sections two and three.

4.2.2. Ligation-Induced Periodontitis Model

Adult mice (6~8 weeks old) underwent general anesthesia with a mixture of ketamine hydrochloride (80 mg/kg) and xylazine (10 mg/kg) administered via intraperitoneal injection. Mice were then postured in a small animal plate in semisupination. To conduct the mechanical ligation model, a sterilized 6.0 nylon thread was wrapped around the right lower first molars. The

suture was gently pushed into gingival sulcus without damaging normal tissue and bilaterally knotting mesio-buccally. The left side remained un-ligated as control.

4.2.3. Micro-CT Scanning and Assessment of Alveolar Bone Loss

After ligation, the mice mandibles were analyzed with a high-resolution micro-CT scanner (Scanco Medical, Basserdorf, Switzerland). The scanning protocol was also set at high resolution, and the X-ray energy settings were 70 kV and 114 μA as previously described [288]. The scanned slice stack was reconstructed into a three-dimensional model and evaluated in Imaris software. Alveolar bone loss (ABL) is represented by the linear distance of Cementoenamel junction (CEJ) to the alveolar crest (AC). The more severe bone loss is, the higher the CEJ-AC distance is. Specifically, CEJ and AC were localized by two point-pins in the "measurement" tab of Imaris.

4.2.4. Paraffin sectioning and H&E staining assay

Next, right and left side mandibles from adult mice following ligation were harvested and fixed in 4% paraformaldehyde overnight, then underwent decalcification in 0.5M EDTA (pH 7.4) at room temperature and shaken for three weeks. Later, the decalcified jaws were dehydrated in gradient ethanol in each different percentage for an hour 50%, 70% Ethanol, 80%, 95% overnight, along with 100% Ethanol 1h *3 times and xylene 1h *3 times. After immersion in a xylene-paraffin (1:1 vol ratio) solution for two hours and paraffin for 1h *3 times, samples were embedded in paraffin, and cut into 5-μm serial proximal-distal sections. Subsequently, slides were deparaffinized, rehydrated, and went through serial solutions as 3* 3 min in Xylene, 3 * 3 min in 100% ethanol, 3 * 3 min in 95% ethanol, 3 * 3 min in 70% ethanol, 3 * 3 min in 50% ethanol and 1 * 5 min in distilled water. Then, sections were stained with Hematoxylin & Eosin for morphology analysis as described in section three.

4.2.5. EdU Incorporation Assay

5-ethynyl-2'-deoxyuridine (EdU) can incorporate into the proliferative DNA chain and be detected through its reaction with fluorescence azides. Likewise, EdU staining is a highly sensitive and efficient method to assay cell proliferation activity. Also, the reagents are almost 1/500th the size of an antibody molecule, and easily penetrate intact hard tissue. To perform EdU staining, we gave adult mice an intraperitoneal injection of EdU (Invitrogen, #A10044) two hours before sacrifice in the dosage of 60ug/g per body weight. Cryo-section slices were later incubated in EdU labeling cocktail for thirty minutes after a PBST wash 3 * 5min. Additionally, the labeling used for this process dye contained Tris-buffered saline (100 mM final, pH 7.6), CuSO4 (4 mM final, Acros #197730010), Sulfo-Cyanine 3 Azide (2-5 uM final, Lumiprobe #D1330) and Sodium Ascorbate (100 mM final, made fresh each use, Acros #352685000).

4.2.6. Confocal imaging assay

Confocal images were captured under a Leica SP 5000 fluorescence microscope with filter settings for DAPI/FITC/TRITC and acquired using Leica LAS AF software. Accordingly, laser energy was set equally at 40% for all sample imaging. Corresponding band-pass filters were set as for DAPI (Ex. 405 nm, BP410-490) and tdTomato (Ex. 543 nm, BP550-595). Furthermore, tiling or individual images were taken at a 1024x1024 frame resolution, 200 Hz frequency with a recommended Z stack interval, while the pinhole for the internal detector was set as 1A.U. Then, Gli1+ cells number were counted manually in six randomly chosen areas of interest within PDL space separately at the root tip area, furcation and interdental septum. Moreover, the relative percentage of Gli1+ cells was calculated as the Gli1+ cells number/total cells (DAPI+) number on both the ligation and non-ligation side.

4.2.7. Real-Time PCR

Molars from five mice were gathered for a one-time assay. One month after ligation, first molars on both sides were extracted with intact PDL attached for real-time PCR assay. Total RNA was also extracted from PDL using RNA Miniprep Kit (Bioland R01-01). Then, the molars were immediately transferred into a 1.5ml tube containing 500ul Buffer LY with the addition of 10ul b-mercaptoethanol and the tissue was homogenized by a rotor starter for a period of seconds. Next, lysis buffer was repeatedly pipetted with a 28G syringe needle on ice twenty times. The solution was then centrifuged at 13,000 rpm for two minutes and the supernatant was transferred to a clean 1.5 mL tube. 1/2 volume 96-100% ethanol was added into the lysate and pipetted five times to mix the solution. Afterwards, the solution was transferred to an RNA column and centrifuged at 13,000 rpm for one minute and flow-through was discarded. Following this process, 400 µL Buffer RB was added to the column and centrifuged at 13,000 rpm for thirty seconds. Then, 500 µL RNA wash buffer was added to the column and centrifuged at 13,000 rpm for thirty seconds—this step was only repeated once. Next, the column was centrifuged with the lid open at 13,000 rpm for one minute. At last, the column was transferred to an RNase-free 1.5 mL tube and 50 µL DEPC-treated ddH2O was added to the center of the column. After centrifuging at 13,000 rpm for one minute, the RNA was eluted for the following cDNA synthesis. The reaction system involved consisted of a 10ul 2x Reaction Mix (Bioland FS01), 9ul total RNA templates, and a 1ul PowerScript Plus RNase. After brief centrifugation, the reaction system was incubated at 25°C for ten minutes and another fifteen minutes at 50°C. The reaction was later halted by heating it at 85°C for five minutes. Then, the system was chilled at 4°C.Next, real-time PCR was performed using a 2x qPCR MasterMix (No ROX) kit (Bioland QP01-00) assay with a SYBR Green I. 10ul reaction solutionprepared as 5ul 2x qPCR MasterMix (No

ROX) + 0.1ul forward primer +0.1ul reverse primer + 4.3 nuclease-free water+ 0.5ul temple DNA. For subsequent thermal cycling, a CFX96 Real-Time System (Bio-Rad iCycler) was used at 95 °C for ten minutes, then forty cycles of 95 °C for fifteen seconds and 60 °C for sixty seconds. Furthermore, the relative mRNA expression level of each gene was calculated on the basis of a standard curve of cycle thresholds and normalized to reference genes with either β-actin, tubulin or GNDPH expression as the internal control. Afterwards, real-time PCR was performed in triplicate for each sample. Additionally, all experiments in this section were repeated four times. Also, the osteogenic related genes' expression level was evaluated via real-time PCR following the same protocol. The result was calculated as follows:

ΔCq=Cq target gene-Cq reference gene

ΔΔCq= ΔCq ligation side- ΔCq non-ligation side

2- ΔΔCq=fold difference of target gene expression

All the primers used are shown in Table 3

4.2.8. X-Gal Staining

Both ligation and non-ligation side mandibles were harvested from Axin2-Lacz reporter mice one month after ligation model construction. They were fixed in 0.5% glutaraldehyde solution containing 2mM $MgCl_2$ at 4℃ overnight and decalcified in 0.25M EDTA with 2mM $MgCl_2$ at 4℃ for one week. Next, samples were dehydrated with a gradient 30% and then 60% sucrose with 2mM $MgCl_2$ at 4℃ until the sample sank down. Frozen sections were soon obtained. After PBS with 2mM $MgCl_2$ wash for ten minutes on ice, slices were postfixed in cold 0.5% glutaraldehyde solution with 2mM $MgCl_2$ for ten minutes also on ice. Slides were later rinsed with cold PBS plus 2mM $MgCl_2$ solution for 2*10min. Additionally, the ß-gal staining solution was used to stain LacZ positive cells at 37℃ for two days. Slides were then washed

with PBS at RT twice for five minutes. 4% PFA was also used to postfix the slices at RT for thirty minutes. Next, Nuclear Fast Red was used to counterstain the slices for two minutes. Then, after a two minutes dehydration in 70% ethanol, Eosin was used to stain the cytoplasm. The slices were further dehydrated with gradient ethanol solutions at 80% and 95% for two minutes and 100% 2*2min. At last, slides were mounted with mounting medium (Vol ratio xylene: permount =1:1).

4.2.9. The FACS (Fluorescence-Activated Cell Sorting) Analysis of Gli1+ Cells Counting

Mandibular first molars were carefully extracted from the alveolar bone. Attached bone debris was then gently removed. Molars were placed into 1.5ml tube containing 600 µl tissue digestion solution (200 U/ml DNase I (Sigma; 1:100), 4 mg/ml Dispase (1:10) and 3 mg/ml Collagenase, type 1 (Worthington Biochemical Corporation; 1:10) in HBSS plus Ca2+ and Mg2+). Next, ten molars were gathered into one tube and incubated at 37 ℃ for two hours. After a brief vortex (three times for five seconds at medium speed), the supernatant was transferred to another tube which contained 600 µl staining medium (2% goat serum in HBSS without Ca2+ and Mg2+) on ice and centrifuged at 1,500 rpm for five minutes at 4℃. Later, the pellet was resuspended with 500 µl staining medium by pipetting five times. Each sample was then examined using a flow cytometry machine with a gating analysis. The results were analyzed and displayed by Flowjo software to obtain the relative Gli1+ cells' percentage on the ligation side and non-ligation side of molar PDL.

4.2.10. PEGASOS Tissue Clearing Method

Mice were sacrificed by transcardial perfusion with 50ml 0.02% heparin-PBS (w/vol) (Sigma-Aldrich, 84020) and 20ml 4% PFA —as described in a previous study 241 under the administration of xylazine and ketamine anesthetics (Xylazine 10-12.5 mg/kg; Ketamine, 80-100

mg/kg body weight). Afterwards, mandibles were collected and fixed in 4% PFA overnight at RT. Samples were then immersed in 0.5 M EDTA (pH=7.0) solution at 37°C to decalcify for four days. This step was followed by decolorization with 25% (vol % in dH2O) EDTP solution (Sigma-Aldrich, 122262) for one day to remove remaining blood heme under constant shaking at 37°C and also stepwise delipidation. This segment was performed at 37°C, with shaking for six hours in each of the following sequentially: 30% (vol% in dH2O) Tert-Buturnol (TB, Sigma-Aldrich, 360538), 50%TB, 70%TB and overnight dehydration with TB-poly (ethylene glycol) methyl ether methacrylate average Mn500 (PEGMMA500) (Sigma-Aldrich, 447943) (vol ratio7:3). All the above mediums' pH was adjusted to 9.5 or above with 3% vol pure EDTP. Finally, samples were immersed in clearing medium benzyl benzoate (BB) (Sigma-Aldrich, B6630) -PEG-MMA500 (R.I=1.543) with 5% EDTP before imaging.

4.2.11. Statistical Analysis

SPSS software version 21.0 was used for statistical analysis. A Paired t test was conducted for mean comparison and P value of less than 0.05 is considered statistically significant. *$p<0.05$, ** $p<0.01$, ***$p<0.001$. Moreover, Prism 7 was used to display the quantification results. Data was shown as Mean ± SEM.

4.3. Results

4.3.1. Periodontitis Compromised Gli1+ MSCs' Contribution to Periodontal Tissue Through De-Activation

Ligation model was constructed on 6~8 weeks old Gli1-CreERT2; Ai14 mice. Two weeks were given for periodontitis establishment. Then, two shots of tamoxifen were given to trace Gli1+ cells for another two weeks and two months. Both ligation side and non-ligation side mandibles were collected for micro-CT, H&E staining and lineage tracing assay. Four weeks

after placement, the ligature caused severe alveolar bone loss compared with the non-ligation side (Fig 15.a-d). Next, H&E staining showed a widened PDL space and decreased AC height of the ligated molar (Fig. 15 d) when compared with the un-ligated molar (Fig. 15b). Also, inflammatory polymorphonuclear neutrophils (PMNs), lymphocytes were noticed infiltrating into PDL (arrow in Fig. 15d1), which was identical to clinical periodontitis pathological manifestation. However, there was no obvious inflammatory cell infiltration on the non-ligation side (Fig. 15b1). Quantification results indicated that alveolar bone height decreased ~500 mm compared with the non-ligation side (Fig. 15e) whereas PDL width increased ~45 mm on the ligation side (Fig. 15f). Furthermore, an overview of lineage tracing results implied that two weeks after the ligation model establishment, the Gli1+ cells normally distributed within PDL on both the non-ligation side and ligation side two days after tamoxifen induction (Fig. 15g,h). Meanwhile, three weeks after ligation, reduced EdU+/Gli1+ cells were noticed on the ligation side compared with the non-ligation side (Fig. 15i,j). Correspondingly, due to compromised Gli1+ MSCs activation, less cells in the ligation side of the periodontium were detected in contrast to non-ligation side periodontium and Gli1+ cells in periodontium on the ligation side were less than the control side as indicated by two weeks of lineage tracing (Fig. 15k,l). In addition, quantification results showed that Gli1+ cells accounted for ~18% of PDL cells and there was no significant difference between the ligation and non-ligation side. Likewise, two weeks lineage tracing results showed that Gli1+ cells could be normally activated and gave to ~60% PDL cells on the control side but only to ~20% on the ligation side (Fig. 15m). Then, local magnification revealed that on the non-ligation side, Gli1+ cells normally contributed to PDL in the root tip, furcation and interdental septum areas (Fig. 15k1-3) which accounted for around 60% PDL cells (Fig. 15n). While on the ligation side, a dramatic decrease in Gli1+ cells inside PDL

was noticed (Fig. 15l1-3,n), especially in furcation and interdental septum areas where Gli1+ cells occupied only 15%~20% PDL because of to the closer distance to the pathogenic ligature insult (Fig. 15n).

Besides the results above, ABL was found more severe with ligation time (Fig. 16a-d). Later, at ten weeks post ligation, CEJ-AC distance increased by two folds on the ligation side than the non-ligation side (Fig. 16e). Accordingly, ligation led to increased PDL width by ~50 mm (Fig. 16d,f). Also, PMNs infiltration was found in PDL tissue (arrow in Fig. 16d1) which was absent on the non-ligation side (Fig. 16b1). Subsequently, Gli1+ cell distribution reduced on the ligation side (Fig. 16g,h). On a different note, following a tracing period of two months on the non-ligation side, Gli+ MSCs showed the possibility of contributing to the majority of PDL (80%~100%). Yet under periodontitis, Gli1+ MSC activation was compromised. For instance, only about 60% PDL component was at the root tip, considering the remainder that was 50% in furcation and 20% in interdental septum areas, derived from Gli1+ periodontal MSCs (Fig. 16g1-3,h1-3,i). Also, Gli1+ MSC commitment to cementum (Fig. 16g1) and alveolar bone (Fig. 16g2) was compromised on the ligation side in comparison with the non-ligation side (Fig. 16h1,h2). Similarly, quantification results indicated that Gli1+ MSCs derived cementocytes accounted for ~50% cementum cells on the non-ligation side while only ~25% cementocytes were Gli1 positive on the ligation side (asterisks in Fig. 16 g1,h1, Fig. 16j). In return to the non-ligation side, about 60% osteocytes inside the furcation area alveolar bone were Gli1+ MSCs derived, but on the ligation side only ~40% were Gli1+ (arrows in Fig. 16g2,h2, Fig. 16k). Therefore, evidence proves that chronic periodontitis ultimately repressed lineage commitment ability of Gli1+ periodontal MSCs.

4.3.2. Chronic periodontitis inhibited Gli1+ MSCs maintenance

One connected issue caused by chronic periodontitis is its refractory nature towards conventional treatment. Tooth scaling and root planning are not effective enough for alveolar bone regrowth. Hence, failure of tissue regeneration after pathogenic insult removal suggests the existence of inhibited Gli1+ MSCs in a periodontitis situation. To investigate chronic periodontitis' impact on Gli1+ MSCs maintenance, we performed an intervention experiment. First, a ligature was placed on the lower right first molars of mice. One month later, the ligature insult was removed and two or three months were given for Gli1+ MSCs to regenerate periodontal tissue while the lower left first molars remained un-ligated as a control. Unfortunately, no regain of alveolar bone was noticed on the ligature removal side no matter if two or three months passed after removal (Fig. 17a, b, d, e). However, CEJ-AC distance increased by 50% on the ligature removal side than the non-ligation side (Fig. 17c). This fact implied the compromised MSCs maintenance.

To testify this point, we collected total PDL cells on both the non-ligation and ligation side molars of adult Gli1-Cre^{ERT2}; tdTomato mice four days after tamoxifen injection. Gli1+ periodontal MSCs (Dapi^{low}/PE-A^{hi}) were then sorted and their frequency within total isolated cells was calculated automatically after FACS assay. Later, quantification demonstrated that Gli1+ MSCs accounted for ~1.2% of total cells collected from non-ligation side molars whereas within ligation side molars, Gli1+ MSCs only accounted for ~0.3% (Fig. 17g). Therefore, significant decrease of Gli1+ MSCs percentage suggested that periodontitis consumed Gli1+ periodontal MSCs.

Then, we performed a longer-term ligation-periodontitis model on Gli1-CreERT2; tdTomato mice. Two days after tamoxifen injection, Gli1+ MSCs were shown reduced on the

ligation side three and six months after ligation (Fig. 17h-k). Then, quantification results indicated that in comparison with the non-ligation side, Gli1+ cells percentage reduced 40% ~50% on the ligation side (Fig. 17l).

4.3.3. Vasculature Density was Reduced in a Periodontitis Situation

PDL is known as the highly vascularized supporting tissues of the teeth. This vasculature provides a reliable microenvironment for the homeostasis of Gli1+ periodontium MSCs. However, little is known so far about the vasculature changes under untreated advanced periodontitis. Further, Vascular Endothelial-Cadherin (Cdh5) is a specific marker to label blood vessel endothelial cells [242]. Thus, we conducted research using a ligation-induced periodontitis model on six weeks old Cdh5-Cre; tdTomato mice. Two months later, both side mandibles were collected to clear with the PEGASOS method as described earlier [255] (Fig. 18a,b). Under the confocal microscope (Leica, SP8), the whole vasculature system of the ligated and non-ligated first molar was visualized for morphological comparison at a three-dimensional scale. The overall vascularity of PDL on the ligation side decreased significantly compared with the un-ligated molar (Fig. 18c, d). Vasculature shrinkage was also noticed on the ligation side molar regardless if it was in the coral 1/3, middle 1/3 or apical 1/3 segment of PDL, featured by a reduction in blood vessel diameter and density (Fig. 18c1, d1, c2, d2, c3, d3, e-g). Likewise, quantification results indicated that the vasculature density decreased by ~20% in coronal 1/3 PDL, ~15% in the middle 1/3 PDL and ~40% in apical 1/3 PDL. Overall, loss of the vasculature niche helps explain the compromised periodontal MSCs bioactivity.

4.3.4. Wnt Activity Was Down-Regulated During Periodontitis

Our data has proven the significance of Wnt signaling for Gli1+ periodontal MSCs activation under normal conditions. To evaluate Wnt signaling activity in periodontitis

conditions, a ligation-periodontitis model was completed on 6~8 week old Axin2-lacZ mice. Following a one month time period, a stronger lacz stain was observed inside the non-ligation side PDL than the ligation side no matter if it was in the root apical region (Fig. 19a in comparison of Fig. 19d), furcation (Fig. 19b versus Fig. 19e) or the interdental septum areas (Fig. 19c compared with Fig. 19f). Quantification also demonstrated that on the non-ligation side, ~60% cells inside the root apex part of PDL were Axin2 positive and responded to Wnt signaling, while on the ligation side only ~30% cells were Axin2+ (Fig. 19g). In the furcation area, Wnt responsive cells occupied ~60% PDL on the non-ligation side and ~40% on the ligation side (Fig. 19h). Similarly, Axin2+ cells accounted for ~60% cells within non-ligated molars' PDL in the interdental septum area and ~40% PDL cells on the ligation side were labeled by Axin2 (Fig. 19i). To further examine Wnt signaling activity at the molecular level, RNA was separately extracted from ligated and un-ligated molars' PDL for RT-PCR assay one month after periodontitis induction. Hence, the results of this experiment confirmed that Wnt signaling activity was down-regulated at all checkpoints under periodontitis. For example, on the ligation side, relative expression of target genes in canonical Wnt signaling pathway reduced to various extents, including Axin2 (down to 40% of the non-ligation/control side level), Ctnnb (decreased by 20%), TCF7 (reduced ~60%), LEF1 (half decrease), cyclin D (only had a remaining 60% of expression activity) (Fig. 19j). Along with Wnt down regulation, osteogenic genes were also negatively affected. The expression of Bone Morphogenetic Protein 4 (BMP4), which is involved in MSCs' osteoblastic commitment, experienced a 60% reduction. Furthermore, transcription factor SP7 (also called Osterix) functions as a master regulator of bone formation through promoting osteogenic precursors to differentiate into osteoblasts. Its relative expression was down-regulated to about 50% of the non-ligation side. Correspondingly, Runt-Related

Transcription Factor 2 (Runx2) is responsible for osteoblasts' differentiation into terminal osteocytes. On the ligation side, its expression level was only 60% of that of the non-ligation side (Fig. 19j). Collectively, the above data convinced us that chronic periodontal tissue infection depressed canonical Wnt signaling activity.

4.3.5. Over-Activation of Wnt Signaling Partially Rescued Tissue Loss and Gli1+ MSCs Inhibition During Periodontitis

Since our experiment showed that Wnt activity can be subject to periodontitis, it gave us a hint that over-activation of Wnt signaling may counteract periodontitis induced tissue loss. We implemented a ligation model on adult Gli1-Cre^{ERT2}; Ctnnbfl/-$^{(exon3)}$; tdTomato mice. Two weeks after ligature placement, tamoxifen was given to induce b-catenin/Wnt signaling overexpression within Gli1+ cells and tracing took place meanwhile for another two weeks. Both sides of the mandibles were then collected from the mutant mice for a micro-CT and confocal imaging assay.

Micro-CT results showed that in the Wnt over-activated mutant mice, the distance between CEJ and AC was similar on both the ligation and non-ligation side (Fig. 20a-d) and statistics analysis showed no significant difference (Fig. 20e). The increase of Wnt signaling activity could help maintain alveolar bone height even under periodontitis. Then, confocal images showed that two weeks after tamoxifen injection, Gli1+ MSCs were activated to populate among the entire periodontium on both sides (Fig. 20f, g, f1-3, g1-3) with ~85% of PDL components labeled as Gli1+ cells on the non-ligation side while on the ligation places, the labeling efficiency was equally high within PDL space by ~75% in the root tip area, ~85% in the furcation area, and ~70% in interdental septum area, which is not much different from non-ligation side, as indicated in the quantification (Fig. 20h). Thus, the over-activation of Wnt

signaling could alleviate periodontal tissue loss under periodontitis by counteracting Gli1+ MSC deactivation.

4.4. Discussion

Complicated crosstalk exists between stem cells and the immune system. In basic science, MSCs are non-immunogenic in favor of their allogeneic transplantation without host immunosuppression [289]. In fact, mesenchymal stem cells do not trigger CD4+ cell activation. They are able to escape lysis by CD8+ cytotoxic lymphocytes and Natural Killer (NK) cell-specific lysis [290] and are comparatively more resistant to cytotoxic T cells lysis. By the same token, MSCs inhibit dendritic cells' maturation and antigen presentation capability [291], transforming the M1 pro-inflammatory macrophage to a M2 anti-inflammatory phenotype [9 292] and suppressing the de novo production of TNF-a from mast cells [291]. As for the existence of an acquired immune system, MSCs negatively regulate the proliferation and activation of lymphocytes, NK cells, and T Helper (Th) cells but promote Regulatory T Cells'(Tregs) proliferation as well as immunomodulatory properties [9 292]. MSCs inhibit Th1 cell development but induce a bias towards Th2 differentiation [293]. Accordingly, a high concentration of MSCs negatively affect the chemotactic properties of B cells by downregulating the expression of chemokine receptors CXCR4, CXCR5 and CCR7B as well as the chemotaxis to CXCL12, the CXCR4 ligand, and CXCL13, the CXCR5 ligand. Therefore, an abundance of studies are focusing on the application of ex vivo MSCs to enhance biomaterials' tissue regeneration ability under infection. Interestingly, the compromised tissue regeneration under periodontitis contradicts this fact, which suggests the impaired MSCs function.

Even with all of the information discovered thus far, another point of discussion is that Wnt signaling has been proven important in Gli1+ periodontal stem cell bioactivity. In fact a

canonical Wnt signaling blockage in the periodontium results in major defects within PDL and alveolar bone formation [260]. Meanwhile, enhancing Wnt activity by genetically knocking out Wnt inhibitors such as SOST or pharmacologically administering sclerostin antibody could restore alveolar bone osteocyte morphology, PDL phenotype, and bioactive molecule function in a periodontitis mouse model [272]. However, our current data indicated a major treatment problem— the vasculature niche and canonical Wnt signaling activity within Gli1+ MSCs were both interrupted during periodontitis. The resultant inhibition of Gli1+ periodontal MSCs maintenance and activation is closely related to periodontal tissue loss. Yet, we also did not exclude the involvement of osteoclasts in the alveolar bone loss. For instance, varying studies have demonstrated that RANKL-mediated osteoclastogenesis played a pivotal role in periodontitis bone resorption [294] [102]. Likewise, activated T lymphocytes may mediate bone resorption through excessive secretion of RANKL [102] [295] [296]. Accordingly, a ligation-induced periodontitis model induced upregulation in osteoclastic related mRNA expression [297]. Furthermore, inhibition of osteoclastogenesis could attenuate ligation induced periodontitis in rats [298].

To continue on the path of disease knowledge, in vivo MSCs are subjected to an undermined microenvironment which is under chronic tissue infection. In periodontitis, the major source of PAMPs is LPS from P.g. TLR4, the exclusive receptor for LPS. It has been found expressed on PDLMSCs' surface in various in vitro studies. However, in our experiments, we found no overlap between Gli1+ MSCs and TLR4 in either PDL or a sagittal suture. Instead, TLR4 was particularly located on blood vessels' lumen while the Gili+ cells were on the outside of it. Then, we crossed TLR4flox mice with G.T mice and performed the ligation model on their offspring which yielded no anti-periodontitis effects on the mutant mice. In addition to that

revelation, the ABL on the ligation side was substantially more severe than the non-ligation side (data not shown). Collectively, this data indicated that Gli1+ MSCs were negative for TLR4. Thus, the underlying mechanism for the suppression of Gli1+ MSCs under periodontitis is more complicated than expected. It is a combined effect of proinflammatory factors instead of sole TRL4/MyD88 signaling within Gli1+ MSCs. However, we have reservations about this statement because some previous studies conclude that under inflammation, the TLR expression of pre-conditioned MSCs is positively related to the dosing of inflammatory ligands and incubation time. Also, transplanted IL1r1/MyD88 KO MSCs were shown with higher regeneration ability than widetype MSCs [163]. In this experiment, we might not have given a long enough time for periodontitis to induce TLR expression in Gli1+ periodontal MSCs.

Despite some time-related ponderings on other parts of the experiments, the ligation model for the study was widely used in the field with good reproductivity regardless of the mice's background. Two weeks was enough time to establish periodontitis with soft and hard tissue loss. In our investigation, we also discovered that some researchers modified this model by soaking their ligature in a P.gingivalis (Pg) suspension [299]. Gavage is another method to induce an oral cavity infection. In this scenario, animals are subjected to an oral inoculation of Pg suspension placed directly into the oral cavity carefully with a micropipette in two days intervals [297]. Unfortunately, the operation is challenging and repetitive with a low efficacy rate. Usually, it takes longer than four weeks to reproduce significant alveolar bone loss. The final way found to purposely infect the oral cavity is to directly inject heat-killed P.g into vestibular and oral gingiva using a microfine insulin syringe. The protocol needs to be repeated in two-day intervals throughout the whole experiment duration. The localized injection could cause rapid and severe periodontal tissue destruction and an increase in pro-inflammatory cytokine

expressions, such as IL-1β, IL-6, and TNF-α [300] [301]. The disadvantage of this method is the demanding nature of the operation.

One item impacted by this intentional infection is periodontal tissue, known as highly vascularized supporting tissues of the teeth. However, little is known about the vascular changes in chronic periodontitis. Some studies mentioned a significant increase in blood vessel diameters, basement membrane thickness, and numerical density within the connective tissue subjacent to the periodontal pocket lining epithelium [302]. Accordingly, morphological changes were explained as an epithelial response to microbial flora in the local environment. However, in our study, we compared the vasculature differences within PDL between physiological and pathological conditions for the first time using a PEGASOS based 3D imaging technique. A three-dimensional view indicated vessel shrinkage and decrease in vasculature density during late stage periodontitis which could be the origin of impaired MSCs bioactivity. This fact also implies the necessity to enhance blood vessel regeneration when transplanting MSCs for periodontal tissue wound repair in a periodontitis situation.

In addition, we demonstrated in this study that enhanced Wnt signaling was able to counteract the depression from tissue infection to maintain periodontal tissue homeostasis, which may provide insight for potential stem cell-based tissue regeneration for biomaterials study and periodontal disease treatments.

5. CONCLUSION

Stem cells play a critical role in tissue homeostasis. To illustrate, periodontal MSCs are supposed to be a hierarchical priority, giving rise to the whole periodontium and obtaining involvement in the tissue injury repair process. The disease which directly influences this process is called periodontitis, a common chronic periodontal tissue disease that affects millions of people worldwide. The hardness of tissue regeneration under periodontitis implies the dysfunction of periodontal MSCs within the infectious microenvironment. Hence, researchers wanted to find out more about the disease. To date, there have been various studies focusing on phenotype changes caused by periodontitis, its underlying mechanism, and potential treatment strategies including periodontal tissue engineering and drug administration. In addition, all relevant studies are either in forms of in vitro MSCs culture treated with periodontitis PAMPs or the evaluation of periodontitis impacts on terminal differentiated tissues. However, the in vivo response of periodontal MSCs to periodontal diseases is poorly understood due to the lack of a reliable in vivo marker for periodontal MSCs. An in vitro study could never replace an in vivo study because the stem cell niche is extremely important for stem cell behavior.

To assist in remedying the lack of the latter study, there have been several in vivo periodontal MSCs markers reported, including αSMA, Axin2, and PTHrP. Among this group, αSMA's labeling efficiency is pretty low with only a small portion of osteoblasts and cementocytes expressed in SMA9 even seven weeks after labeling [68]; Wnt-responsive Axin2+ cells are quiescent within PDL and highly proliferative upon injury. They migrate away from the PDL into the tooth extraction socket and become osteoprogenitors [69]. Unfortunately, their contribution to PDL and cementum is unknown. Likewise, Axin2 is not a unique marker for periodontium. Although there could be exceptions, cementoblasts and odontoblasts were also

found Axin2 positive. Another MSC marker is PTHrP+ cells, which are important for molar root development and give rise to the majority of PDL and parts of osteocytes. However, PTHrP+ cells' contribution to tissue turnover in adults is minor [70]. For adult periodontal MSCs identification, all of the above markers are not convincing enough. Therefore, we examined Gli1 expression within adult molar periodontium based on a previous study about Gli1 as the perfect marker for mouse incisor MSCs and suture MSCs. In our study, lineage tracing experiments proved that Gli1+ cells could give rise to the majority of the periodontium complex no matter if it was at a young age such as P3-P14 or in adults. Also, Gli1+ cells could quickly respond to injury with an accelerated lineage commitment activity. Surprisingly, we found that in vivo Gli1+ cells express none of the traditional MSCs surface markers such as CD73, CD44 or CD146, although in vitro Gli1+ cells did. In this way, we successfully identified Gli1 as a good in vivo marker for periodontal MSCs.

Besides just performing that successful marker search, we took advantage of the PEGASOS tissue clearing technique and detected a neurovascular bundle as the Gli1+ periodontal MSCs niche in vivo. In this scenario, we found that Gli1+ cells closely surround blood vessels and nerves, populating along with them. Because nerve and blood vessels are confluent at the root tip area, the primitive Gli1+ MSCs are mostly located at the apex region. This conclusion was in line with previous studies on Gli1+ cells [228 59] and other stem cells [303 224]. In addition, this observation asserted that when compared with other tissue stem cell markers including aSMA, LepR, NG2, and PDGF, Gli1+ cells not only show the best performance in labeling periodontium, but also more primitively give rise to some populations such as aSMA+ cells and LepR+ cells.

Even though there has been notable activity in our work so far pertaining to the advance of periodontal MSC markers and a designated niche, we decided to take the project a step farther. Many past studies have clarified the importance of Wnt signaling in periodontium homeostasis [304] [267] [259] with the conclusion that Wnt signaling helps balance between fibrous tissue and osseous tissues. Nevertheless, few of them have linked Wnt to periodontal MSCs in situ. In our study, we first proved the existence of Wnt signaling within Gli1+ periodontal MSCs. Then, through a gain and loss of function study, we directly demonstrated the functional reliance of Gli1+ cells on Wnt signaling activation. A β-catenin knockout led to the failure of Gli1+ cells activation and periodontium loss. Conversely, a gain-of-function mutation in β-catenin enhanced the proliferation and activation of Gli1+ cells, which resulted in cementum overgrowth.

After those procedures were finished, we were able to investigate the in vivo response of Gli1+ MSCs to periodontitis and the associated regulatory mechanism through performing ligation induced periodontitis model on Gli1-Cre mice. Lineage tracing data at different time points after tooth ligation revealed the failure of Gli1+ cells' activation to populate along PDL, as well as form a commitment to cementum and alveolar bone. We found severe alveolar bone loss and widened PDL detected by Micro-CT and H&E staining on the ligation side. The data was finally gathered from multiple phases of the experiments and we came to several brief conclusions. First, established periodontitis could consume Gli1+ MSCs behind what may be their impaired vascular niche. Accordingly, canonical Wnt signaling activity was evaluated by Axin2-LacZ reporter mice and Realtime PCR. Later, down-regulation was noticed on the ligation side of the mice. Further, the rescue experiment by Wnt over-activation confirms the necessity of Wnt signaling in Gli1+ MSCs mediated periodontal tissue regeneration. Thus, all of the data collectively implied that Wnt agonists or genetic Wnt signaling activation could be a possible

approach to treat periodontitis. Additionally, blood vessel regrowth is essential for tissue regeneration.

Nonetheless, there are some questions remaining to be answered. First, we need to further explore the NVB niche. Our current data implied that Gli1+ periodontal MSCs are in spatially close relation to vasculature and nerves. However, we have not identified the specific vasculature and nerve type that support Gli1+ MSCs function and how these structures participate in the regulation of periodontal MSCs. To answer this question, we need to isolate Gli1hi and Gli1low cells from adult molar periodontium to run an RNA sequence to screen out highly expressed genes, especially those related to vasculature and nerves. Then, to confirm their role in MSCs regulation, we will do a traditional gain and loss of function study to examine phenotype changes and lineage tracing maps of Gli1+ MSCs. If possible, physically cutting off specific blood vessels or nerves can be used to verify their function.

Secondly, we want to perform additional research on Wnt signaling. This concept is known as a short-range intercellular signal in an autocrine model [85] [305]. During our study, we verified that Gli1+ MSCs themselves express Wnt, but stem cells are quiescent. The MSCs niche cells are presumed to be the major Wnt source controlling MSCs' bioactivity. In future studies, Wnt canonical and noncanonical signaling activity will be monitored after niche cell depletion to demonstrate Wnt`s distribution within the NVB niche. Besides considering the interaction between the dual types of Wnt signaling, it is necessary to elucidate the precise role of the non-canonical Wnt signaling pathway in Gli1+ MSCs regulation. To solve this puzzle, non-canonical Wnt signaling reporter mice are required to map the distribution pattern within adult molar periodontium. Afterwards, a loss and gain of function study should be performed for detailed information.

Third, the underlying mechanism causing the inhibition of Gli1+ MSCs during periodontitis should be further studied. To move forward with this investigation, we will digest and isolate adult Gli1+ cells from ligated and un-ligated adult molar PDL for an RNA sequencing assay. Differently expressed genes will then be analyzed via a loss and gain of function study for the ultimate purpose of a building and implementing a detailed mechanism study. Also, with supplementary efforts, we hope to have a better understanding of the molecular pathogenesis in periodontal disease. This awareness is especially relevant to periodontal MSCs, which will help us to design a stem cell treatment therapy for periodontitis in the near future.

REFERENCES

1. Pittenger MF, Mackay AM, Beck SC, et al. Multilineage potential of adult human mesenchymal stem cells. *Science* 1999;284:143-147.

2. Gronthos S, Mankani M, Brahim J, Robey PG, Shi S. Postnatal human dental pulp stem cells (DPSCs) in vitro and in vivo. *Proc Natl Acad Sci U S A* 2000;97:13625-13630.

3. Miura M, Gronthos S, Zhao M, et al. SHED: stem cells from human exfoliated deciduous teeth. *Proc Natl Acad Sci U S A* 2003;100:5807-5812.

4. Seo BM, Miura M, Gronthos S, et al. Investigation of multipotent postnatal stem cells from human periodontal ligament. *Lancet (London, England)* 2004;364:149-155.

5. Sonoyama W, Liu Y, Fang D, et al. Mesenchymal stem cell-mediated functional tooth regeneration in swine. *PLoS One* 2006;1:e79.

6. Agha-Hosseini F, Jahani MA, Jahani M, Mirzaii-Dizgah I, Ali-Moghaddam K. In vitro isolation of stem cells derived from human dental pulp. *Clinical transplantation* 2010;24:E23-28.

7. Rashedi I, Gomez-Aristizabal A, Wang XH, Viswanathan S, Keating A. TLR3 or TLR4 Activation Enhances Mesenchymal Stromal Cell-Mediated Treg Induction via Notch Signaling. *Stem Cells* 2017;35:265-275.

8. Morsczeck C, Gotz W, Schierholz J, et al. Isolation of precursor cells (PCs) from human dental follicle of wisdom teeth. *Matrix biology : journal of the International Society for Matrix Biology* 2005;24:155-165.

9. Zhang Q, Shi S, Liu Y, et al. Mesenchymal stem cells derived from human gingiva are capable of immunomodulatory functions and ameliorate inflammation-related tissue destruction in experimental colitis. *J Immunol* 2009;183:7787-7798.

10. Horwitz EM, Le Blanc K, Dominici M, et al. Clarification of the nomenclature for MSC: The International Society for Cellular Therapy position statement. *Cytotherapy* 2005;7:393-395.

11. Dominici M, Le Blanc K, Mueller I, et al. Minimal criteria for defining multipotent mesenchymal stromal cells. The International Society for Cellular Therapy position statement. *Cytotherapy* 2006;8:315-317.

12. Guimaraes-Camboa N, Cattaneo P, Sun Y, et al. Pericytes of Multiple Organs Do Not Behave as Mesenchymal Stem Cells In Vivo. *Cell Stem Cell* 2017;20:345-359.e345.

13. Bianco P, Riminucci M, Gronthos S, Robey PG. Bone marrow stromal stem cells: nature, biology, and potential applications. *Stem Cells* 2001;19:180-192.

14. Dellavalle A, Maroli G, Covarello D, et al. Pericytes resident in postnatal skeletal muscle differentiate into muscle fibres and generate satellite cells. *Nat Commun* 2011;2:499.

15. Zuk PA, Zhu M, Ashjian P, et al. Human adipose tissue is a source of multipotent stem cells. *Molecular biology of the cell* 2002;13:4279-4295.

16. Gargett CE, Chan RW, Schwab KE. Endometrial stem cells. *Current opinion in obstetrics & gynecology* 2007;19:377-383.

17. Harvanova D, Tothova T, Sarissky M, Amrichova J, Rosocha J. Isolation and characterization of synovial mesenchymal stem cells. *Folia biologica* 2011;57:119-124.

18. Patel AN, Park E, Kuzman M, Benetti F, Silva FJ, Allickson JG. Multipotent menstrual blood stromal stem cells: isolation, characterization, and differentiation. *Cell transplantation* 2008;17:303-311.

19. Weiss ML, Troyer DL. Stem Cells in the Umbilical Cord. *Stem Cell Rev* 2006;2:155-162.

20. Weiss ML, Medicetty S, Bledsoe AR, et al. Human umbilical cord matrix stem cells: preliminary characterization and effect of transplantation in a rodent model of Parkinson's disease. *Stem Cells* 2006;24:781-792.

21. Grompe M. Tissue stem cells: new tools and functional diversity. *Cell Stem Cell* 2012;10:685-689.

22. Mendez-Ferrer S, Michurina TV, Ferraro F, et al. Mesenchymal and haematopoietic stem cells form a unique bone marrow niche. *Nature* 2010;466:829-834.

23. He H, Yu J, Liu Y, et al. Effects of FGF2 and TGFbeta1 on the differentiation of human dental pulp stem cells in vitro. *Cell biology international* 2008;32:827-834.

24. Gronthos S, Brahim J, Li W, et al. Stem cell properties of human dental pulp stem cells. *J Dent Res* 2002;81:531-535.

25. Shi S, Bartold PM, Miura M, Seo BM, Robey PG, Gronthos S. The efficacy of mesenchymal stem cells to regenerate and repair dental structures. *Orthodontics & craniofacial research* 2005;8:191-199.

26. Batouli S, Miura M, Brahim J, et al. Comparison of stem-cell-mediated osteogenesis and dentinogenesis. *J Dent Res* 2003;82:976-981.

27. Arthur A, Shi S, Zannettino AC, Fujii N, Gronthos S, Koblar SA. Implanted adult human dental pulp stem cells induce endogenous axon guidance. *Stem Cells* 2009;27:2229-2237.

28. Yu J, He H, Tang C, et al. Differentiation potential of STRO-1+ dental pulp stem cells changes during cell passaging. *BMC cell biology* 2010;11:32.

29. Zhang W, Walboomers XF, Van Kuppevelt TH, et al. In vivo evaluation of human dental pulp stem cells differentiated towards multiple lineages. *Journal of tissue engineering and regenerative medicine* 2008;2:117-125.

30. Gomes JA, Geraldes Monteiro B, Melo GB, et al. Corneal reconstruction with tissue-engineered cell sheets composed of human immature dental pulp stem cells. *Invest Ophthalmol Vis Sci* 2010;51:1408-1414.

31. Kiraly M, Kadar K, Horvathy DB, et al. Integration of neuronally predifferentiated human dental pulp stem cells into rat brain in vivo. *Neurochem Int* 2011;59:371-381.

32. Sugiyama M, Iohara K, Wakita H, et al. Dental pulp-derived CD31(-)/CD146(-) side population stem/progenitor cells enhance recovery of focal cerebral ischemia in rats. *Tissue Eng Part A* 2011;17:1303-1311.

33. Gandia C, Arminan A, Garcia-Verdugo JM, et al. Human dental pulp stem cells improve left ventricular function, induce angiogenesis, and reduce infarct size in rats with acute myocardial infarction. *Stem Cells* 2008;26:638-645.

34. Xuan K, Li B, Guo H, et al. Deciduous autologous tooth stem cells regenerate dental pulp after implantation into injured teeth. *Science translational medicine* 2018;10.

35. Sakai VT, Zhang Z, Dong Z, et al. SHED differentiate into functional odontoblasts and endothelium. *J Dent Res* 2010;89:791-796.

36. Nakamura S, Yamada Y, Katagiri W, Sugito T, Ito K, Ueda M. Stem cell proliferation pathways comparison between human exfoliated deciduous teeth and dental pulp stem cells by gene expression profile from promising dental pulp. *J Endod* 2009;35:1536-1542.

37. Kerkis I, Kerkis A, Dozortsev D, et al. Isolation and characterization of a population of immature dental pulp stem cells expressing OCT-4 and other embryonic stem cell markers. *Cells, tissues, organs* 2006;184:105-116.

38. Koyama N, Okubo Y, Nakao K, Bessho K. Evaluation of pluripotency in human dental pulp cells. *Journal of oral and maxillofacial surgery : official journal of the American Association of Oral and Maxillofacial Surgeons* 2009;67:501-506.

39. Seo BM, Sonoyama W, Yamaza T, et al. SHED repair critical-size calvarial defects in mice. *Oral diseases* 2008;14:428-434.

40. Zheng Y, Liu Y, Zhang CM, et al. Stem cells from deciduous tooth repair mandibular defect in swine. *J Dent Res* 2009;88:249-254.

41. Govindasamy V, Abdullah AN, Ronald VS, et al. Inherent differential propensity of dental pulp stem cells derived from human deciduous and permanent teeth. *J Endod* 2010;36:1504-1515.

42. Wang J, Wang X, Sun Z, et al. Stem cells from human-exfoliated deciduous teeth can differentiate into dopaminergic neuron-like cells. *Stem Cells Dev* 2010;19:1375-1383.

43. Sonoyama W, Liu Y, Yamaza T, et al. Characterization of the apical papilla and its residing stem cells from human immature permanent teeth: a pilot study. *J Endod* 2008;34:166-171.

44. Huang GT, Sonoyama W, Liu Y, Liu H, Wang S, Shi S. The hidden treasure in apical papilla: the potential role in pulp/dentin regeneration and bioroot engineering. *J Endod* 2008;34:645-651.

45. Vollkommer T, Gosau M, Felthaus O, Reichert TE, Morsczeck C, Gotz W. Genome-wide gene expression profiles of dental follicle stem cells. *Acta odontologica Scandinavica* 2015;73:93-100.

46. Guo W, Gong K, Shi H, et al. Dental follicle cells and treated dentin matrix scaffold for tissue engineering the tooth root. *Biomaterials* 2012;33:1291-1302.

47. Yokoi T, Saito M, Kiyono T, et al. Establishment of immortalized dental follicle cells for generating periodontal ligament in vivo. *Cell and tissue research* 2007;327:301-311.

48. Handa K, Saito M, Tsunoda A, et al. Progenitor cells from dental follicle are able to form cementum matrix in vivo. *Connective tissue research* 2002;43:406-408.

49. El-Sayed KM, Paris S, Graetz C, et al. Isolation and characterisation of human gingival margin-derived STRO-1/MACS(+) and MACS(-) cell populations. *International journal of oral science* 2015;7:80-88.

50. Zhang Q, Nguyen AL, Shi S, et al. Three-dimensional spheroid culture of human gingiva-derived mesenchymal stem cells enhances mitigation of chemotherapy-induced oral mucositis. *Stem Cells Dev* 2012;21:937-947.

51. Tang L, Li N, Xie H, Jin Y. Characterization of mesenchymal stem cells from human normal and hyperplastic gingiva. *J Cell Physiol* 2011;226:832-842.

52. Wang F, Yu M, Yan X, et al. Gingiva-derived mesenchymal stem cell-mediated therapeutic approach for bone tissue regeneration. *Stem Cells Dev* 2011;20:2093-2102.

53. Smith CE, Warshawsky H. Cellular renewal in the enamel organ and the odontoblast layer of the rat incisor as followed by radioautography using 3H-thymidine. *The Anatomical record* 1975;183:523-561.

54. Feng J, Mantesso A, De Bari C, Nishiyama A, Sharpe PT. Dual origin of mesenchymal stem cells contributing to organ growth and repair. *Proc Natl Acad Sci U S A* 2011;108:6503-6508.

55. Zhou BO, Yue R, Murphy MM, Peyer JG, Morrison SJ. Leptin-receptor-expressing mesenchymal stromal cells represent the main source of bone formed by adult bone marrow. *Cell Stem Cell* 2014;15:154-168.

56. Chan CK, Seo EY, Chen JY, et al. Identification and specification of the mouse skeletal stem cell. *Cell* 2015;160:285-298.

57. Worthley DL, Churchill M, Compton JT, et al. Gremlin 1 identifies a skeletal stem cell with bone, cartilage, and reticular stromal potential. *Cell* 2015;160:269-284.

58. Kaukua N, Shahidi MK, Konstantinidou C, et al. Glial origin of mesenchymal stem cells in a tooth model system. *Nature* 2014;513:551-554.

59. Zhao H, Feng J, Seidel K, et al. Secretion of shh by a neurovascular bundle niche supports mesenchymal stem cell homeostasis in the adult mouse incisor. *Cell Stem Cell* 2014;14:160-173.

60. An Z, Sabalic M, Bloomquist RF, Fowler TE, Streelman T, Sharpe PT. A quiescent cell population replenishes mesenchymal stem cells to drive accelerated growth in mouse incisors. *Nat Commun* 2018;9:378.

61. Hanna JH, Saha K, Jaenisch R. Pluripotency and cellular reprogramming: facts, hypotheses, unresolved issues. *Cell* 2010;143:508-525.

62. Zhu W, Zhang Q, Zhang Y, Cen L, Wang J. PDL regeneration via cell homing in delayed replantation of avulsed teeth. *J Transl Med* 2015;13:357.

63. Liu Y, Zheng Y, Ding G, et al. Periodontal ligament stem cell-mediated treatment for periodontitis in miniature swine. *Stem Cells* 2008;26:1065-1073.

64. Park JY, Jeon SH, Choung PH. Efficacy of periodontal stem cell transplantation in the treatment of advanced periodontitis. *Cell transplantation* 2011;20:271-285.

65. Lin Y, Gallucci GO, Buser D, Bosshardt D, Belser UC, Yelick PC. Bioengineered periodontal tissue formed on titanium dental implants. *J Dent Res* 2011;90:251-256.

66. Feng F, Akiyama K, Liu Y, et al. Utility of PDL progenitors for in vivo tissue regeneration: a report of 3 cases. *Oral diseases* 2010;16:20-28.

67. Gault P, Black A, Romette JL, et al. Tissue-engineered ligament: implant constructs for tooth replacement. *Journal of clinical periodontology* 2010;37:750-758.

68. Roguljic H, Matthews BG, Yang W, Cvija H, Mina M, Kalajzic I. In vivo identification of periodontal progenitor cells. *J Dent Res* 2013;92:709-715.

69. Yuan X, Pei X, Zhao Y, Tulu US, Liu B, Helms JA. A Wnt-Responsive PDL Population Effectuates Extraction Socket Healing. *J Dent Res* 2018;97:803-809.

70. Takahashi A, Nagata M, Gupta A, et al. Autocrine regulation of mesenchymal progenitor cell fates orchestrates tooth eruption. *Proc Natl Acad Sci U S A* 2019;116:575-580.

71. Zhao H, Feng J, Ho TV, Grimes W, Urata M, Chai Y. The suture provides a niche for mesenchymal stem cells of craniofacial bones. *Nat Cell Biol* 2015;17:386-396.

72. Guo Y, Yuan Y, Wu L, et al. BMP-IHH-mediated interplay between mesenchymal stem cells and osteoclasts supports calvarial bone homeostasis and repair. *Bone research* 2018;6:30.

73. Yu HM, Jerchow B, Sheu TJ, et al. The role of Axin2 in calvarial morphogenesis and craniosynostosis. *Development (Cambridge, England)* 2005;132:1995-2005.

74. Maruyama T, Jeong J, Sheu TJ, Hsu W. Stem cells of the suture mesenchyme in craniofacial bone development, repair and regeneration. *Nat Commun* 2016;7:10526.

75. Gonzales KAU, Fuchs E. Skin and Its Regenerative Powers: An Alliance between Stem Cells and Their Niche. *Developmental cell* 2017;43:387-401.

76. Gao X, Xu C, Asada N, Frenette PS. The hematopoietic stem cell niche: from embryo to adult. *Development (Cambridge, England)* 2018;145.

77. Ding L, Morrison SJ. Haematopoietic stem cells and early lymphoid progenitors occupy distinct bone marrow niches. *Nature* 2013;495:231-235.

78. Bruns I, Lucas D, Pinho S, et al. Megakaryocytes regulate hematopoietic stem cell quiescence through CXCL4 secretion. *Nat Med* 2014;20:1315-1320.

79. Zhao M, Perry JM, Marshall H, et al. Megakaryocytes maintain homeostatic quiescence and promote post-injury regeneration of hematopoietic stem cells. *Nat Med* 2014;20:1321-1326.

80. Rompolas P, Deschene ER, Zito G, et al. Live imaging of stem cell and progeny behaviour in physiological hair-follicle regeneration. *Nature* 2012;487:496-499.

81. Hsu YC, Li L, Fuchs E. Transit-amplifying cells orchestrate stem cell activity and tissue regeneration. *Cell* 2014;157:935-949.

82. Tang YL, Tang Y, Zhang YC, Qian K, Shen L, Phillips MI. Improved graft mesenchymal stem cell survival in ischemic heart with a hypoxia-regulated heme oxygenase-1 vector. *Journal of the American College of Cardiology* 2005;46:1339-1350.

83. Bresson L, Faraldo MM, Di-Cicco A, Quintanilla M, Glukhova MA, Deugnier MA. Podoplanin regulates mammary stem cell function and tumorigenesis by potentiating Wnt/beta-catenin signaling. *Development (Cambridge, England)* 2018;145.

84. Shi Y, He G, Lee WC, McKenzie JA, Silva MJ, Long F. Gli1 identifies osteogenic progenitors for bone formation and fracture repair. *Nat Commun* 2017;8:2043.

85. Lim X, Tan SH, Yu KL, Lim SB, Nusse R. Axin2 marks quiescent hair follicle bulge stem cells that are maintained by autocrine Wnt/beta-catenin signaling. *Proc Natl Acad Sci U S A* 2016;113:E1498-1505.

86. Schepers A, Clevers H. Wnt signaling, stem cells, and cancer of the gastrointestinal tract. *Cold Spring Harb Perspect Biol* 2012;4:a007989.

87. Frank DB, Peng T, Zepp JA, et al. Emergence of a Wave of Wnt Signaling that Regulates Lung Alveologenesis by Controlling Epithelial Self-Renewal and Differentiation. *Cell Rep* 2016;17:2312-2325.

88. Lee JH, Tammela T, Hofree M, et al. Anatomically and Functionally Distinct Lung Mesenchymal Populations Marked by Lgr5 and Lgr6. *Cell* 2017;170:1149-1163.e1112.

89. Jiang M, Zheng C, Shou P, et al. SHP1 Regulates Bone Mass by Directing Mesenchymal Stem Cell Differentiation. *Cell Rep* 2016;16:769-780.

90. Sharma RP, Chopra VL. Effect of the Wingless (wg1) mutation on wing and haltere development in Drosophila melanogaster. *Dev Biol* 1976;48:461-465.

91. Cadigan KM, Nusse R. Wnt signaling: a common theme in animal development. *Genes & development* 1997;11:3286-3305.

92. Wodarz A, Nusse R. Mechanisms of Wnt signaling in development. *Annual review of cell and developmental biology* 1998;14:59-88.

93. Hurlstone A, Clevers H. T-cell factors: turn-ons and turn-offs. *The EMBO journal* 2002;21:2303-2311.

94. Hagen T, Sethi JK, Foxwell N, Vidal-Puig A. Signalling activity of beta-catenin targeted to different subcellular compartments. *The Biochemical journal* 2004;379:471-477.

95. Nelson WJ, Nusse R. Convergence of Wnt, beta-catenin, and cadherin pathways. *Science* 2004;303:1483-1487.

96. Baron R, Kneissel M. WNT signaling in bone homeostasis and disease: from human mutations to treatments. *Nat Med* 2013;19:179-192.

97. Takada I, Kouzmenko AP, Kato S. Wnt and PPARgamma signaling in osteoblastogenesis and adipogenesis. *Nature reviews Rheumatology* 2009;5:442-447.

98. Visweswaran M, Pohl S, Arfuso F, et al. Multi-lineage differentiation of mesenchymal stem cells - To Wnt, or not Wnt. *The international journal of biochemistry & cell biology* 2015;68:139-147.

99. Ko JH, Lee HJ, Jeong HJ, et al. Mesenchymal stem/stromal cells precondition lung monocytes/macrophages to produce tolerance against allo- and autoimmunity in the eye. *Proc Natl Acad Sci U S A* 2016;113:158-163.

100. Huelsken J, Behrens J. The Wnt signalling pathway. *Journal of cell science* 2002;115:3977-3978.

101. Komiya Y, Habas R. Wnt signal transduction pathways. *Organogenesis* 2008;4:68-75.

102. Yasuda H, Shima N, Nakagawa N, et al. Osteoclast differentiation factor is a ligand for osteoprotegerin/osteoclastogenesis-inhibitory factor and is identical to TRANCE/RANKL. *Proc Natl Acad Sci U S A* 1998;95:3597-3602.

103. Murphy LL, Hughes CC. Endothelial cells stimulate T cell NFAT nuclear translocation in the presence of cyclosporin A: involvement of the wnt/glycogen synthase kinase-3 beta pathway. *J Immunol* 2002;169:3717-3725.

104. Veltri A, Lang C, Lien WH. Concise Review: Wnt Signaling Pathways in Skin Development and Epidermal Stem Cells. *Stem Cells* 2018;36:22-35.

105. Kim KA, Kakitani M, Zhao J, et al. Mitogenic influence of human R-spondin1 on the intestinal epithelium. *Science* 2005;309:1256-1259.

106. Yin X, Li J, Salmon B, et al. Wnt Signaling and Its Contribution to Craniofacial Tissue Homeostasis. *J Dent Res* 2015;94:1487-1494.

107. Kretzschmar K, Clevers H. Wnt/beta-catenin signaling in adult mammalian epithelial stem cells. *Dev Biol* 2017;428:273-282.

108. Xian L, Georgess D, Huso T, et al. HMGA1 amplifies Wnt signalling and expands the intestinal stem cell compartment and Paneth cell niche. *Nat Commun* 2017;8:15008.

109. Adam RC, Yang H, Ge Y, et al. Temporal Layering of Signaling Effectors Drives Chromatin Remodeling during Hair Follicle Stem Cell Lineage Progression. *Cell Stem Cell* 2018;22:398-413.e397.

110. Farin HF, Jordens I, Mosa MH, et al. Visualization of a short-range Wnt gradient in the intestinal stem-cell niche. *Nature* 2016;530:340-343.

111. Degirmenci B, Valenta T, Dimitrieva S, Hausmann G, Basler K. GLI1-expressing mesenchymal cells form the essential Wnt-secreting niche for colon stem cells. *Nature* 2018;558:449-453.

112. Korinek V, Barker N, Moerer P, et al. Depletion of epithelial stem-cell compartments in the small intestine of mice lacking Tcf-4. *Nature genetics* 1998;19:379-383.

113. van Es JH, Haegebarth A, Kujala P, et al. A critical role for the Wnt effector Tcf4 in adult intestinal homeostatic self-renewal. *Molecular and cellular biology* 2012;32:1918-1927.

114. Fevr T, Robine S, Louvard D, Huelsken J. Wnt/beta-catenin is essential for intestinal homeostasis and maintenance of intestinal stem cells. *Molecular and cellular biology* 2007;27:7551-7559.

115. Kuhnert F, Davis CR, Wang HT, et al. Essential requirement for Wnt signaling in proliferation of adult small intestine and colon revealed by adenoviral expression of Dickkopf-1. *Proc Natl Acad Sci U S A* 2004;101:266-271.

116. Pinto D, Gregorieff A, Begthel H, Clevers H. Canonical Wnt signals are essential for homeostasis of the intestinal epithelium. *Genes & development* 2003;17:1709-1713.

117. van de Wetering M, Sancho E, Verweij C, et al. The beta-catenin/TCF-4 complex imposes a crypt progenitor phenotype on colorectal cancer cells. *Cell* 2002;111:241-250.

118. Muncan V, Sansom OJ, Tertoolen L, et al. Rapid loss of intestinal crypts upon conditional deletion of the Wnt/Tcf-4 target gene c-Myc. *Molecular and cellular biology* 2006;26:8418-8426.

119. Lim X, Tan SH, Koh WL, et al. Interfollicular epidermal stem cells self-renew via autocrine Wnt signaling. *Science* 2013;342:1226-1230.

120. Jing H, Liao L, An Y, et al. Suppression of EZH2 Prevents the Shift of Osteoporotic MSC Fate to Adipocyte and Enhances Bone Formation During Osteoporosis. *Molecular therapy : the journal of the American Society of Gene Therapy* 2016;24:217-229.

121. Niehrs C, Acebron SP. Mitotic and mitogenic Wnt signalling. *The EMBO journal* 2012;31:2705-2713.

122. Li L, Clevers H. Coexistence of quiescent and active adult stem cells in mammals. *Science* 2010;327:542-545.

123. Park JR, Jung JW, Lee YS, Kang KS. The roles of Wnt antagonists Dkk1 and sFRP4 during adipogenesis of human adipose tissue-derived mesenchymal stem cells. *Cell Prolif* 2008;41:859-874.

124. Ehrlund A, Mejhert N, Lorente-Cebrian S, et al. Characterization of the Wnt inhibitors secreted frizzled-related proteins (SFRPs) in human adipose tissue. *The Journal of clinical endocrinology and metabolism* 2013;98:E503-508.

125. Mahdi T, Hanzelmann S, Salehi A, et al. Secreted frizzled-related protein 4 reduces insulin secretion and is overexpressed in type 2 diabetes. *Cell metabolism* 2012;16:625-633.

126. Zaragosi LE, Wdziekonski B, Fontaine C, Villageois P, Peraldi P, Dani C. Effects of GSK3 inhibitors on in vitro expansion and differentiation of human adipose-derived stem cells into adipocytes. *BMC cell biology* 2008;9:11.

127. Gaur T, Rich L, Lengner CJ, et al. Secreted frizzled related protein 1 regulates Wnt signaling for BMP2 induced chondrocyte differentiation. *J Cell Physiol* 2006;208:87-96.

128. Jin EJ, Park JH, Lee SY, Chun JS, Bang OS, Kang SS. Wnt-5a is involved in TGF-beta3-stimulated chondrogenic differentiation of chick wing bud mesenchymal cells. *The international journal of biochemistry & cell biology* 2006;38:183-195.

129. Fischer L, Boland G, Tuan RS. Wnt signaling during BMP-2 stimulation of mesenchymal chondrogenesis. *Journal of cellular biochemistry* 2002;84:816-831.

130. Luo S, Shi Q, Zha Z, et al. Inactivation of Wnt/beta-catenin signaling in human adipose-derived stem cells is necessary for chondrogenic differentiation and maintenance. *Biomedicine & pharmacotherapy = Biomedecine & pharmacotherapie* 2013;67:819-824.

131. Im GI, Quan Z. The effects of Wnt inhibitors on the chondrogenesis of human mesenchymal stem cells. *Tissue Eng Part A* 2010;16:2405-2413.

132. Im GI, Lee JM, Kim HJ. Wnt inhibitors enhance chondrogenesis of human mesenchymal stem cells in a long-term pellet culture. *Biotechnology letters* 2011;33:1061-1068.

133. Liu G, Vijayakumar S, Grumolato L, et al. Canonical Wnts function as potent regulators of osteogenesis by human mesenchymal stem cells. *The Journal of cell biology* 2009;185:67-75.

134. Kato M, Patel MS, Levasseur R, et al. Cbfa1-independent decrease in osteoblast proliferation, osteopenia, and persistent embryonic eye vascularization in mice deficient in Lrp5, a Wnt coreceptor. *The Journal of cell biology* 2002;157:303-314.

135. Boyden LM, Mao J, Belsky J, et al. High bone density due to a mutation in LDL-receptor-related protein 5. *The New England journal of medicine* 2002;346:1513-1521.

136. Bennett CN, Longo KA, Wright WS, et al. Regulation of osteoblastogenesis and bone mass by Wnt10b. *Proc Natl Acad Sci U S A* 2005;102:3324-3329.

137. Yamada A, Iwata T, Yamato M, Okano T, Izumi Y. Diverse functions of secreted frizzled-related proteins in the osteoblastogenesis of human multipotent mesenchymal stromal cells. *Biomaterials* 2013;34:3270-3278.

138. Yao W, Cheng Z, Shahnazari M, Dai W, Johnson ML, Lane NE. Overexpression of secreted frizzled-related protein 1 inhibits bone formation and attenuates parathyroid hormone bone anabolic effects. *Journal of bone and mineral research : the official journal of the American Society for Bone and Mineral Research* 2010;25:190-199.

139. Nakanishi R, Akiyama H, Kimura H, et al. Osteoblast-targeted expression of Sfrp4 in mice results in low bone mass. *Journal of bone and mineral research : the official journal of the American Society for Bone and Mineral Research* 2008;23:271-277.

140. Bodine PV, Billiard J, Moran RA, et al. The Wnt antagonist secreted frizzled-related protein-1 controls osteoblast and osteocyte apoptosis. *Journal of cellular biochemistry* 2005;96:1212-1230.

141. Di Meglio P, Perera GK, Nestle FO. The multitasking organ: recent insights into skin immune function. *Immunity* 2011;35:857-869.

142. Hanahan D, Weinberg RA. Hallmarks of cancer: the next generation. *Cell* 2011;144:646-674.

143. Aurora AB, Olson EN. Immune modulation of stem cells and regeneration. *Cell Stem Cell* 2014;15:14-25.

144. Forbes SJ, Rosenthal N. Preparing the ground for tissue regeneration: from mechanism to therapy. *Nat Med* 2014;20:857-869.

145. Takemura N, Kawasaki T, Kunisawa J, et al. Blockade of TLR3 protects mice from lethal radiation-induced gastrointestinal syndrome. *Nat Commun* 2014;5:3492.

146. Liu Y, Wang L, Kikuiri T, et al. Mesenchymal stem cell-based tissue regeneration is governed by recipient T lymphocytes via IFN-gamma and TNF-alpha. *Nat Med* 2011;17:1594-1601.

147. Li X, Wang S, Zhu R, Li H, Han Q, Zhao RC. Lung tumor exosomes induce a pro-inflammatory phenotype in mesenchymal stem cells via NFkappaB-TLR signaling pathway. *Journal of hematology & oncology* 2016;9:42.

148. Keyes BE, Fuchs E. Stem cells: Aging and transcriptional fingerprints. *The Journal of cell biology* 2018;217:79-92.

149. Zolezzi JM, Inestrosa NC. Wnt/TLR Dialog in Neuroinflammation, Relevance in Alzheimer's Disease. *Front Immunol* 2017;8:187.

150. Wynn TA, Vannella KM. Macrophages in Tissue Repair, Regeneration, and Fibrosis. *Immunity* 2016;44:450-462.

151. Ren J, Stroncek DF, Zhao Y, et al. Intra-subject variability in human bone marrow stromal cell (BMSC) replicative senescence: molecular changes associated with BMSC senescence. *Stem cell research* 2013;11:1060-1073.

152. Mahla RS, Reddy MC, Prasad DV, Kumar H. Sweeten PAMPs: Role of Sugar Complexed PAMPs in Innate Immunity and Vaccine Biology. *Front Immunol* 2013;4:248.

153. Fortier ME, Kent S, Ashdown H, Poole S, Boksa P, Luheshi GN. The viral mimic, polyinosinic:polycytidylic acid, induces fever in rats via an interleukin-1-dependent mechanism. *Am J Physiol Regul Integr Comp Physiol* 2004;287:R759-766.

154. Sultan M, Coyle KM, Vidovic D, Thomas ML, Gujar S, Marcato P. Hide-and-seek: the interplay between cancer stem cells and the immune system. *Carcinogenesis* 2016.

155. Feng G, Zheng K, Cao T, et al. Repeated stimulation by LPS promotes the senescence of DPSCs via TLR4/MyD88-NF-kappaB-p53/p21 signaling. *Cytotechnology* 2018.

156. Gong Y, Slee RB, Fukai N, et al. LDL receptor-related protein 5 (LRP5) affects bone accrual and eye development. *Cell* 2001;107:513-523.

157. Karin M. How NF-kappaB is activated: the role of the IkappaB kinase (IKK) complex. *Oncogene* 1999;18:6867-6874.

158. Blasius AL, Beutler B. Intracellular toll-like receptors. *Immunity* 2010;32:305-315.

159. Lester SN, Li K. Toll-like receptors in antiviral innate immunity. *J Mol Biol* 2014;426:1246-1264.

160. Chen GY, Nunez G. Sterile inflammation: sensing and reacting to damage. *Nature reviews Immunology* 2010;10:826-837.

161. Arslan F, Smeets MB, Riem Vis PW, et al. Lack of fibronectin-EDA promotes survival and prevents adverse remodeling and heart function deterioration after myocardial infarction. *Circ Res* 2011;108:582-592.

162. DelaRosa O, Lombardo E. Modulation of adult mesenchymal stem cells activity by toll-like receptors: implications on therapeutic potential. *Mediators of inflammation* 2010;2010:865601.

163. Martino MM, Maruyama K, Kuhn GA, et al. Inhibition of IL-1R1/MyD88 signalling promotes mesenchymal stem cell-driven tissue regeneration. *Nat Commun* 2016;7:11051.

164. Pevsner-Fischer M, Morad V, Cohen-Sfady M, et al. Toll-like receptors and their ligands control mesenchymal stem cell functions. *Blood* 2007;109:1422-1432.

165. Poulain-Godefroy O, Le Bacquer O, Plancq P, et al. Inflammatory role of Toll-like receptors in human and murine adipose tissue. *Mediators of inflammation* 2010;2010:823486.

166. J SP, Hu P, Burke SJ, Collier JJ, Chen J, Zhao L. The effects of NOD activation on adipocyte differentiation. *Obesity (Silver Spring, Md)* 2013;21:737-747.

167. Chang LY, Lai YL, Yu TH, Chen YT, Hung SL. Effects of areca nut extract on lipopolysaccharides-enhanced adhesion and migration of human mononuclear leukocytes. *Journal of periodontology* 2014;85:859-867.

168. Tang Y, Zhou X, Gao B, et al. Modulation of Wnt/beta-catenin signaling attenuates periapical bone lesions. *J Dent Res* 2014;93:175-182.

169. Wang J, Dai J, Liu B, Gu S, Cheng L, Liang J. Porphyromonas gingivalis lipopolysaccharide activates canonical Wnt/beta-catenin and p38 MAPK signalling in stem cells from the apical papilla. *Inflammation* 2013;36:1393-1402.

170. Li D, Fu L, Zhang Y, et al. The effects of LPS on adhesion and migration of human dental pulp stem cells in vitro. *Journal of dentistry* 2014;42:1327-1334.

171. He W, Wang Z, Zhou Z, et al. Lipopolysaccharide enhances Wnt5a expression through toll-like receptor 4, myeloid differentiating factor 88, phosphatidylinositol 3-OH kinase/AKT and nuclear factor kappa B pathways in human dental pulp stem cells. *J Endod* 2014;40:69-75.

172. He W, Qu T, Yu Q, et al. Lipopolysaccharide enhances decorin expression through the Toll-like receptor 4, myeloid differentiating factor 88, nuclear factor-kappa B, and mitogen-activated protein kinase pathways in odontoblast cells. *J Endod* 2012;38:464-469.

173. Xing Q, Ye Q, Fan M, Zhou Y, Xu Q, Sandham A. Porphyromonas gingivalis lipopolysaccharide inhibits the osteoblastic differentiation of preosteoblasts by activating Notch1 signaling. *J Cell Physiol* 2010;225:106-114.

174. Kedia S, Rampal R, Paul J, Ahuja V. Gut microbiome diversity in acute infective and chronic inflammatory gastrointestinal diseases in North India. *Journal of gastroenterology* 2016;51:660-671.

175. Sodhi CP, Shi XH, Richardson WM, et al. Toll-like receptor-4 inhibits enterocyte proliferation via impaired beta-catenin signaling in necrotizing enterocolitis. *Gastroenterology* 2010;138:185-196.

176. Liu X, Lu R, Xia Y, Wu S, Sun J. Eukaryotic signaling pathways targeted by Salmonella effector protein AvrA in intestinal infection in vivo. *BMC microbiology* 2010;10:326.

177. Marchetti B, Pluchino S. Wnt your brain be inflamed? Yes, it Wnt! *Trends in molecular medicine* 2013;19:144-156.

178. Kanneganti TD, Lamkanfi M, Nunez G. Intracellular NOD-like receptors in host defense and disease. *Immunity* 2007;27:549-559.

179. Franchi L, Warner N, Viani K, Nunez G. Function of Nod-like receptors in microbial recognition and host defense. *Immunological reviews* 2009;227:106-128.

180. Jorgensen I, Miao EA. Pyroptotic cell death defends against intracellular pathogens. *Immunological reviews* 2015;265:130-142.

181. Franchi L, Munoz-Planillo R, Nunez G. Sensing and reacting to microbes through the inflammasomes. *Nat Immunol* 2012;13:325-332.

182. Galluzzi L, Vitale I, Aaronson SA, et al. Molecular mechanisms of cell death: recommendations of the Nomenclature Committee on Cell Death 2018. *Cell death and differentiation* 2018;25:486-541.

183. Naji A, Muzembo BA, Yagyu K, et al. Endocytosis of indium-tin-oxide nanoparticles by macrophages provokes pyroptosis requiring NLRP3-ASC-Caspase1 axis that can be prevented by mesenchymal stem cells. *Sci Rep* 2016;6:26162.

184. Kim HS, Shin TH, Yang SR, et al. Implication of NOD1 and NOD2 for the differentiation of multipotent mesenchymal stem cells derived from human umbilical cord blood. *PLoS One* 2010;5:e15369.

185. Wang L, Chen K, Wan X, Wang F, Guo Z, Mo Z. NLRP3 inflammasome activation in mesenchymal stem cells inhibits osteogenic differentiation and enhances adipogenic differentiation. *Biochem Biophys Res Commun* 2017;484:871-877.

186. Singh V, Holla S, Ramachandra SG, Balaji KN. WNT-inflammasome signaling mediates NOD2-induced development of acute arthritis in mice. *J Immunol* 2015;194:3351-3360.

187. Zhou L, Dorfer CE, Chen L, Fawzy El-Sayed KM. Porphyromonas gingivalis lipopolysaccharides affect gingival stem/progenitor cells attributes through NF-kappaB, but not Wnt/beta-catenin, pathway. *Journal of clinical periodontology* 2017;44:1112-1122.

188. Chen S, Shen D, Popp NA, et al. Responses of Multipotent Retinal Stem Cells to IL-1β, IL-18, or IL-17. *Journal of Ophthalmology* 2015;2015:9.

189. Huang J, Chen L. IL-1beta inhibits osteogenesis of human bone marrow-derived mesenchymal stem cells by activating FoxD3/microRNA-496 to repress wnt signaling. *Genesis* 2017;55.

190. Gao Y, Grassi F, Ryan MR, et al. IFN-gamma stimulates osteoclast formation and bone loss in vivo via antigen-driven T cell activation. *The Journal of clinical investigation* 2007;117:122-132.

191. Suzawa M, Takada I, Yanagisawa J, et al. Cytokines suppress adipogenesis and PPAR-gamma function through the TAK1/TAB1/NIK cascade. *Nat Cell Biol* 2003;5:224-230.

192. Gaspersic R, Stiblar-Martincic D, Osredkar J, Skaleric U. In vivo administration of recombinant TNF-alpha promotes bone resorption in mice. *Journal of periodontal research* 2003;38:446-448.

193. Wang L, Zhao Y, Shi S. Interplay between mesenchymal stem cells and lymphocytes: implications for immunotherapy and tissue regeneration. *J Dent Res* 2012;91:1003-1010.

194. Yang SR, Park JR, Kang KS. Reactive Oxygen Species in Mesenchymal Stem Cell Aging: Implication to Lung Diseases. *Oxidative medicine and cellular longevity* 2015;2015:486263.

195. Kawai T, Akira S. Toll-like receptors and their crosstalk with other innate receptors in infection and immunity. *Immunity* 2011;34:637-650.

196. Atashi F, Modarressi A, Pepper MS. The role of reactive oxygen species in mesenchymal stem cell adipogenic and osteogenic differentiation: a review. *Stem Cells Dev* 2015;24:1150-1163.

197. Brown GC, Borutaite V. There is no evidence that mitochondria are the main source of reactive oxygen species in mammalian cells. *Mitochondrion* 2012;12:1-4.

198. McNally JS, Davis ME, Giddens DP, et al. Role of xanthine oxidoreductase and NAD(P)H oxidase in endothelial superoxide production in response to oscillatory shear stress. *American journal of physiology Heart and circulatory physiology* 2003;285:H2290-2297.

199. O'Donnell VB, Azzi A. High rates of extracellular superoxide generation by cultured human fibroblasts: involvement of a lipid-metabolizing enzyme. *The Biochemical journal* 1996;318 (Pt 3):805-812.

200. Starkov AA. The role of mitochondria in reactive oxygen species metabolism and signaling. *Annals of the New York Academy of Sciences* 2008;1147:37-52.

201. Gross E, Sevier CS, Heldman N, et al. Generating disulfides enzymatically: reaction products and electron acceptors of the endoplasmic reticulum thiol oxidase Ero1p. *Proc Natl Acad Sci U S A* 2006;103:299-304.

202. Roy P, Roy SK, Mitra A, Kulkarni AP. Superoxide generation by lipoxygenase in the presence of NADH and NADPH. *Biochim Biophys Acta* 1994;1214:171-179.

203. Schroder K, Wandzioch K, Helmcke I, Brandes RP. Nox4 acts as a switch between differentiation and proliferation in preadipocytes. *Arterioscler Thromb Vasc Biol* 2009;29:239-245.

204. Pittenger MF, Martin BJ. Mesenchymal stem cells and their potential as cardiac therapeutics. *Circ Res* 2004;95:9-20.

205. Liu SP, Ding DC, Wang HJ, et al. Nonsenescent Hsp27-upregulated MSCs implantation promotes neuroplasticity in stroke model. *Cell transplantation* 2010;19:1261-1279.

206. Kobayashi CI, Suda T. Regulation of reactive oxygen species in stem cells and cancer stem cells. *J Cell Physiol* 2012;227:421-430.

207. D'Autreaux B, Toledano MB. ROS as signalling molecules: mechanisms that generate specificity in ROS homeostasis. *Nat Rev Mol Cell Biol* 2007;8:813-824.

208. Eto H, Kato H, Suga H, et al. The fate of adipocytes after nonvascularized fat grafting: evidence of early death and replacement of adipocytes. *Plastic and reconstructive surgery* 2012;129:1081-1092.

209. Rodrigues M, Turner O, Stolz D, Griffith LG, Wells A. Production of reactive oxygen species by multipotent stromal cells/mesenchymal stem cells upon exposure to fas ligand. *Cell transplantation* 2012;21:2171-2187.

210. Zou X, Li H, Chen L, Baatrup A, Bunger C, Lind M. Stimulation of porcine bone marrow stromal cells by hyaluronan, dexamethasone and rhBMP-2. *Biomaterials* 2004;25:5375-5385.

211. Denu RA, Hematti P. Effects of Oxidative Stress on Mesenchymal Stem Cell Biology. *Oxidative medicine and cellular longevity* 2016;2016:2989076.

212. Valle-Prieto A, Conget PA. Human mesenchymal stem cells efficiently manage oxidative stress. *Stem Cells Dev* 2010;19:1885-1893.

213. Orciani M, Gorbi S, Benedetti M, et al. Oxidative stress defense in human-skin-derived mesenchymal stem cells versus human keratinocytes: Different mechanisms of protection and cell selection. *Free Radic Biol Med* 2010;49:830-838.

214. Ko E, Lee KY, Hwang DS. Human umbilical cord blood-derived mesenchymal stem cells undergo cellular senescence in response to oxidative stress. *Stem Cells Dev* 2012;21:1877-1886.

215. Hou J, Han ZP, Jing YY, et al. Autophagy prevents irradiation injury and maintains stemness through decreasing ROS generation in mesenchymal stem cells. *Cell death & disease* 2013;4:e844.

216. Kanda Y, Hinata T, Kang SW, Watanabe Y. Reactive oxygen species mediate adipocyte differentiation in mesenchymal stem cells. *Life sciences* 2011;89:250-258.

217. Zhang Y, Marsboom G, Toth PT, Rehman J. Mitochondrial respiration regulates adipogenic differentiation of human mesenchymal stem cells. *PLoS One* 2013;8:e77077.

218. Suh HN, Kim MJ, Jung YS, Lien EM, Jun S, Park JI. Quiescence Exit of Tert(+) Stem Cells by Wnt/beta-Catenin Is Indispensable for Intestinal Regeneration. *Cell Rep* 2017;21:2571-2584.

219. Sallman DA, Cluzeau T, Basiorka AA, List A. Unraveling the Pathogenesis of MDS: The NLRP3 Inflammasome and Pyroptosis Drive the MDS Phenotype. *Frontiers in oncology* 2016;6:151.

220. Kajla S, Mondol AS, Nagasawa A, et al. A crucial role for Nox 1 in redox-dependent regulation of Wnt-beta-catenin signaling. *Faseb j* 2012;26:2049-2059.

221. Lin Z, Fateh A, Salem DM, Intini G. Periosteum: biology and applications in craniofacial bone regeneration. *J Dent Res* 2014;93:109-116.

222. Covas DT, Panepucci RA, Fontes AM, et al. Multipotent mesenchymal stromal cells obtained from diverse human tissues share functional properties and gene-expression profile with CD146+ perivascular cells and fibroblasts. *Exp Hematol* 2008;36:642-654.

223. Schwab KE, Gargett CE. Co-expression of two perivascular cell markers isolates mesenchymal stem-like cells from human endometrium. *Human reproduction (Oxford, England)* 2007;22:2903-2911.

224. Crisan M, Yap S, Casteilla L, et al. A perivascular origin for mesenchymal stem cells in multiple human organs. *Cell Stem Cell* 2008;3:301-313.

225. Traktuev DO, Merfeld-Clauss S, Li J, et al. A population of multipotent CD34-positive adipose stromal cells share pericyte and mesenchymal surface markers, reside in a periendothelial location, and stabilize endothelial networks. *Circ Res* 2008;102:77-85.

226. Murray IR, West CC, Hardy WR, et al. Natural history of mesenchymal stem cells, from vessel walls to culture vessels. *Cellular and molecular life sciences : CMLS* 2014;71:1353-1374.

227. Selliseth NJ, Selvig KA. The vasculature of the periodontal ligament: a scanning electron microscopic study using corrosion casts in the rat. *Journal of periodontology* 1994;65:1079-1087.

228. Kramann R, Schneider RK, DiRocco DP, et al. Perivascular Gli1+ progenitors are key contributors to injury-induced organ fibrosis. *Cell Stem Cell* 2015;16:51-66.

229. Ding L, Saunders TL, Enikolopov G, Morrison SJ. Endothelial and perivascular cells maintain haematopoietic stem cells. *Nature* 2012;481:457-462.

230. Maeda T. Sensory innervation of the periodontal ligament in the incisor and molar of the monkey, Macaca fuscata. An immunohistochemical study for neurofilament protein and glia-specific S-100 protein. *Archivum histologicum Japonicum = Nihon soshikigaku kiroku* 1987;50:437-454.

231. Katayama Y, Battista M, Kao WM, et al. Signals from the sympathetic nervous system regulate hematopoietic stem cell egress from bone marrow. *Cell* 2006;124:407-421.

232. Mendez-Ferrer S, Battista M, Frenette PS. Cooperation of beta(2)- and beta(3)-adrenergic receptors in hematopoietic progenitor cell mobilization. *Annals of the New York Academy of Sciences* 2010;1192:139-144.

233. Knox SM, Lombaert IM, Reed X, Vitale-Cross L, Gutkind JS, Hoffman MP. Parasympathetic innervation maintains epithelial progenitor cells during salivary organogenesis. *Science* 2010;329:1645-1647.

234. Knox SM, Lombaert IM, Haddox CL, et al. Parasympathetic stimulation improves epithelial organ regeneration. *Nat Commun* 2013;4:1494.

235. Roelink H, Augsburger A, Heemskerk J, et al. Floor plate and motor neuron induction by vhh-1, a vertebrate homolog of hedgehog expressed by the notochord. *Cell* 1994;76:761-775.

236. Hebrok M, Kim SK, St Jacques B, McMahon AP, Melton DA. Regulation of pancreas development by hedgehog signaling. *Development (Cambridge, England)* 2000;127:4905-4913.

237. Kawahira H, Ma NH, Tzanakakis ES, McMahon AP, Chuang PT, Hebrok M. Combined activities of hedgehog signaling inhibitors regulate pancreas development. *Development (Cambridge, England)* 2003;130:4871-4879.

238. St-Jacques B, Hammerschmidt M, McMahon AP. Indian hedgehog signaling regulates proliferation and differentiation of chondrocytes and is essential for bone formation. *Genes & development* 1999;13:2072-2086.

239. Ingham PW, McMahon AP. Hedgehog signaling in animal development: paradigms and principles. *Genes & development* 2001;15:3059-3087.

240. Rimkus TK, Carpenter RL, Qasem S, Chan M, Lo HW. Targeting the Sonic Hedgehog Signaling Pathway: Review of Smoothened and GLI Inhibitors. *Cancers* 2016;8.

241. Tran Hle B, Doan VN, Le HT, Ngo LT. Various methods for isolation of multipotent human periodontal ligament cells for regenerative medicine. *In vitro cellular & developmental biology Animal* 2014;50:597-602.

242. Vestweber D. VE-cadherin: the major endothelial adhesion molecule controlling cellular junctions and blood vessel formation. *Arterioscler Thromb Vasc Biol* 2008;28:223-232.

243. Soteriou D, Fuchs Y. A matter of life and death: stem cell survival in tissue regeneration and tumour formation. *Nature reviews Cancer* 2018;18:187-201.

244. Horiuchi K, Amizuka N, Takeshita S, et al. Identification and characterization of a novel protein, periostin, with restricted expression to periosteum and periodontal ligament and increased expression by transforming growth factor beta. *Journal of bone and mineral research : the official journal of the American Society for Bone and Mineral Research* 1999;14:1239-1249.

245. Keating A. Mesenchymal stromal cells. *Current opinion in hematology* 2006;13:419-425.

246. Batlle E, Clevers H. Cancer stem cells revisited. *Nat Med* 2017;23:1124-1134.

247. Dameshghi S, Zavaran-Hosseini A, Soudi S, Shirazi FJ, Nojehdehi S, Hashemi SM. Mesenchymal stem cells alter macrophage immune responses to Leishmania major infection in both susceptible and resistance mice. *Immunol Lett* 2016;170:15-26.

248. Acar M, Kocherlakota KS, Murphy MM, et al. Deep imaging of bone marrow shows non-dividing stem cells are mainly perisinusoidal. *Nature* 2015;526:126-130.

249. Lin G, Garcia M, Ning H, et al. Defining stem and progenitor cells within adipose tissue. *Stem Cells Dev* 2008;17:1053-1063.

250. Shi S, Gronthos S. Perivascular niche of postnatal mesenchymal stem cells in human bone marrow and dental pulp. *Journal of bone and mineral research : the official journal of the American Society for Bone and Mineral Research* 2003;18:696-704.

251. Yue R, Zhou BO, Shimada IS, Zhao Z, Morrison SJ. Leptin Receptor Promotes Adipogenesis and Reduces Osteogenesis by Regulating Mesenchymal Stromal Cells in Adult Bone Marrow. *Cell Stem Cell* 2016;18:782-796.

252. Dassule HR, Lewis P, Bei M, Maas R, McMahon AP. Sonic hedgehog regulates growth and morphogenesis of the tooth. *Development (Cambridge, England)* 2000;127:4775-4785.

253. Martinez C, Smith PC, Rodriguez JP, Palma V. Sonic hedgehog stimulates proliferation of human periodontal ligament stem cells. *J Dent Res* 2011;90:483-488.

254. Seidel K, Ahn CP, Lyons D, et al. Hedgehog signaling regulates the generation of ameloblast progenitors in the continuously growing mouse incisor. *Development (Cambridge, England)* 2010;137:3753-3761.

255. Jing D, Zhang S, Luo W, et al. Tissue clearing of both hard and soft tissue organs with the PEGASOS method. *Cell research* 2018.

256. Chung K, Deisseroth K. CLARITY for mapping the nervous system. *Nat Methods* 2013;10:508-513.

257. Hama H, Hioki H, Namiki K, et al. ScaleS: an optical clearing palette for biological imaging. *Nature neuroscience* 2015;18:1518-1529.

258. Yang Z, Balic A, Michon F, Juuri E, Thesleff I. Mesenchymal Wnt/beta-Catenin Signaling Controls Epithelial Stem Cell Homeostasis in Teeth by Inhibiting the Antiapoptotic Effect of Fgf10. *Stem Cells* 2015;33:1670-1681.

259. Rooker SM, Liu B, Helms JA. Role of Wnt signaling in the biology of the periodontium. *Dev Dyn* 2010;239:140-147.

260. Lim WH, Liu B, Cheng D, Williams BO, Mah SJ, Helms JA. Wnt signaling regulates homeostasis of the periodontal ligament. *Journal of periodontal research* 2014;49:751-759.

261. Wu Y, Yuan X, Perez KC, et al. Aberrantly elevated Wnt signaling is responsible for cementum overgrowth and dental ankylosis. *Bone* 2018.

262. Salmon B, Liu B, Shen E, et al. WNT-activated bone grafts repair osteonecrotic lesions in aged animals. *Sci Rep* 2017;7:14254.

263. Yin X, Li J, Chen T, et al. Rescuing failed oral implants via Wnt activation. *Journal of clinical periodontology* 2016;43:180-192.

264. Lim WH, Liu B, Mah SJ, Yin X, Helms JA. Alveolar bone turnover and periodontal ligament width are controlled by Wnt. *Journal of periodontology* 2015;86:319-326.

265. Salic A, Mitchison TJ. A chemical method for fast and sensitive detection of DNA synthesis in vivo. *Proc Natl Acad Sci U S A* 2008;105:2415-2420.

266. Kim TH, Bae CH, Jang EH, et al. Col1a1-cre mediated activation of beta-catenin leads to aberrant dento-alveolar complex formation. *Anatomy & cell biology* 2012;45:193-202.

267. Lim WH, Liu B, Hunter DJ, Cheng D, Mah SJ, Helms JA. Downregulation of Wnt causes root resorption. *American journal of orthodontics and dentofacial orthopedics : official publication of the American Association of Orthodontists, its constituent societies, and the American Board of Orthodontics* 2014;146:337-345.

268. Liu N, Shi S, Deng M, et al. High levels of beta-catenin signaling reduce osteogenic differentiation of stem cells in inflammatory microenvironments through inhibition of the noncanonical Wnt pathway. *Journal of bone and mineral research : the official journal of the American Society for Bone and Mineral Research* 2011;26:2082-2095.

269. Sugimura R, Li L. Noncanonical Wnt signaling in vertebrate development, stem cells, and diseases. *Birth defects research Part C, Embryo today : reviews* 2010;90:243-256.

270. Lee HJ, Choi EK, Park JB, Han KD, Oh S. Tooth Loss Predicts Myocardial Infarction, Heart Failure, Stroke, and Death. *J Dent Res* 2019;98:164-170.

271. Han J, Menicanin D, Gronthos S, Bartold PM. Stem cells, tissue engineering and periodontal regeneration. *Australian dental journal* 2014;59 Suppl 1:117-130.

272. Ren Y, Han X, Ho SP, et al. Removal of SOST or blocking its product sclerostin rescues defects in the periodontitis mouse model. *Faseb j* 2015;29:2702-2711.

273. Yang RB, Mark MR, Gray A, et al. Toll-like receptor-2 mediates lipopolysaccharide-induced cellular signalling. *Nature* 1998;395:284-288.

274. Good DW, George T, Watts BA, 3rd. Toll-like receptor 2 is required for LPS-induced Toll-like receptor 4 signaling and inhibition of ion transport in renal thick ascending limb. *The Journal of biological chemistry* 2012;287:20208-20220.

275. Kato H, Taguchi Y, Tominaga K, Umeda M, Tanaka A. Porphyromonas gingivalis LPS inhibits osteoblastic differentiation and promotes pro-inflammatory cytokine production in human periodontal ligament stem cells. *Archives of oral biology* 2014;59:167-175.

276. Kukolj T, Trivanovic D, Djordjevic IO, et al. Lipopolysaccharide can modify differentiation and immunomodulatory potential of periodontal ligament stem cells via ERK1,2 signaling. *J Cell Physiol* 2018;233:447-462.

277. Cho HH, Kim YJ, Kim SJ, et al. Endogenous Wnt signaling promotes proliferation and suppresses osteogenic differentiation in human adipose derived stromal cells. *Tissue engineering* 2006;12:111-121.

278. Yu Y, Bi CS, Wu RX, et al. Effects of short-term inflammatory and/or hypoxic pretreatments on periodontal ligament stem cells: in vitro and in vivo studies. *Cell and tissue research* 2016;366:311-328.

279. Kong X, Liu Y, Ye R, et al. GSK3beta is a checkpoint for TNF-alpha-mediated impaired osteogenic differentiation of mesenchymal stem cells in inflammatory microenvironments. *Biochim Biophys Acta* 2013;1830:5119-5129.

280. Chen X, Hu C, Wang G, et al. Nuclear factor-kappaB modulates osteogenesis of periodontal ligament stem cells through competition with beta-catenin signaling in inflammatory microenvironments. *Cell death & disease* 2013;4:e510.

281. Chan WK, Lau AS, Li JC, Law HK, Lau YL, Chan GC. MHC expression kinetics and immunogenicity of mesenchymal stromal cells after short-term IFN-gamma challenge. *Exp Hematol* 2008;36:1545-1555.

282. Chan JL, Tang KC, Patel AP, et al. Antigen-presenting property of mesenchymal stem cells occurs during a narrow window at low levels of interferon-gamma. *Blood* 2006;107:4817-4824.

283. Graves DT, Fine D, Teng YT, Van Dyke TE, Hajishengallis G. The use of rodent models to investigate host-bacteria interactions related to periodontal diseases. *Journal of clinical periodontology* 2008;35:89-105.

284. Graves DT, Kang J, Andriankaja O, Wada K, Rossa C, Jr. Animal models to study host-bacteria interactions involved in periodontitis. *Frontiers of oral biology* 2012;15:117-132.

285. Polak D, Wilensky A, Shapira L, et al. Mouse model of experimental periodontitis induced by Porphyromonas gingivalis/Fusobacterium nucleatum infection: bone loss and host response. *Journal of clinical periodontology* 2009;36:406-410.

286. Kesavalu L, Sathishkumar S, Bakthavatchalu V, et al. Rat model of polymicrobial infection, immunity, and alveolar bone resorption in periodontal disease. *Infection and immunity* 2007;75:1704-1712.

287. Genco CA, Van Dyke T, Amar S. Animal models for Porphyromonas gingivalis-mediated periodontal disease. *Trends in microbiology* 1998;6:444-449.

288. Zhang H, Liu P, Wang S, et al. Transgenic expression of dentin phosphoprotein inhibits skeletal development. *European journal of histochemistry : EJH* 2016;60:2587.

289. Fawzy El-Sayed KM, Elahmady M, Adawi Z, et al. The periodontal stem/progenitor cell inflammatory-regenerative cross talk: A new perspective. *Journal of periodontal research* 2018.

290. Angoulvant D, Clerc A, Benchalal S, et al. Human mesenchymal stem cells suppress induction of cytotoxic response to alloantigens. *Biorheology* 2004;41:469-476.

291. Su WR, Zhang QZ, Shi SH, Nguyen AL, Le AD. Human gingiva-derived mesenchymal stromal cells attenuate contact hypersensitivity via prostaglandin E2-dependent mechanisms. *Stem Cells* 2011;29:1849-1860.

292. Zhang QZ, Nguyen AL, Yu WH, Le AD. Human oral mucosa and gingiva: a unique reservoir for mesenchymal stem cells. *J Dent Res* 2012;91:1011-1018.

293. Aggarwal S, Pittenger MF. Human mesenchymal stem cells modulate allogeneic immune cell responses. *Blood* 2005;105:1815-1822.

294. Liu D, Xu JK, Figliomeni L, et al. Expression of RANKL and OPG mRNA in periodontal disease: possible involvement in bone destruction. *International journal of molecular medicine* 2003;11:17-21.

295. Nagasawa T, Kiji M, Yashiro R, et al. Roles of receptor activator of nuclear factor-kappaB ligand (RANKL) and osteoprotegerin in periodontal health and disease. *Periodontology 2000* 2007;43:65-84.

296. Taubman MA, Valverde P, Han X, Kawai T. Immune response: the key to bone resorption in periodontal disease. *Journal of periodontology* 2005;76:2033-2041.

297. de Molon RS, Mascarenhas VI, de Avila ED, et al. Long-term evaluation of oral gavage with periodontopathogens or ligature induction of experimental periodontal disease in mice. *Clinical oral investigations* 2016;20:1203-1216.

298. Li J, Li Y, Pan S, Zhang L, He L, Niu Y. Paeonol attenuates ligation-induced periodontitis in rats by inhibiting osteoclastogenesis via regulating Nrf2/NF-kappaB/NFATc1 signaling pathway. *Biochimie* 2019;156:129-137.

299. Do MJ, Kim K, Lee H, et al. Development of animal experimental periodontitis models. *Journal of periodontal & implant science* 2013;43:147-152.

300. Orth RK, O'Brien-Simpson NM, Dashper SG, Reynolds EC. Synergistic virulence of Porphyromonas gingivalis and Treponema denticola in a murine periodontitis model. *Molecular oral microbiology* 2011;26:229-240.

301. Buduneli E, Vardar-Sengul S, Buduneli N, Atilla G, Wahlgren J, Sorsa T. Matrix metalloproteinases, tissue inhibitor of matrix metalloproteinase-1, and laminin-5 gamma2 chain immunolocalization in gingival tissue of endotoxin-induced periodontitis in rats: effects of low-dose doxycycline and alendronate. *Journal of periodontology* 2007;78:127-134.

302. Chapple CC, Kumar RK, Hunter N. Vascular remodelling in chronic inflammatory periodontal disease. *Journal of oral pathology & medicine : official publication of the International Association of Oral Pathologists and the American Academy of Oral Pathology* 2000;29:500-506.

303. Morrison SJ, Scadden DT. The bone marrow niche for haematopoietic stem cells. *Nature* 2014;505:327-334.

304. Tamura M, Nemoto E. Role of the Wnt signaling molecules in the tooth. *The Japanese dental science review* 2016;52:75-83.

305. Clevers H, Loh KM, Nusse R. Stem cell signaling. An integral program for tissue renewal and regeneration: Wnt signaling and stem cell control. *Science* 2014;346:1248012.

APPENDIX A

FIGURES

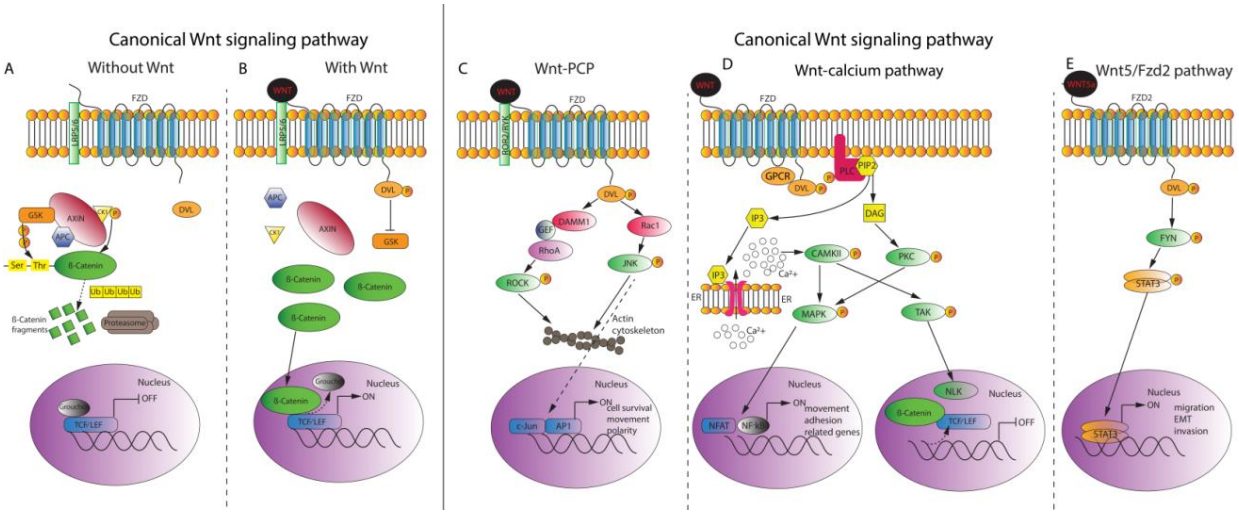

Figure 1 Overview of the Canonical and Noncanonical Wnt Pathway
(A). In the canonical pathway, without Wnt ligands, the destruction complex phosphorylates ß-catenin is later ubiquitinated and targeted to degradation in the proteasome. The absence of ß-catenin represses Wnt downstream genes. (B). For a canonical pathway with the binding of Wnt ligands, recruited Dvl blocks GSK and destruction complex disassembled to stabilize ß-catenin. The nucleus translocation elicits target genes' expression. (C). Depiction of the noncanonical Wnt-PCP pathway. With the Dvl and coreceptor ROR2/RYK bonded, two Rho family GTPases, RhoA, and Rac1 stimulate respective ROCK and JNK activity. Both kinases directly regulate the cytoskeleton and JNK also triggers the expression of target genes regulating cell survival, movement, and polarity. (D). Schematic representation of the Wnt-Calcium pathway. Wnt ligands'FZD binding mediates Dvl activation with a G protein-coupled receptor. Then, Dvl activates PLC to decompose PIP2 into IP3 and DAG. IP3 leads to an intracellular Ca2+ release from the ER, which in turn phosphorylates CAMKII. CAMKII activates NFAT to regulate cell movement and adhesion via MAPK. Wnt-Calcium pathway inhibits Wnt/ß-catenin signaling through TAK-NLK, which is mediated through a LEF1-b-catenin dissociation from DNA. DAG activates NFAT downstream genes through PKC. (F). Schematic of the Wnt5a/Fzd2 pathway involved in tumor metastasis-related genes expression via FYN activated STAT3.

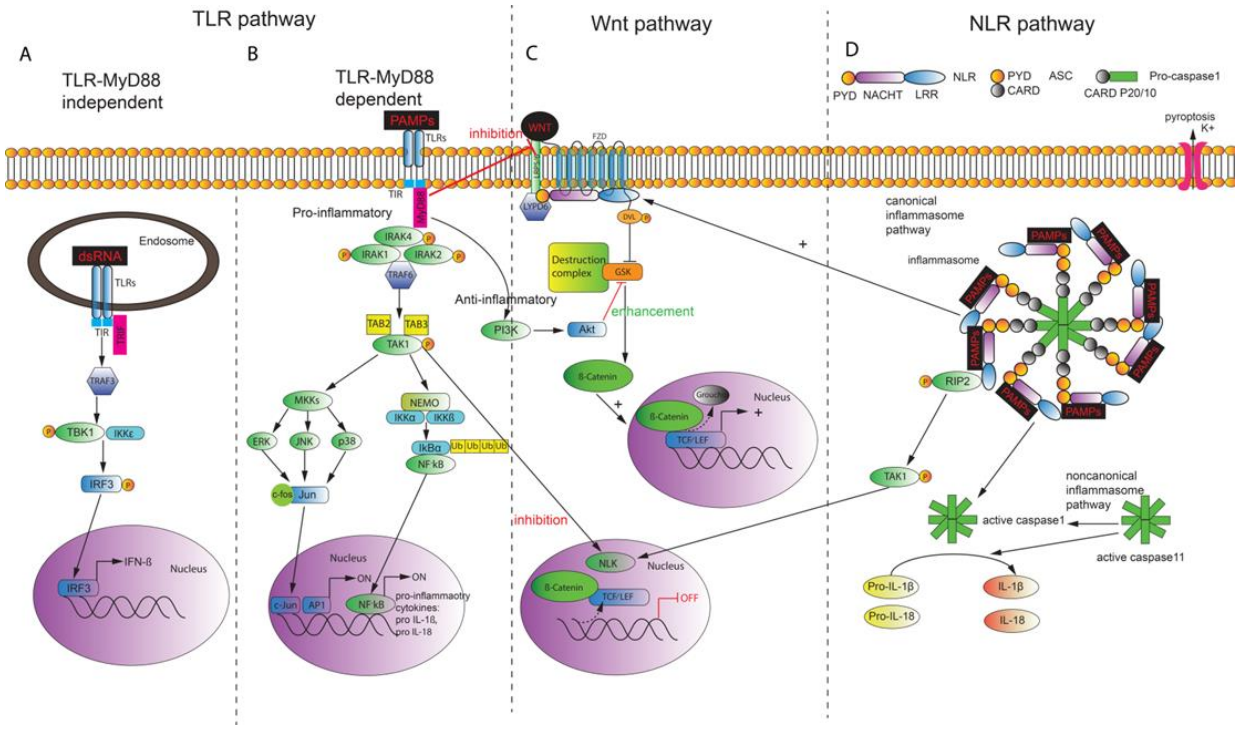

Figure 2 TLR Pathway and NLR Pathway Including Their Modification to Wnt/ß-Catenin Signaling

(A). Depiction of the TLR-MyD88 independent pathway with a terminal IFN-1ß secretion. Intracellular PAMPs-dsRNA in endosomes are recognized by TLR3 and IKKε/TBK1 are recruited to phosphorylate IRF3 via TRIF and TRAF3. IRF3 translocates into the nucleus to trigger IFN-1ß expression. (B). Overview of the TLR-MyD88 dependent pathway inducing pro-inflammatory cytokines such as pro-IL-1ß and pro-IL-18. Upon extracellular PAMPs binding, TLRs recruit MyD88 to cytoplasmic TIR. Consequently, MyD88 associates with IRAKs, a process in which IRAK4 phosphorylates IRAK1 and 2 and promotes association with TRAF6. TAK1 and IKK complex is then activated. The subsequent IkBα degradation frees NF-kB to translocate into the nucleus for target gene expression. TAK1 can also mediate pro-inflammatory cytokines' expression through MKKs/MAPK cascades. (C). Diagram indicating the positive and negative influence of inflammatory pathways on Wnt signaling. Negatively, TLRs/MyD88 inhibits the binding of Wnt ligands to the LRP5/6 Fz receptor complex. Phosphorylated TAK1 activates NLK, which separates b-catenin/TCF-LEF from DNA. Activated NLR could also inhibit Wnt through the same TAK1/NLK pathway after RIP2 attachment and phosphorylation. Positively, the combination of MyD88 triggers an anti-inflammatory pathway via PI3K/AKT activation. AKT then enhances the level of b-catenin and Wnt target genes' expression. Alternatively, activated NLRs interact with Wnt receptors via LYPD6. (D). The NLR pathway, including the canonical/noncanonical inflammasome pathway. After the recognition of extracellular PAMPs by NLRs, ASC directly attaches on NLRs via the PYD domain and pro-caspase1 via CARD. Inflammasomes are self-assembled, leading to the cleavage of caspase-1. The activated caspase-1 catalyzes pro-IL-1ß and pro-IL-18 into functional IL-1ß and IL-18. The K+ ion channel on the inflammatory cell surface is open, dependent on active caspase-1. This circumstance results in pore formation in the cell membrane. In the noncanonical pathway, an activated caspase-11 can directly enhance IL-1ß and IL-18 release and promote the caspase-1 pathway as well.

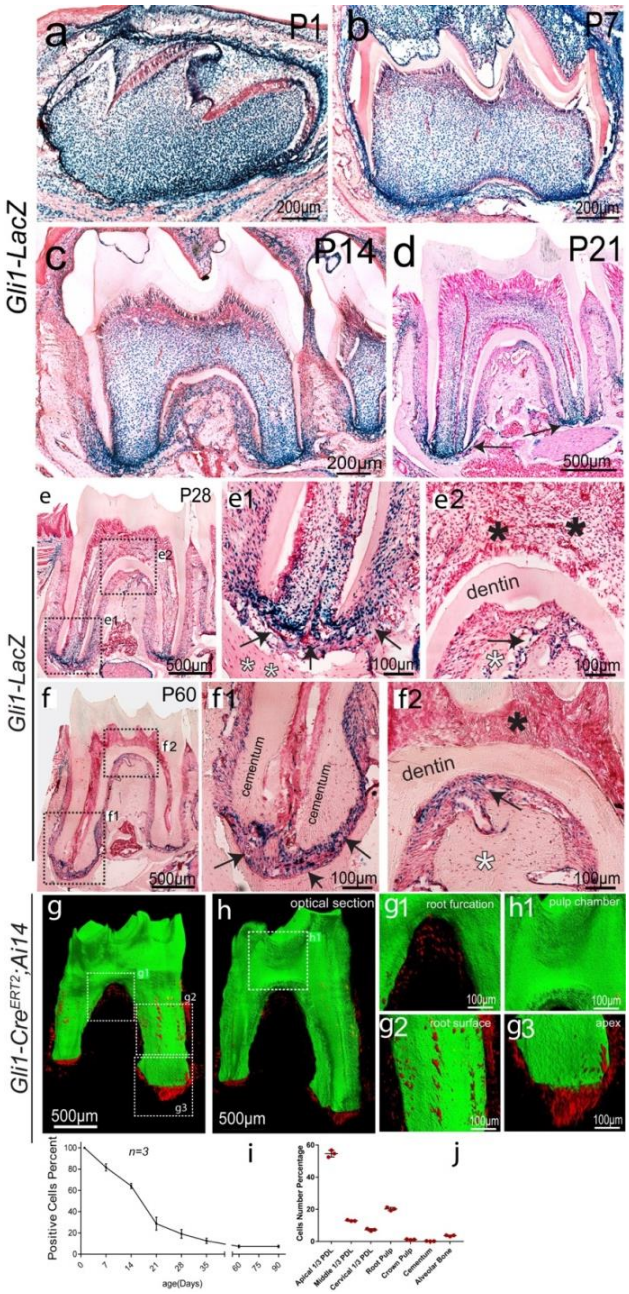

Figure 3 Gli1+ Cells Were Gradually Restricted to the Apical Region of Adult Molars During Postnatal Development.

Mandibles were collected from Gli1-lacZ mice. Lacz staining took place in the lower first molar of groups P1(a), P7(b), P14(c), P21(d), P28(e), and P60(f). The asterisk indicates Gli1+ cells in dental pulp tissue and the arrow indicates Gli1+ cells in PDL. Two doses of tamoxifen were given to Gli1-CreERT2; Ai14 mice to label Gli1+ cells. Four days after injection, mandibles were harvested and cleared with PEGASOS. (g). Three-dimensional images show initial Gli1+ cells distribution within the mice's lower first molar periodontium two days after induction. Boxed regions are enlarged in the right panels (g1-g3). (h). The optical section was acquired to indicate the pulp chamber. Boxed regions are enlarged in the panel on the right (h1). The color green denotes SHG+ mineralized tissue to outline the tooth structure while red areas are Gli1+ cells. Relative Gli1+ cell percentage within molar of differing development ages is quantified in (i). (j). Three-dimensional quantification of relative Gli1+ cell percentage within adult mice molar periodontium in different regions. Values are plotted as mean ± SEM. Scale bars are as shown in panels.

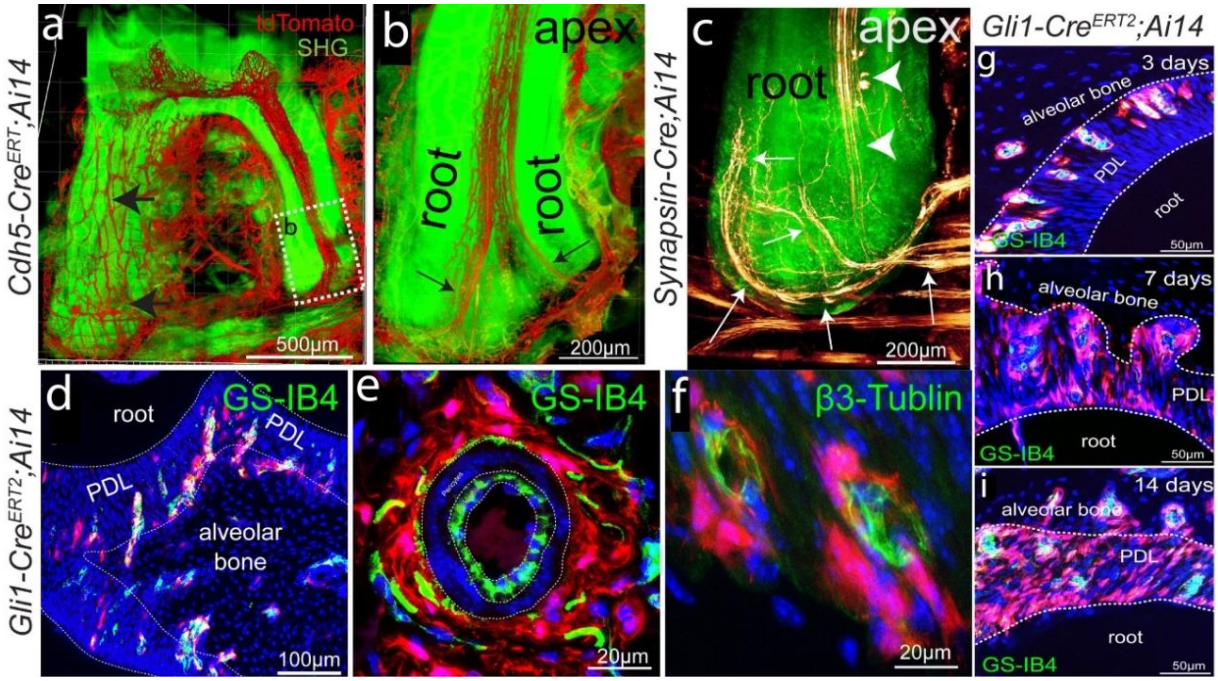

Figure 4 Gli1+ Cells Tightly Surrounded the Neurovasculature Bundle (NVB) and Multiplied Within PDL Along Vasculature

Mandibular molars were collected from adult Cdh5-Cre; tdTomato mice and processed following the PEGASOS clearing method. (a). Three-dimensional view of the vasculature system supporting the lower first molar of adult mice. Arrows highlight the supportive vasculature within PDL. The boxed area was enlarged in (b). Arrows indicate the blood vessels supporting the molar. Mandibular molars were collected from adult Synapsin-Cre; Ai14 mice and cleared with PEGASOS. SHG (in green) was used to label tooth structure. (c). Local three-dimensional view of nerve bundles from an adult first molar surrounding its lower root. Arrows mark the connected nerve. (d). Sagittal section and (e) cross-section of a Gli1-CreERT2; Ai14 mouse molar which was tamoxifen-induced for four days (initial Gli1+ cells appear red) after Gs-IB4 (green) immunohistochemical staining. Gs-IB4 labels vasculature. (f). ß3-tubulin (green) staining of the cross-section in a four days induced Gli1-CreERT2; Ai14 mouse molar`s PDL. Dapi is blue. (g-i). Immunohistochemical staining of Gs-IB4 (vasculature in green) in adult Gli1-CreERT2; Ai14 mouse molars collected on three days (g), seven days (h) or fourteen days (i) after tamoxifen induction. Dotted lines outline the PDL space on the cross-section of mice molars. Scale bars are as shown in each panel.

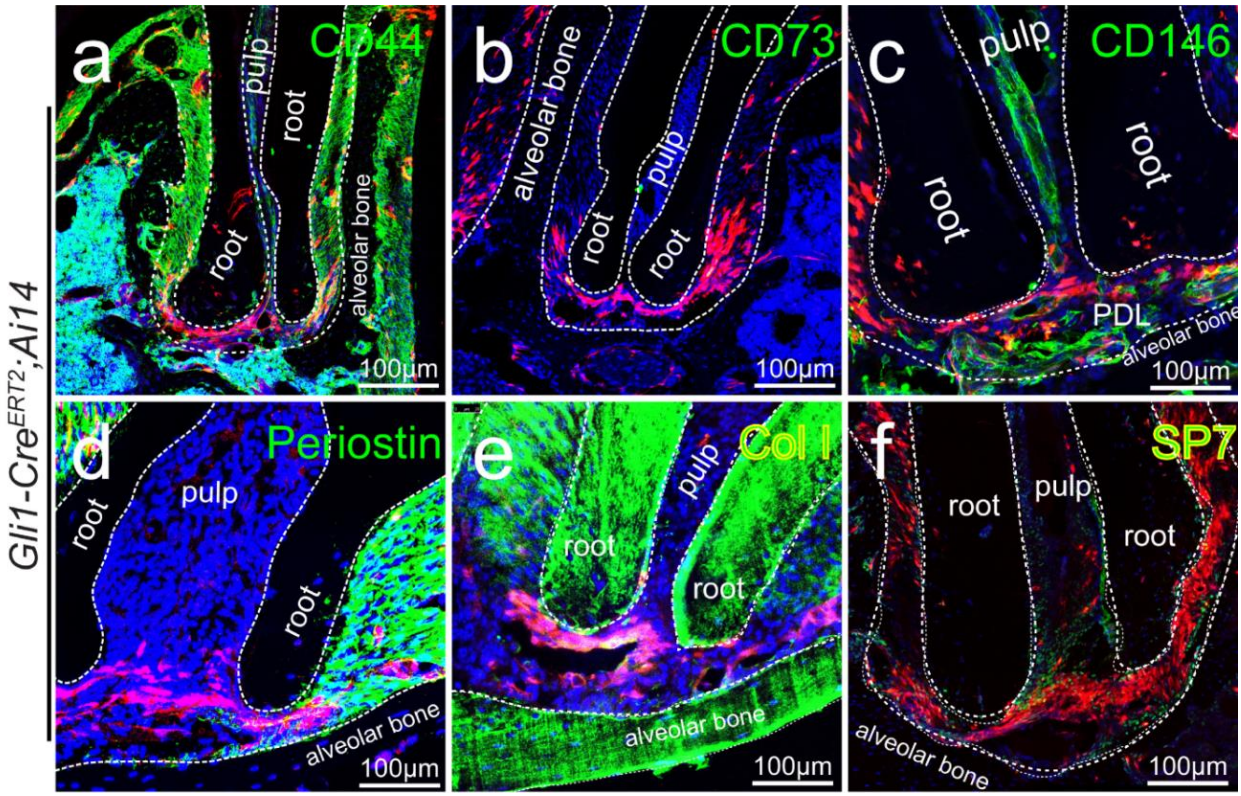

Figure 5 Gli1+ Cells Were Negative for Periodontium Lineage Differentiation Markers and Expressed Typical MSCs Markers in Vitro

Gli1+ cells were marked by inducing adult Gli1-CreERT2; Ai14 mice for two days. (a-c). Immunohistochemical staining of CD44, CD73, and CD146 in induced Gli1-CreERT2; Ai14 mice mandible molars. Red, Gli1+ cells; Green, typical in vitro MSC markers. (d-f). Co-staining assay of periostin (d), type1 collagen (e), and Sp7 (f). Red, Gli1+ cells; Green, markers for mature periodontium tissues. Blue, Dapi, labelled nuclei. Scale bars are as shown in each panel.

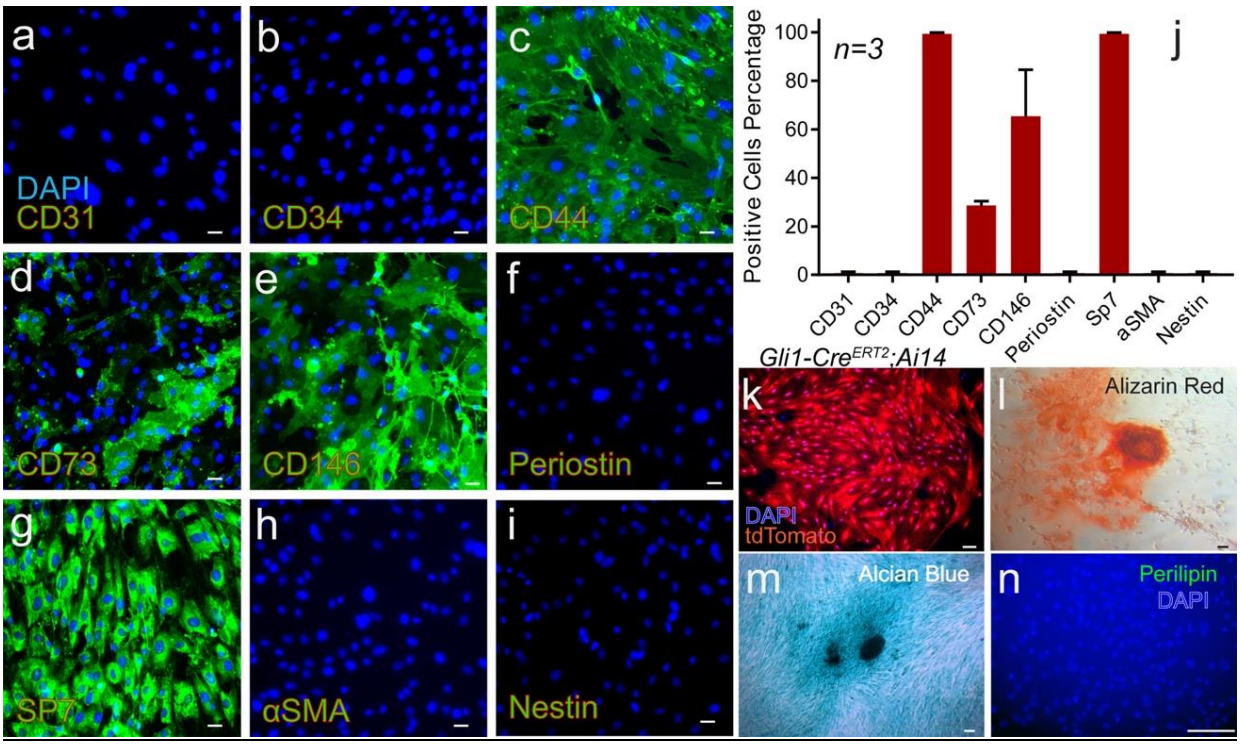

Figure 6 Gli1+ Cells Expressed Typical MSC Markers and Underwent Multilineage Differentiation in Vitro

Adult Gli1-CreERT2; Ai14 mice were induced for two days with tamoxifen and Gli1+ cells were isolated from their molar root surfaces. In vitro expression profile of Gli1+ cells was shown in (a-i). (j). Quantification of results in a-i. Values are plotted as mean ± SEM. (k). Gli1+ cell colony formed on the culture dish. (i). Alizarin red staining of Gli1+ cells two weeks after osteogenic induction. (m). The Alcian blue staining result of Gli1+ cells two weeks after chondrogenic induction. (n). Perilipin staining result of molar mesenchymal Gli1+ cells two weeks after adipogenic induction. Green, MSC markers; Blue (Dapi), Nuclei. The Scale bars, 10um.

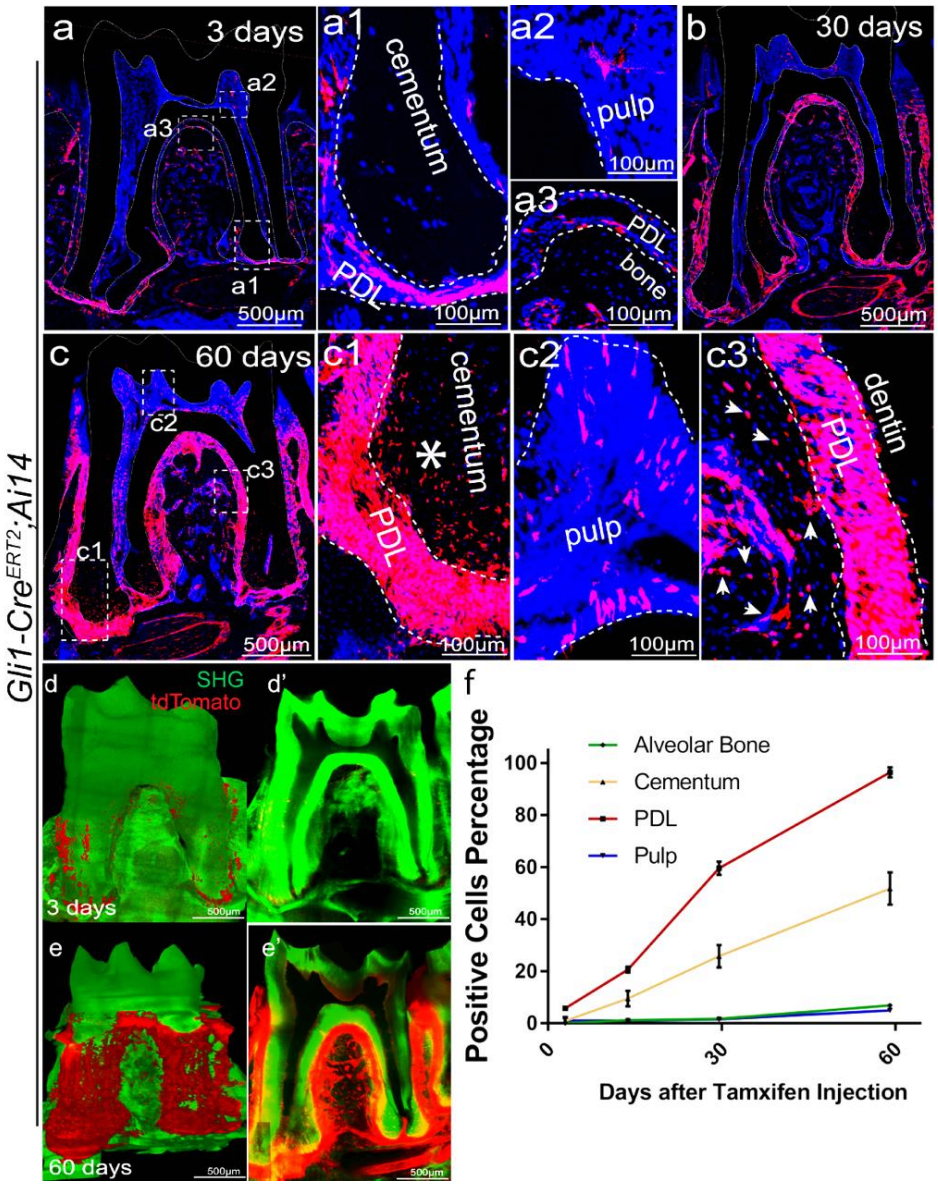

Figure 7 Gli1+ MSCs Contributed to Periodontium Physiological Turnover in Adulthood
One month old Gli1-CreERT2; Ai14 mice were induced with two injections of tamoxifen. Then, their mandibles were collected and sectioned for confocal assay after different time points. (a-c3). The time course of Gli1+ cells tracing (red) for adult Gli1-CreERT2; Ai14 mice three days after tamoxifen induction (a, a1-a3), 30 days after induction (b), and 60 days after induction (c, c1-c3). Boxed areas are shown magnified in the right panels. The asterisk indicates Gli1+ cells in cementum. The arrow represents positively labeled osteocytes and dotted lines outline tooth structure. (d). A three-dimensional view of Gli1+ cells (red) distribution in adult Gli1-CreERT2; Ai14 mice molar periodontium three days after tamoxifen induction. Next, an optical section was acquired to show the dental pulp, cementum and alveolar bone regions inside. (e). Three-dimensional view of Gli1+ cell (in red) distribution in adult GT mouse molar periodontium 60 days after tamoxifen induction. (e'). The optical section was captured to display the dental pulp, cementum and alveolar bone regions inside. SHG appears green to show the tooth structure. (f). Quantification of Gli1+ cells' lineage tracing results from the first two months within adult molar PDL, cementum, alveolar bone, and pulp. Values are plotted as mean ± SEM. Scale bars are as shown in panels.

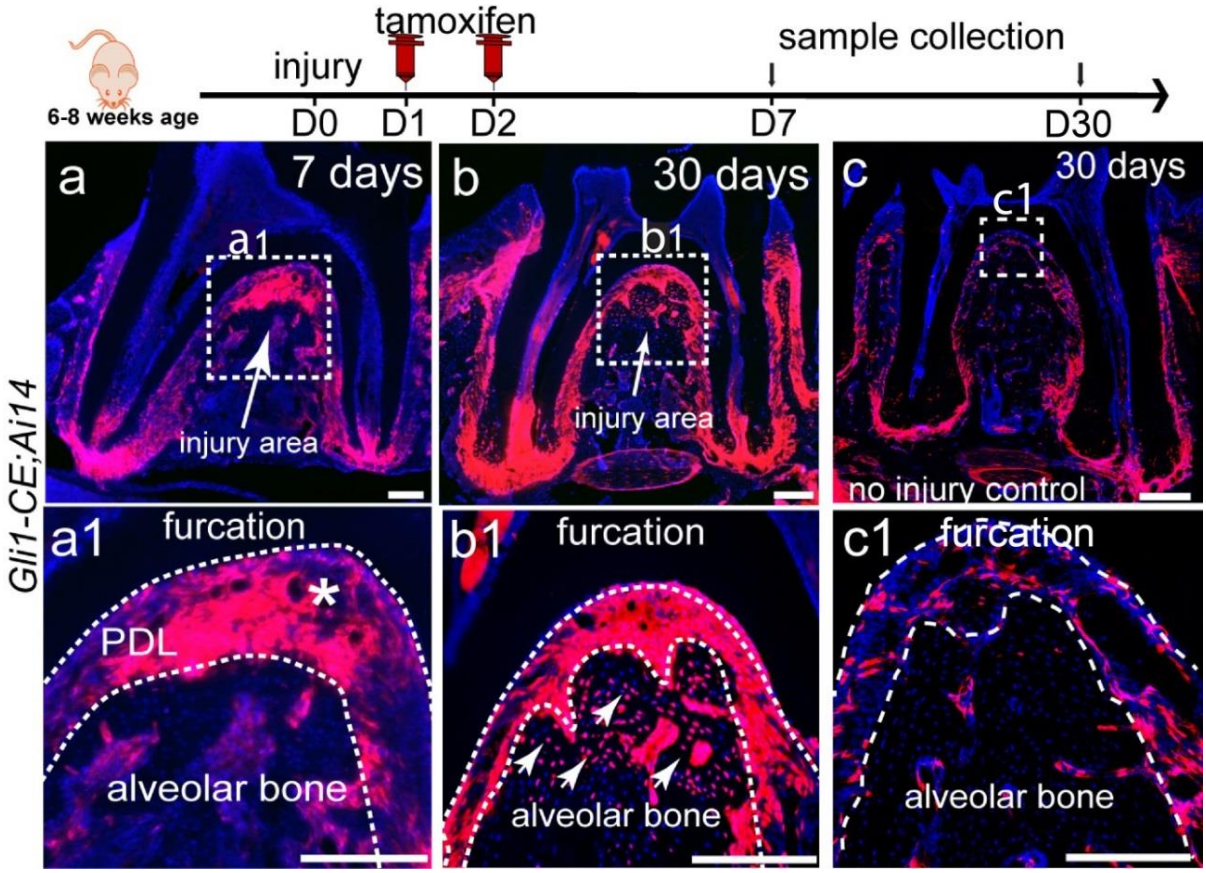

Figure 8 Gli1+ Cells Supported Periodontium Tissue Injury Repair.
An injury model was performed on 6~8 week old Gli1-CreERT2; Ai14 mice on their molars at the furcation area. The mice were induced with two injections of tamoxifen immediately after the injury. Littermate Gli1-CreERT2; Ai14 mice without injury were set as the control group. Then, mandibles were collected 7 and 30 days after injury. Images were acquired afterwards under a confocal microscope. (a). The Lineage tracing result from injured molar sections seven days after receiving a syringe punch. (a1). The local magnification of the injury site indicated in box area (a). The asterisk indicates enhanced Gli1+ activation within PDL at the injury site. (b). The lineage tracing result of molar sections 30 days after injury and tamoxifen administration. (b1). Local magnification of an injury site as the box area in (b). The arrow indicates Gli1+ osteocytes in the injury site. (c). Lineage tracing results of Gli1+ cells within the no injury control group's molar periodontium. (c1). Local magnification of the furcation area as boxed in (c). DAPI is present in blue. Scale bars are as displayed in panels.

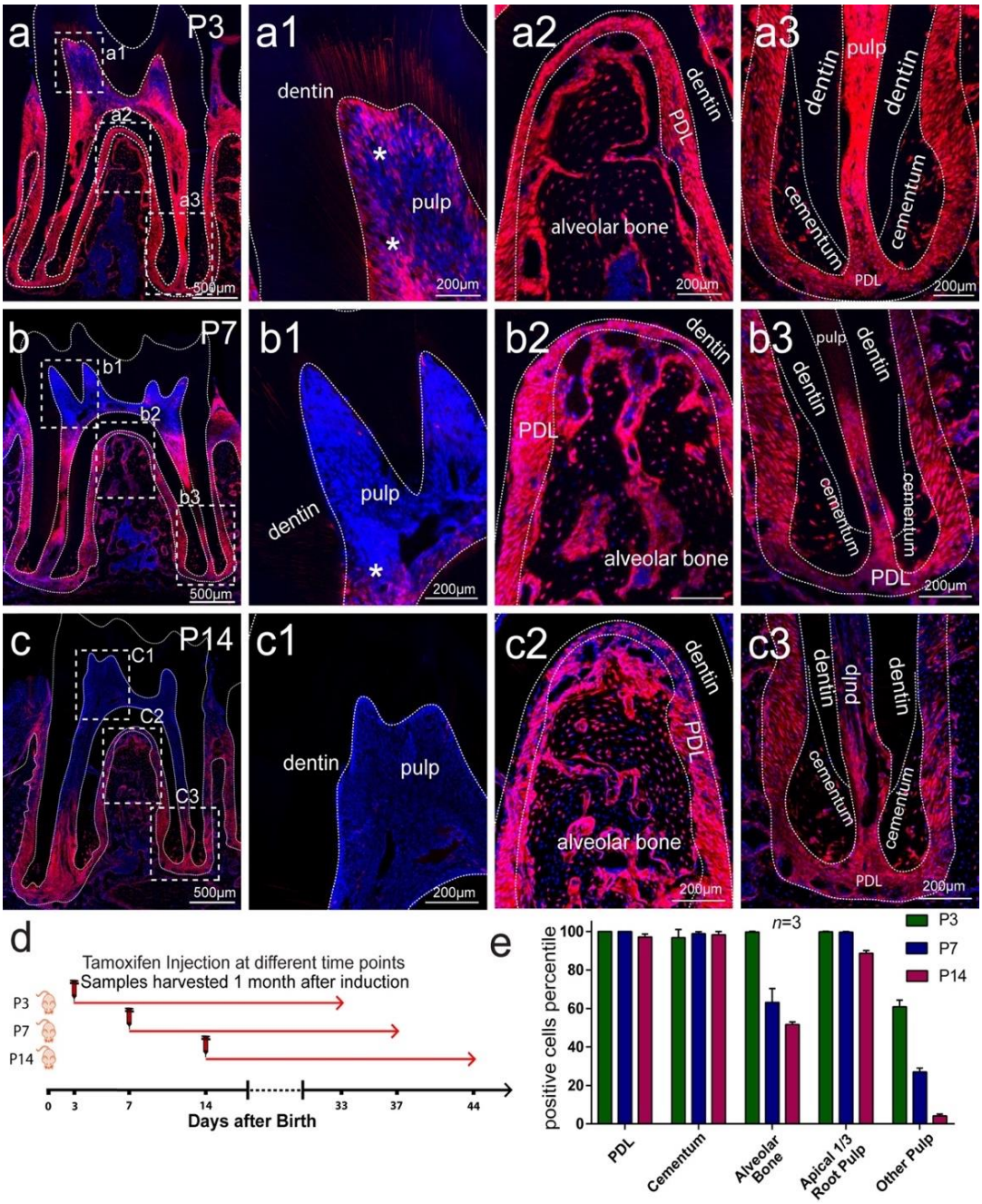

Figure 9 Multipotent Gli1+ Cells Gave Rise to the Entire Molar Periodontium at a Young Age.
(a). The lineage tracing result of P3 Gli1-CreERT2; Ai14 mice one month after tamoxifen injection. Additionally, boxed areas are magnified in the right panels of the figure, demonstrating Gli1+ cells' distribution in the respective crown pulp (a1), furcation (a2), and root tip areas (a3). (b). Lineage tracing result of P7 Gli1-CreERT2; Ai14 mice one month after tamoxifen injection. Boxed areas are enlarged in the right panel, demonstrating Gli1+ cells' distribution in corresponding crown pulp (b1), furcation (b2), and root tip (b3) areas. (c). Lineage tracing result of P14 Gli1-CreERT2; Ai14 mice one month after tamoxifen injection. Boxed areas are magnified in the right panels, demonstrating Gli1+ cells' distribution in several places such as crown pulp (c1), furcation (c2), and root tip on the mice. (c3). Dotted lines outline tooth structure. Asterisks indicate Gli1+ cells in pulp. (d). Tamoxifen administration scheme. (e). Quantification results of a lineage tracing assay as shown in the above panels. Values are shown as mean ± SEM. Scale bars are as shown in panels.

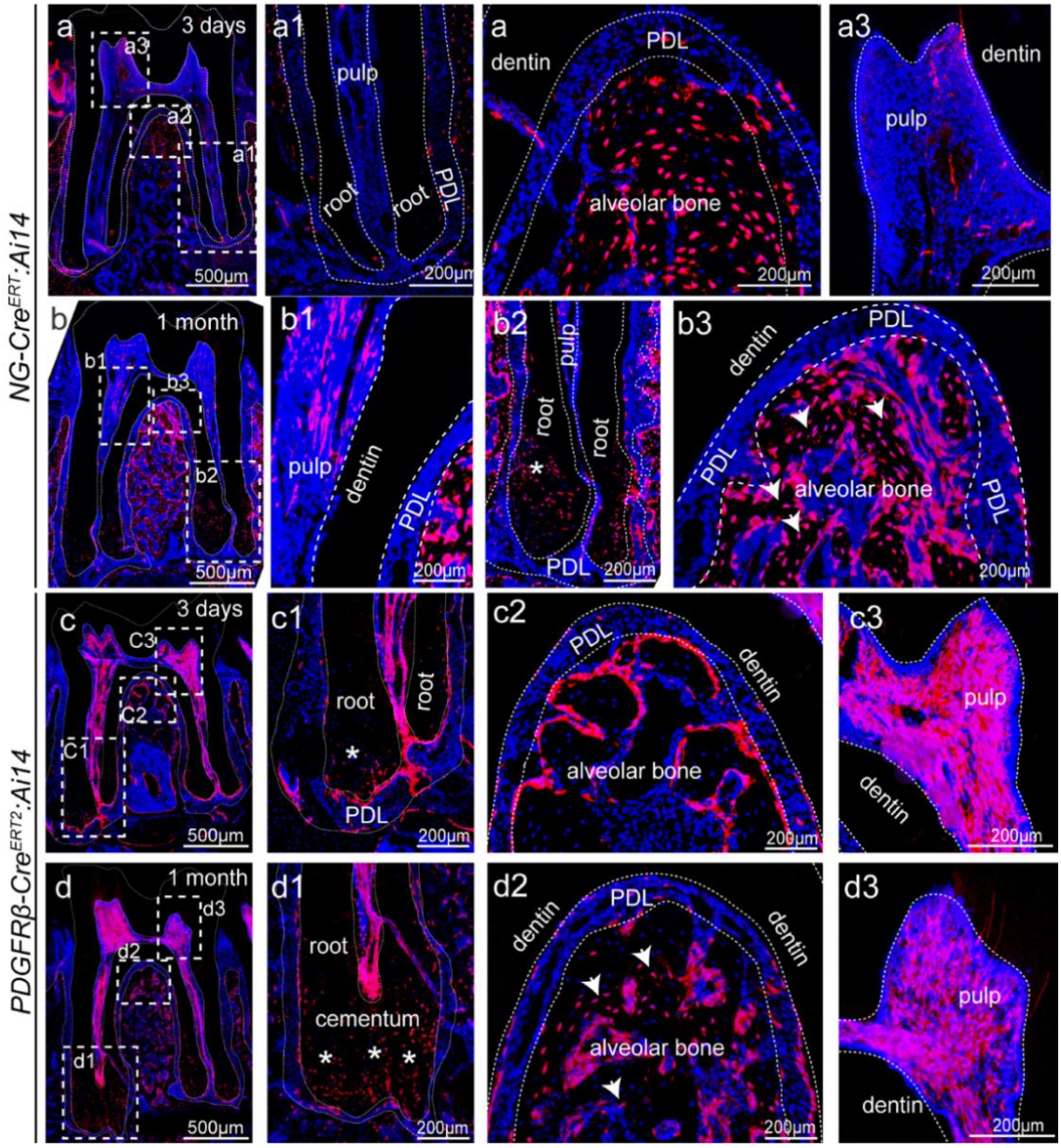

Figure 10 Gli1+ Cells Were the Primitive Stem Cell Populations of Adult Molar Periodontium.
6~8 week old NG2-CreERT2;Ai14 and PDGFRb-CE;tdTomato mice were induced with two injections of tamoxifen. Then, mandibles were collected three days and one month after induction. (a). NG2+ cells' distribution pattern three days after injection. Boxed areas are magnified on the right panels, which display their respective distribution in the molar root tip (a1), furcation (a2) and crown pulp (a3) areas. (b). Lineage tracing results of NG2+ cells one month after injection. Boxed areas are magnified to the right panels showing the root tip (b1), furcation (b2) and crown pulp areas (b3). Asterisk marks the NG2+ cells in cementum. The arrow marks osteocytes derived from NG2+ cells. (c). PDGFRb+ cells' distribution pattern three days after injection. Boxed areas are magnified to the right panels displaying PDGFRb+ cells' specific distribution in the molar root tip (c1), furcation (c2) and crown pulp (c3). Asterisk marks the PDGFRb+ cells in cementum. (d). Lineage tracing results of PDGFRb+ cells one month after tamoxifen injection. Boxed areas are magnified to the right panels showing the root tip area (d1), furcation (d2), and crow pulp areas (d3). Asterisk marks the PDGFRb+ cells in cementum. The arrow designates osteocytes derived from PDGFRb+ cells. Dotted lines outline tooth structure. Red denotes positive cells while blue DAPI represents the nucleus. Scale bars are as shown in panels.

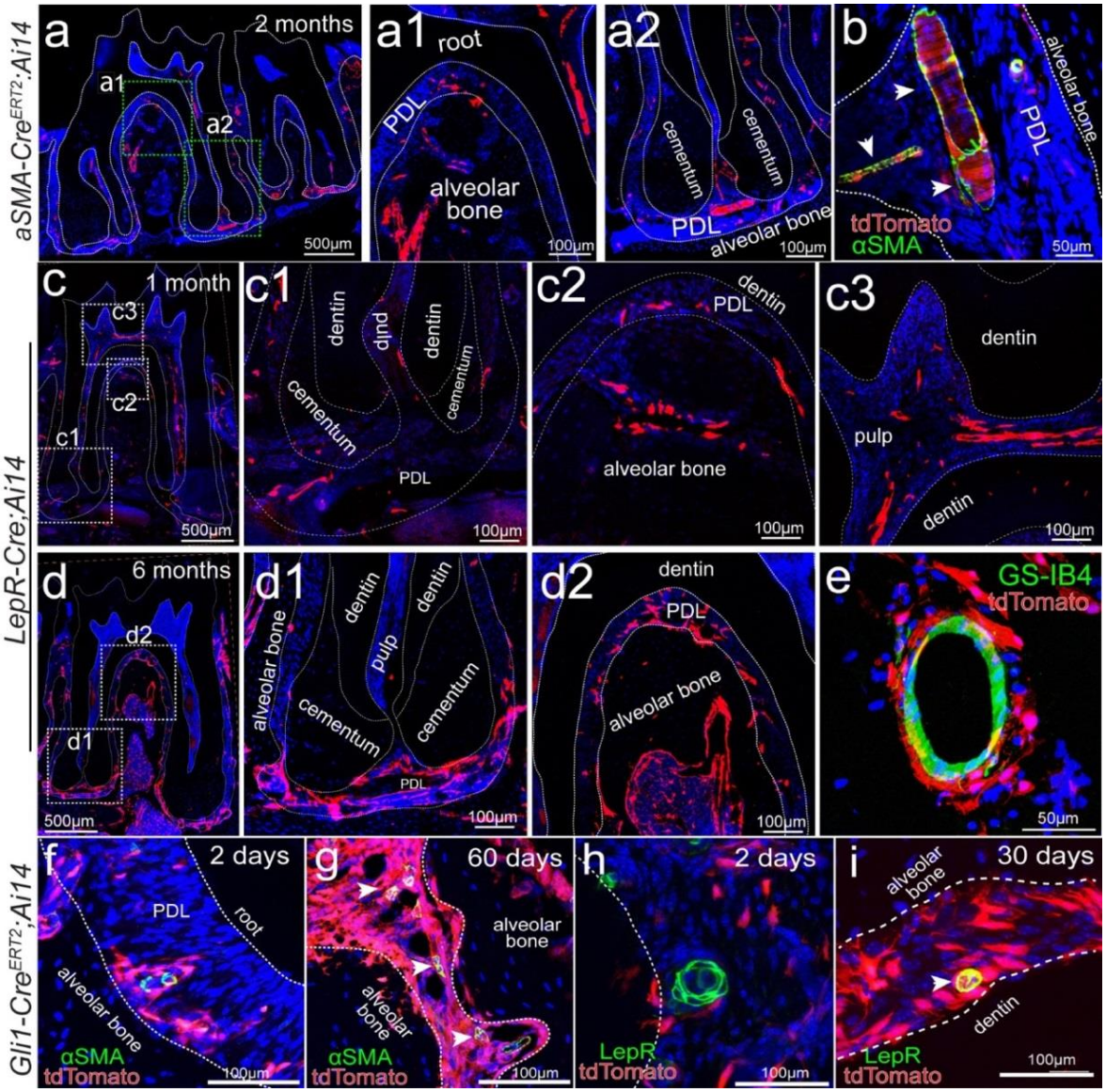

Figure 11 Gli1+ Cells Were the Primitive Stem Cell Populations of Adult Molar Periodontium.

(a).aSMA+ cells' distribution pattern two months after tamoxifen induction in 6~8 week old aSMA-CreERT2;Ai14 mice. Boxed areas are magnified on the right panels, displaying aSMA+ cells' distribution in the mice`s corresponding molar furcation (a1) and root tip (a2) areas r. The scale bar, 500um in a, 100um in a1 and a2. (b) aSMA immunofluorescent staining in a two month induced aSMA-CreERT2;Ai14 mice molar shows co-localization of an aSMA antibody (green) and aSMA+ cells (red). Scale bar, 50um. (c). Confocal images of LepR+ cells' distribution in a one month old LepR-Cre;Ai14 mouse molar. Boxed areas are magnified to the right in panels which display LepR+ cells' distribution in respective root tip (c1), furcation (c2), and crown pulp (c3) areas. Scale bar, 500um in c and100um in c1-c3. (d). Confocal images of LepR+ cells' distribution in a six month old LepR-cre;Ai14 mouse molar. Boxed areas are magnified to the right, with panels displaying LepR+ cells' distribution in the assigned root tip (d1), furcation (d2) areas. Scale bar, 500um in d and100um in d1, d2. (e). Gs-IB4 immunofluorescent staining in a six month old LepR-cre; Ai14 mouse molar shows LepR+ cells (red) surrounding GS-IB4 stained blood vessels (green). Scale bar, 50um. (f). Merged confocal image of aSMA antibody and initial Gli1+ cells in two day induced Gli1-CreERT2; Ai14 mice. (g). aSMA immunofluorescent staining in six day induced Gli1-CreERT2; Ai14 mice. (h). Merged confocal image of LepR antibody and initial Gli1+ cells in two day induced Gli1-CreERT2; Ai14 mice. (g). LepR immunofluorescent staining in thirty day induced Gli1-CreERT2; Ai14 mice. Red, positive cells and blue, DAPI, nucleus. Scale bars are as shown in panels.

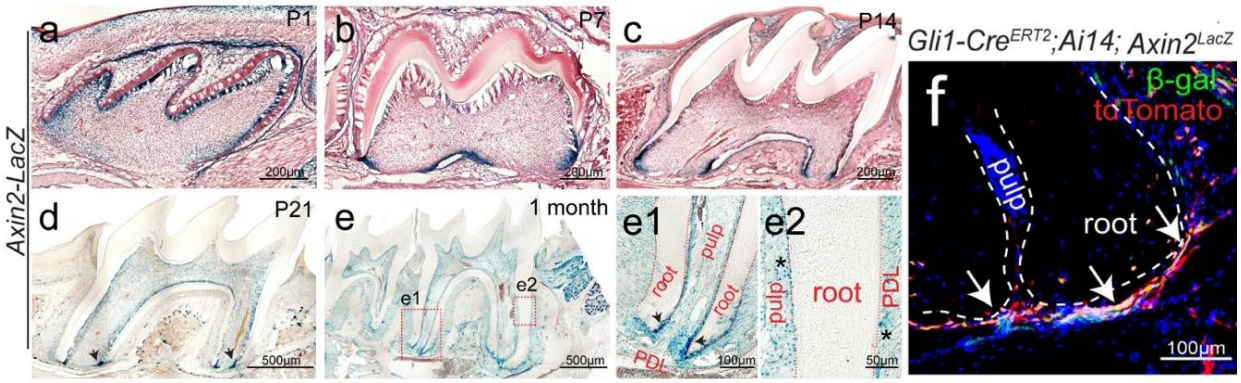

Figure 12 Wnt Signaling was Gradually Restricted to the Adult molar Apical Region and corresponded to Gli1+ MSCs Activity.

LacZ staining was performed on Axin2-LacZ mice molars during the following time periods: P1 (a), P7 (b), P14 (c), P21 (d) and postnatal 1 month (e). Boxed areas in (e) are enlarged in (e1) and (e2). The arrow marks Gli1+ cells gathering in the root apex area. Asterisk denotes Gli1+ odontoblasts. (f). Co-localized Axin2 staining within Gli1+ cells. Red, Gli1+ cells; green, Axin2+ cells; blue, DAPI. Scale bars are as displayed in panels.

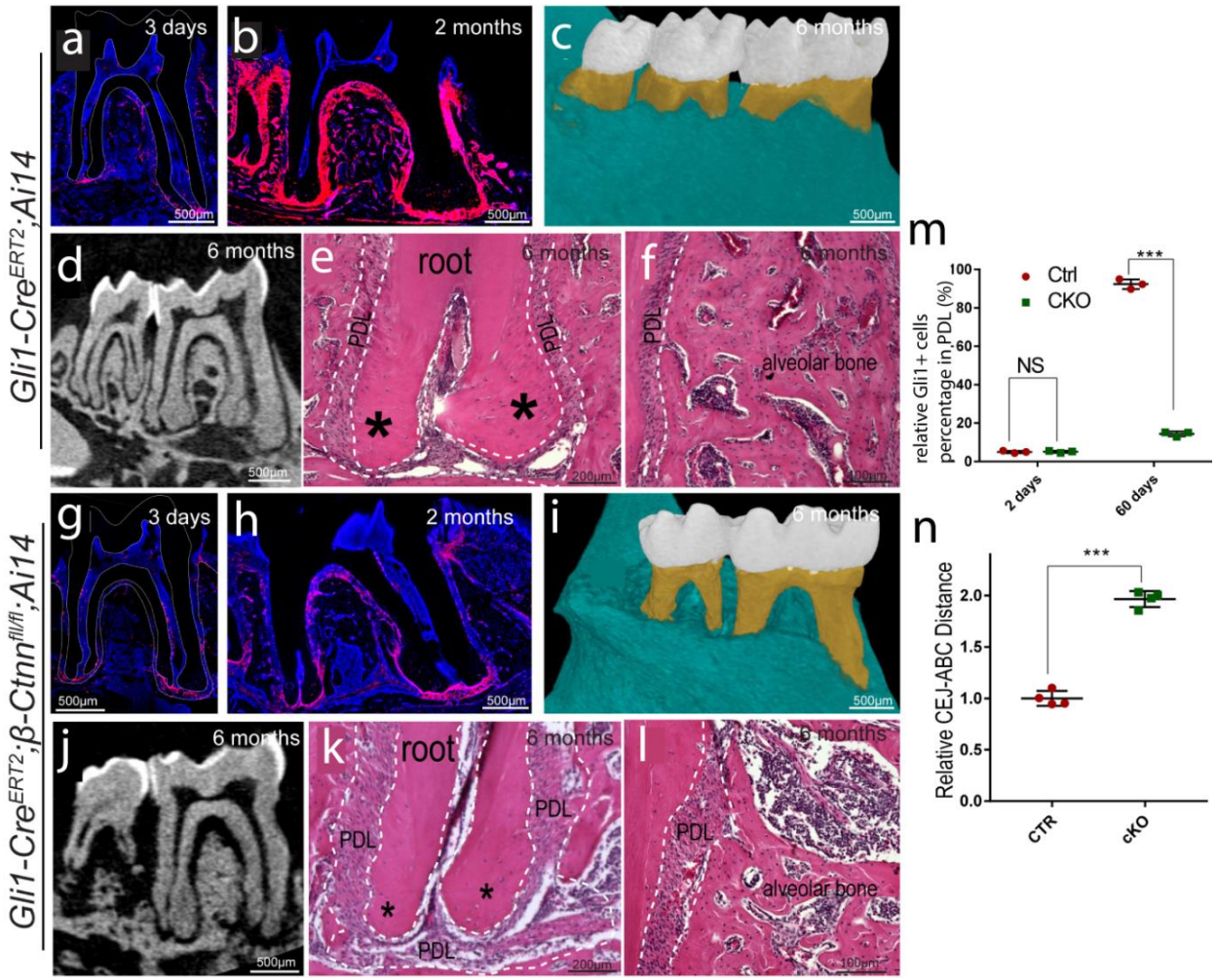

Figure 13 Blockage of the Canonical Wnt Pathway Within Gli1+ MSCs Led to Deactivation and Severe Periodontium Tissue Loss

Gli1-CreERT2; β-Catenin$^{flox/flox}$; Ai14 and littermate Gli1-CreERT2; Ai14 mice at 6~8 weeks of age were induced with tamoxifen and sacrificed three days and two months later. (a,b). Control of the lower first molar showed normal respective Gli1+ cell distribution three days and two months after induction. (c). μCT results of the control lower first molar six months after tamoxifen induction. (d). Longitudinal μCT images of the control lower first molar six months after induction. (e). H&E staining of the control group`s molar root apical region. The asterisk indicates normal cementum morphology. (f). H&E staining of the control molar furcation area. (g,h). Mutant lower 1st molar showed corresponding inhibited Gli1+ cells distribution three days and two months after induction. (i). Overview of μCT results from the mutant lower first molar six months after tamoxifen induction. (j). Longitudinal μCT images of the mutant mice molar six months after induction. (k). H&E staining of the mutant molar's root apical region. The asterisk indicates reduced cementum volume. (l). H&E staining of the mutant molar furcation area. (m). Quantification of results from (a), (b), (g) and (h). (n). Quantification of alveolar bone loss in (c) and (i), represented by the distance between CEJ and ABC. CEJ designates cementum-enamel junction and ABC. Values are plotted as mean ± SEM (***$p < 0.001$; n = 6). NS means no significant differences. Red indicates Gli1+ cells and blue is DAPI use. Scale bars are as shown in panels.

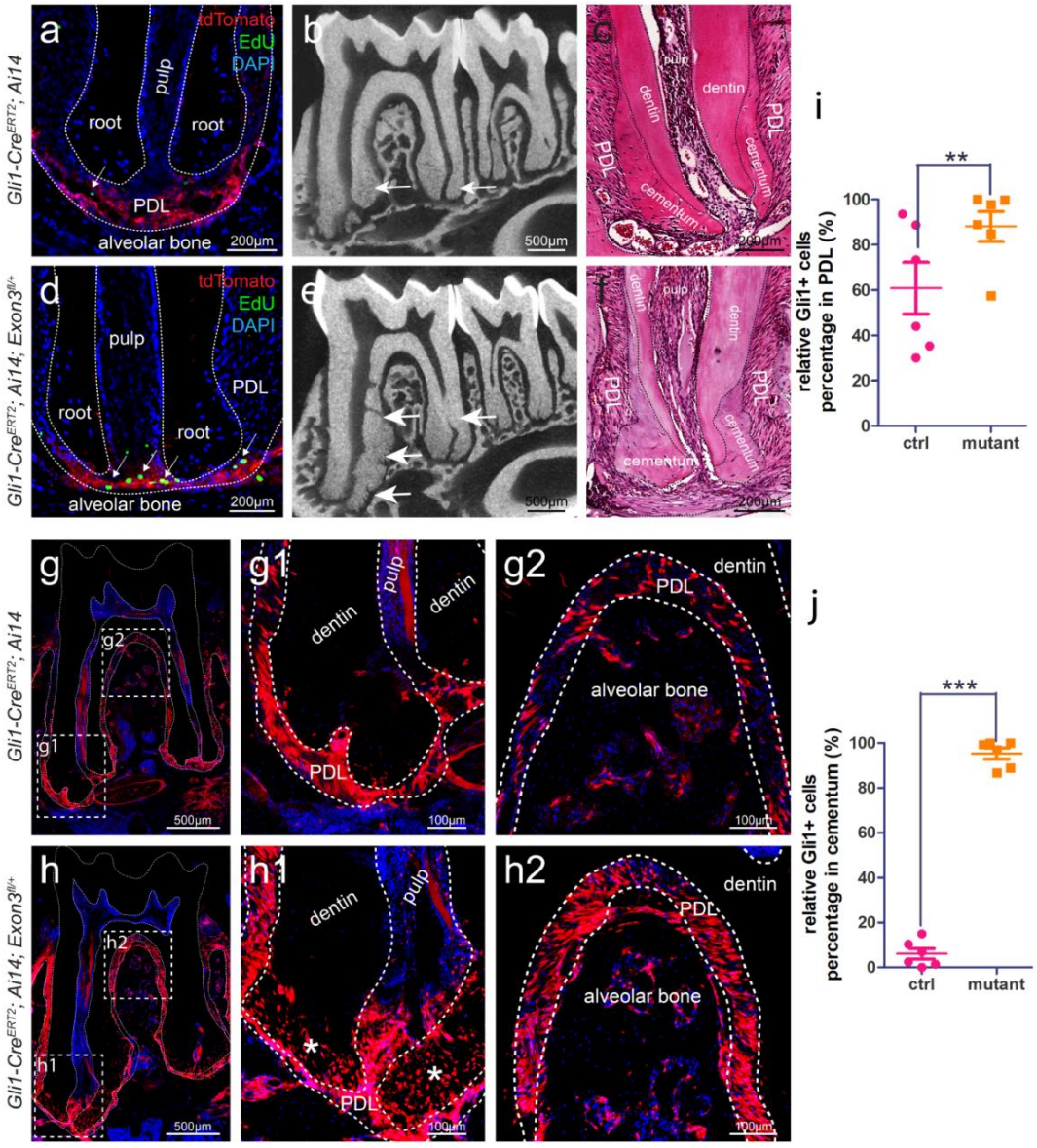

Figure 14 Constitutive Activation of Wnt Signaling Led to Periodontium Overgrowth and Enhanced Gli1+ MSCs Activation

Gli1-CreERT2; Ctnnb$^{fl/-(exon3)}$; Ai14 and littermate Gli1-CreERT2; Ai14 mice at 6~8 weeks of age were induced with tamoxifen for two consecutive days. (a). The control group`s lower first molars showed normal EdU+/Gli1+ cell distribution four days after tamoxifen induction (arrow). (b). Micro-CT result of the control lower first molar. Arrow indicates normal cementum. (c). H&E staining of the control lower first molar root apical region. (d). The Mutant lower first molar showed increased EdU+/Gli1+ cell numbers four days after tamoxifen induction (arrow). (e). Micro-CT scanning results of the mutant lower first molar. Arrow points to enlarged cementum. (f). H&E staining of the mutant lower first molar`s root apex. (g). Lineage tracing of the control lower first molar showed normal Gli1+ cell distribution two weeks after induction. Boxed places were magnified to display Gli1+ cells in the root tip (g1) and furcation areas (g2). (h). Lineage tracing of mutant lower first molar showed over-active Gli1+ cells in periodontium two weeks after induction. Boxed sections are magnified to display details in the root tip (h1) and furcation areas (h2). The asterisk indicates cementocytes derived from Gli1+ MSCs. The arrow highlights osteocytes expressing Gli1 inside the alveolar bone, specifically in its furcation area. (i). Quantification of results from (g1), (h1). (j). Quantification of results from (g2) and (h2). Values are plotted as mean ± SEM (**p<0.01; ***p < 0.001; n = 6). Red is designated for Gli1+ cells, green is , EdU+ cells, and Blue is shown for DAPI. Scale bars are as presented in panels.

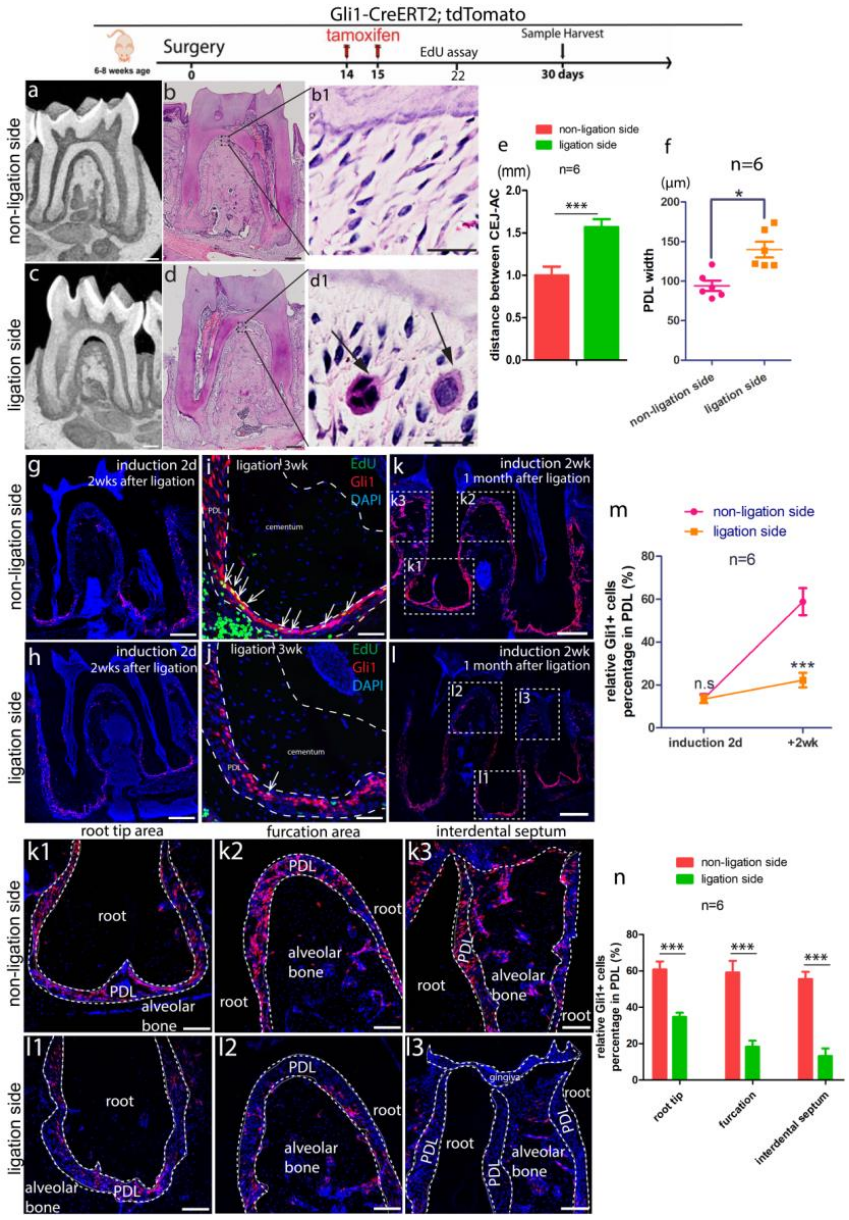

Figure 15 Periodontitis Compromised the Contribution of Gli1+ MSCs to Periodontal Tissue Through Deactivation One Month After Ligation

Ligation-periodontitis model was performed on 6~8 week old Gli1-CreERT2; tdTomato mice. Two weeks after ligation, tamoxifen was injected for lineage tracing. (a). Micro-CT result of the non-ligation side molar one month after ligation. (b). H&E staining of the non-ligation side's first molar one month after ligation. (b1). Local magnification of boxed areas in (b), showing no inflammatory cells inside the PDL space. (c). Micro-CT results of the ligation side`s first molar one month after ligation. (d). H&E staining of the ligation side`s first molar one month after ligation. (d1). Local magnification of boxed areas in (d), showing infiltrated inflammatory leukocytes within PDL. (e). Quantification of the CEJ-AC distance in (a) and (c). (f). Quantification of the PDL width of both non-ligation and ligation side molars in (b), (d). (g,h). Gli1+ cells tracing (red) in adult Gli1-CreERT2; tdTomato mice two days after tamoxifen induction on respective non-ligation and ligation sides two weeks after ligation. (i,j). EdU+/Gli1+ cells inside root tip area PDL on non-ligation and ligation side 3 weeks post ligation. (k,l). Two week lineage tracing results of the non-ligation side (k) and ligation side (l) of Gli1+ periodontal MSCs one month after ligation. Boxed areas are highlighted in (1-3), representing distribution of Gli1+ cells at the root tip (1), furcation (2), and interdental septum (3) areas. (m). Quantification based on the first two weeks of Gli1+ cell lineage tracing results in (g,h,k,l). (n). Quantification of relative Gli1+ cell percentage within PDL in the above three areas. Data is shown as Mean ± SEM (*p<0.05; ***p < 0.001; n = 6). Red indicates Gli1+ cells and green is EdU+ cells while blue is DAPI. Scale bars=200 μm in (a-d), (i,j), (k1-3), (l1-3), 500 μm in (g,h,k,l), and 10 μm in (b1,d1).

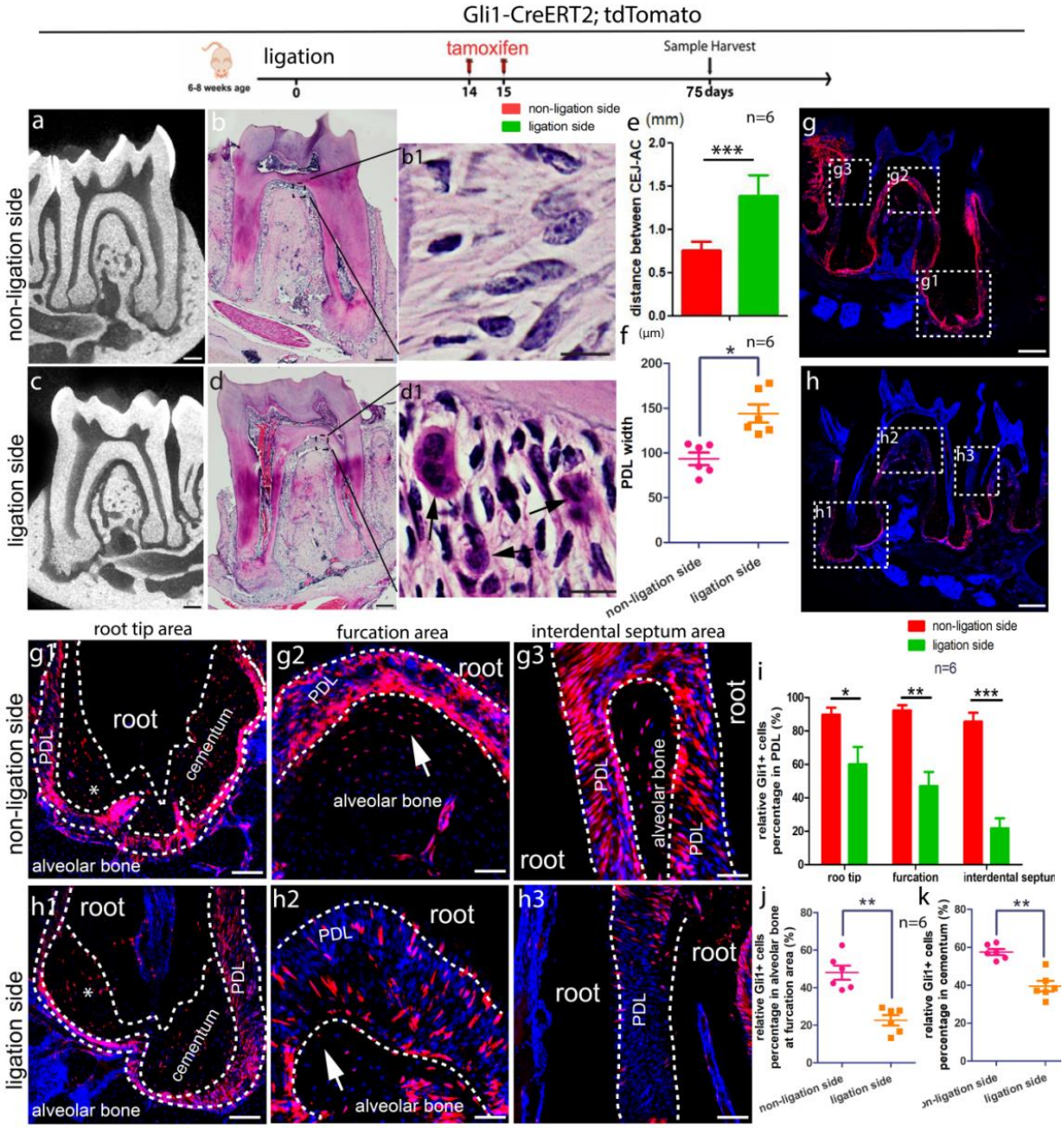

Figure 16 Chronic Periodontitis Compromised Gli1+ MSCs Lineage Commitment Activity

6~8 week old Gli1-CreERT2; tdTomato mice were ligatured on the right side of their lower first molar. Two weeks after ligation, tamoxifen was injected for two months of lineage tracing. (a). Micro-CT results of the non-ligation side's first molar. (b). H&E staining of the non-ligation side`s first molar. (b1). Local magnification of boxed areas in (b) showing no obvious inflammatory cells inside PDL. (c). Micro-CT results of the ligation side's first molar. (d). H&E staining of the ligation side`s first molar. Boxed areas in (d) were enlarged in (d1) to show inflammation characteristic in PDL. The arrow marks inflammatory PMNs' infiltration into PDL tissue. (e). Quantification of the distance between the CEJ and AC of both non-ligation and ligation side molars. (f). Quantification of PDL space in width of both the non-ligation and ligation side molars. (g, h). Overview of lineage tracing result belonging to Gli1+ cells in the periodontium of respective non-ligation and ligation side molars. Boxed areas are magnified in g1-3, h1-3 representing the distribution of Gli1+ cells at the root tip, furcation and interdental septum areas. An arrow indicates osteocytes derived from Gli1+ MSCs. The percentage of Gli1+ cells within PDL in the three boxed areas are quantified in (i). (j). Quantification of lineage tracing in (g2) and (h2), indicating the relative percentage of Gli1+ MSCs derived osteocytes in the furcation area. (k). Quantification of lineage tracing in (g2), (h2) demonstrating the relative percentage of Gli1+ MSCs derived cementocytes in the root tip. Data is shown as Mean ± SEM (*p<0.05; ** p<0.01, ***p < 0.001; n = 6). Red marks Gli1+ cells and blue represents DAPI. Scale bars, 200 μm in (a-d), (g1-3), (h1-3), 500 μm in (g-h), and 10 μm in (b1, d1).

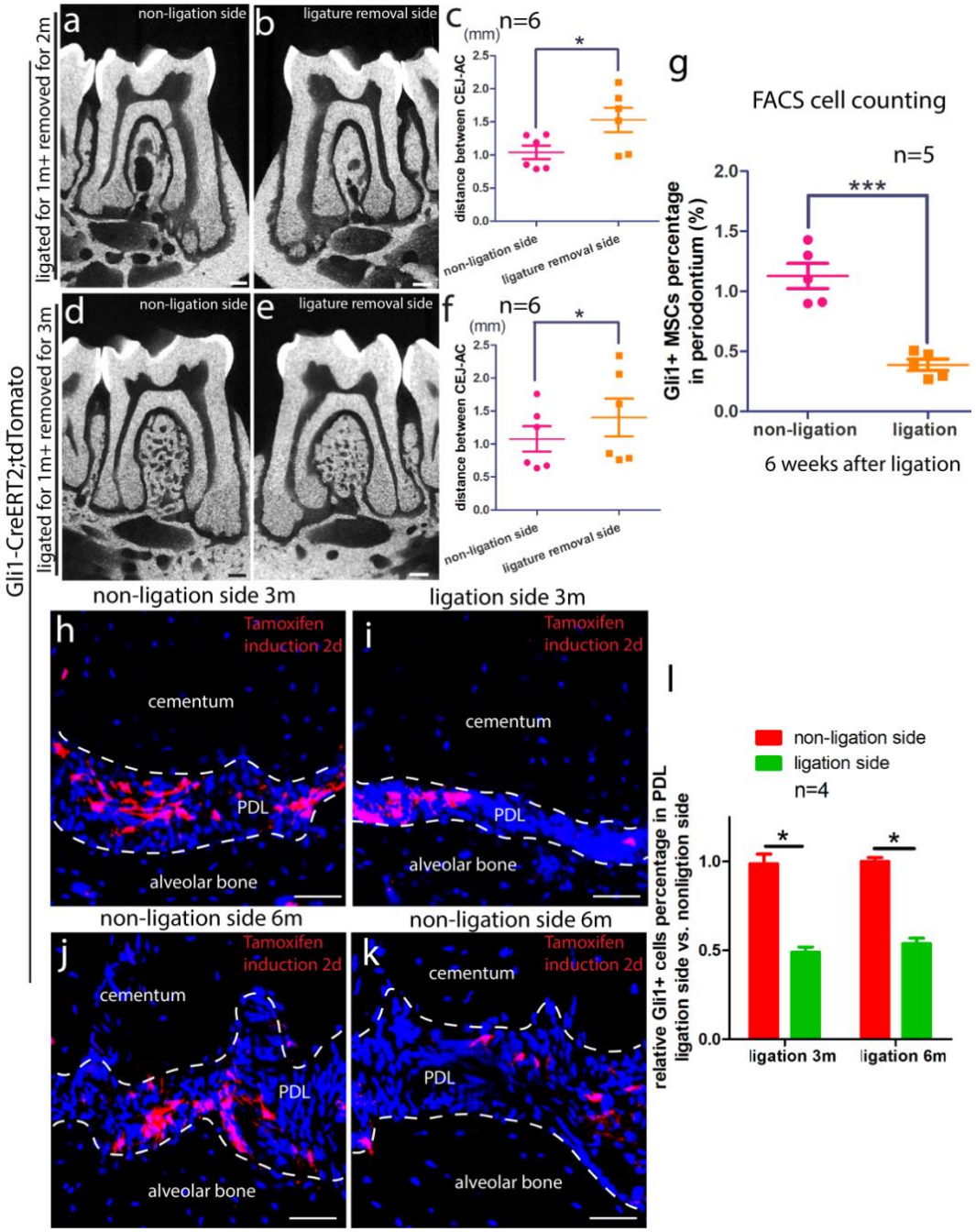

Figure 17 Chronic Periodontitis Inhibited Gli1+ MSCs Maintenance

Ligation-periodontitis model was performed on the lower right first molars. One month after ligation, the ligature was removed and two or three months were given for possible regeneration. Lower left first molars remained un-ligated. (a), (b). Micro-CT result of the non-ligation side and ligature side two months post ligature removal. (c). Quantification of the CEJ-AC distance for both non-ligation and ligature removal side molars in (a),(b). (d), (e). Micro-CT result of the non-ligation side and ligature removal side of the mice three months post ligature removal. (f). Quantification of the CEJ-AC distance within both non-ligation and ligature removal side molars in (d),(e). (g). FACS result of Gli1+ MSCs percentage in PDL cells six weeks post ligation. (h),(i). Local magnification showing Gli1+ MSCs' distribution in PDL three months after ligation model on corresponding areas of non-ligation and ligation. (j),(k). Local magnification showing Gli1+ MSCs distribution in PDL six months after ligation model on respective non-ligation and ligation sides. (l). Quantification result of Gli1+ MSCs' percentage in (h-k). The Gli1+ cells' percentage on the non-ligation side is normalized to 1.0. The ligation side relative to the Gli1+ cells percentage was the ratio to the non-ligation side. n=4. Data is shown as Mean ± SEM (*$p < 0.05$; n = 6). Red, Gli1+ cells; blue, DAPI. Scale bars, 200μm in a, b, d, and e; 100 μm in h, i, j, and k.

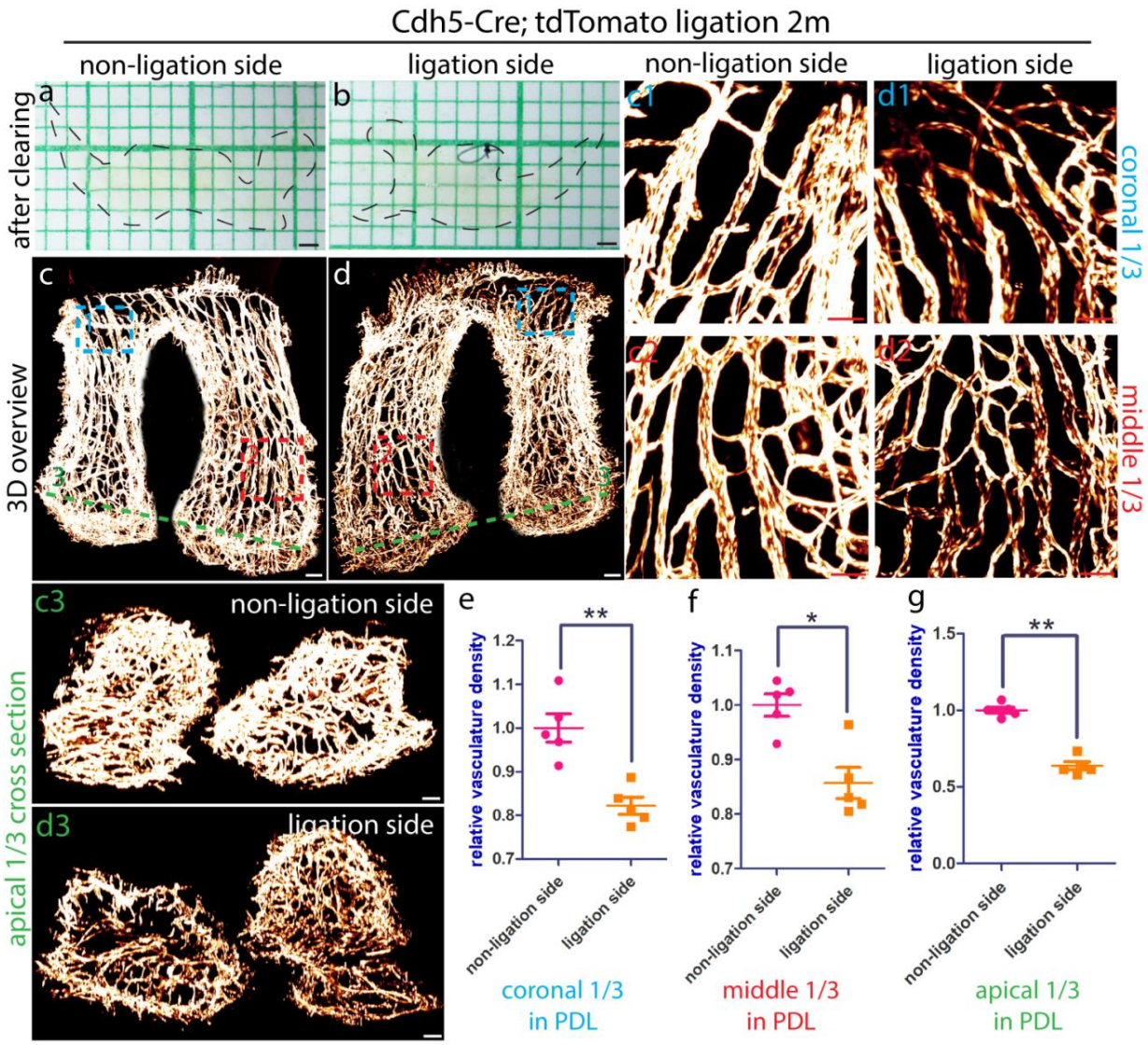

Figure 18 Vascular Density was Reduced in a Periodontitis Situation

Ligation model was performed on adult Cdh5-Cre; tdTomato mice. Two months later, both of their non-ligation side and ligation side mandibles were collected for PEGASOS tissue clearing and 3D imaging. (a), (b). Transparent mandibles were found after PEGASOS tissue clearing on their individual non-ligation and ligation sides. (c), (d). Three-dimensional overview images show PDL vasculature morphology of mice`s lower first molars during non-ligation and ligation. Boxed areas were enlarged to also show the vasculature morphology in coronal 1/3 (c1,d1), middle 1/3 (c2,d2) and apical 1/3 (c3,d3) of PDL. (e-g). Quantification of relative vasculature density on non-ligation and ligation side in respective coronal 1/3, middle 1/3, and apical 1/3 segments. Data is shown as Mean ± SEM (*$p < 0.05$; **$p<0.01$, $n = 5$). The vasculature density of non-ligation side PDL is normalized to 1.0. Glow is categorized as Cdh5+ blood vessels. Scale bars are set as 200 μm in a, b; 100 μm in c,d, c3, d3; 50 μm in c1,d1,c2, and d2.

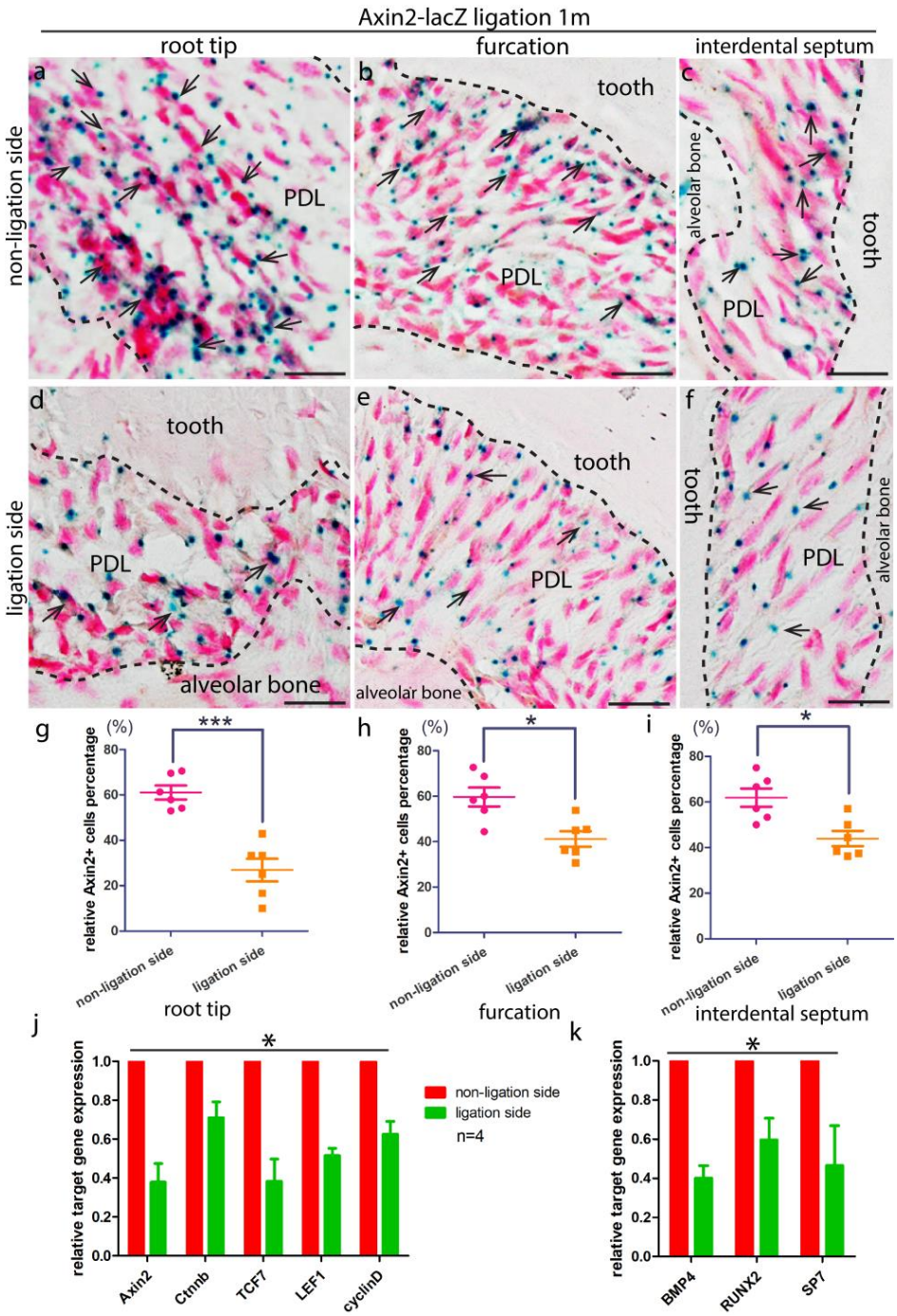

Figure 19 Wnt Activity was Down-Regulated During Periodontitis.

6~8 week old Axin2-lacZ mice were ligatured on lower right 1st molar and sacrificed one month later. LacZ staining was performed on both non-ligation and ligation side molars. (a-c). Axin2+ cell distribution inside non-ligated molars' PDL in the root tip a, furcation, and interdental septum areas. (d-f). Axin2+ cell distribution inside ligated molars' PDL in respective root tip, furcation, and interdental septum areas. Scale bars, 20 μm. Relative Axin2+ cell percentage within PDL in the above three representative areas, quantified accordingly in (g), (h), and (i). Data is shown as Mean ± SEM (*p<0.05; ***p < 0.001; n = 6). (j). Real-time PCR results coming from the relative expression levels of Wnt signaling target genes. (k). Real-time PCR results of the relative expression levels of osteogenic genes. The expression level of the non-ligation side is normalized to 1.0. n=4.

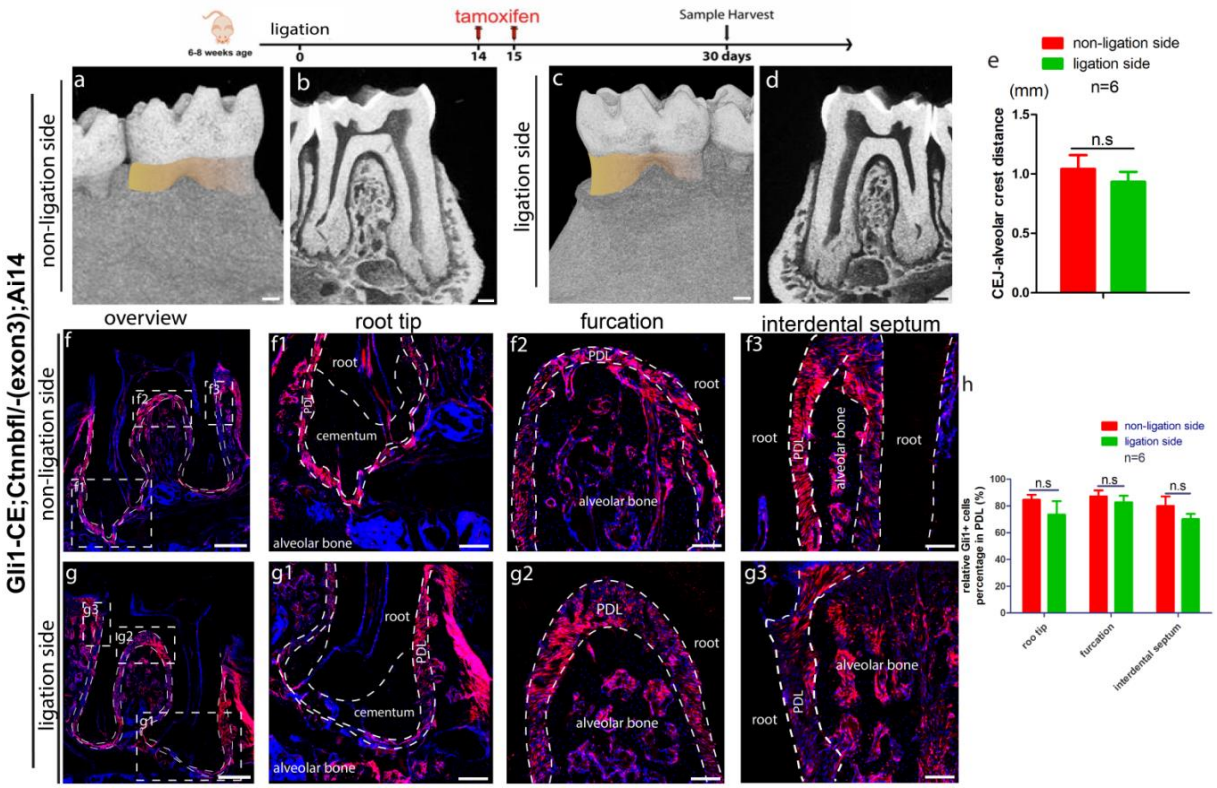

Figure 20 Over-Activation of Wnt Signaling Partially Rescued Tissue Loss and Gli1+ MSCs Inhibition During Periodontitis

6~8 week old Gli1-CreERT2; Ctnnb$^{fl/-(exon3)}$; Ai14 mice were ligatured on their right side lower first molar. Two weeks after ligation, tamoxifen was injected to over-activate Wnt and trace Gli1+ cells for two weeks. (a,b). Micro-CT assay of the non-ligation side molar alveolar bone height in mutant mice. (c,d). Micro-CT assay of alveolar bone height on the ligation side. CEJ-AC distance is quantified in (e). (f). Two weeks lineage tracing results of Gli1+ cell distribution within PDL on the non-ligation side in mutant mice. Boxed areas are magnified in (f1), (f2), and (f3) which highlight respective root tip, furcation, and interdental septum areas. (g). Lineage tracing results of Gli1+ cells within PDL on the molar ligation side in Gli1-CreERT2; Ctnnb$^{fl/-(exon3)}$; Ai14 mice. Boxed areas are magnified in (g1), (g2), and (g3), highlighting the root tip, furcation, and interdental septum areas. (h). Quantification of relative Gli1+ cells percentage within PDL in the above three areas. Data is shown as Mean ± SEM. n=6. n.s, no significant differences. Red denotes Gli1+ cells and blue markings are DAPI. Scale bars, 200mm in (a-d), (f1-3), and (g1-3), 500mm (f, g).

APPENDIX B

TABLES

Table 1 Mice Line Information Used in Section 2

Mouse Lines	Source	References
Gli1-LacZ	JAX#008211	(Bai et al., 2002)
Gli1-Cre ^{ERT2}	JAX#007913	(Ahn and Joyner, 2004)
NG2-Cre	JAX#008533	(Zhu et al., 2008)
ROSA26	JAX#007905	(Madisen et al., 2010)
Cdh5-Cre^{ERT2}	Obtained from Dr. Woo-Ping Ge (UTSW)	(Zhou, Bo et al.,2015)
Synapsin-Cre	JAX#003966	(Repem, D et al., 2006)
LeptinR-Cre	JAX#008320	(Ding, L et al., 2012)
PDGFR-Cre^{ERT2}	Obtained from Dr. Sean. J Morrison (UTSW)	(Xie et al., 1999)
αSma-Cre^{ERT2}	Obtained from Dr. Sean. J Morrison (UTSW)	(Perl et al., 2002)

Table 2 Available Wnt Signaling Reporter Mice Strains

Animal Strain	Reporter	Reference
TOP-GAL	TCF sites, c-fos promoter, LacZ	(Gupta and Fuchs, 1999)
BAT-GAL	TCF sites, Siamois promoter	(Maretto et al, 2003)
LEF-EGFP	TCF sites, EGFP	(Currier et al, 2010)
TCF/Lef:H2B-GFP reporter	TCF sites, H2B-GFP	(Ferrer-Vaquer et al, 2010)
ins-TOPEGFP, ins-TOPGAL	TCF sites, LacZ or GFP	(Moriyama, 2007)
Axin2-LacZ	Insert of LacZ into Axin2	(Lustig et al, 2002)
Axin2-d2EGFP	Axin2 promoter, EGFP	(Jho et al, 2002)
Axin2-mTurquoise2	Insert of mTurquoise into Axin2	(de Roo, 2017)
Axin2-rtTA	Axin2 promoter, rtTA	(Maruyuma, 2010)
Lgr5tm1-cre/ERT2	Cre/ERT2 insert into LGR5	(Barker et al, 2007)
Axin2-Cre/ERT2	Cre/ERT2 insert into Axin2	(Van Amerongen, 2012)
Tcf3-CreER	Cre/ERT2 into TCF3	(Howard et al, 2014)

Table 3 Primer Sequences Used in Section 4 for the qPCR Assay

	name	Forward primer 5'-3'	Reverse primer 5'-3'
Reference Genes	mouse β-actin	ATCAAGATCATTGCTCCTGAG	CTGCTTGCTGATCCACATCTG
	mouse GAPDH	CCTTCATTGACCTCAACTACAT	CAAAGTTGTCATGGATGACC
	mouse Tubulin	CGTGTTCGGCCAGAGTGGTGC	GGGTGAGGGCATGACGCTGAA
Wnt Signal Related Genes	mouse c-myc	GCTGTTTGAAGGCTGGATTTC	GATGAAATAGGGCTGTACGGA
	mouse cyclin D	TGCGTGCAGAAGGAGATTGT	CTTCTTCAAGGGCTCCAGGG
	mouse TCF7	AGGAGATGAGAGCCAAGGTCATTG	TTTTCCTCCTGTGGTGGATTCTTG
	mouse Axin2	TTATCCAGCGACCTGAC	GGTTCCACAGGCGTCATCTC
	mouse Runx2	CCATCCATCCACTCCACCAC	GCCAGAGGCAGAAGTCAGAG
	mouse Ctnnb	AGACAGCTCGTTGTACTGCT	GTGTCGTGATGGCGTAGAAC

Table 3 Continued

	name	Forward primer 5'-3'	Reverse primer 5'-3'
Osteogenic Related Genes	Mouse Osteoprotegerin	GCCACGCAAAAGTGTGGAAT	TTTGGTCCCAGGCAAACTGT
	mouse BMP4	GGAGGAGGAGGAAGAGCAGA	TGCTGCTGAGGTTGAAGAGG
	mouse SP7	CGATTCCCCCTGAGCTTTGT	CCCATTGGACTTCCCCCTTC